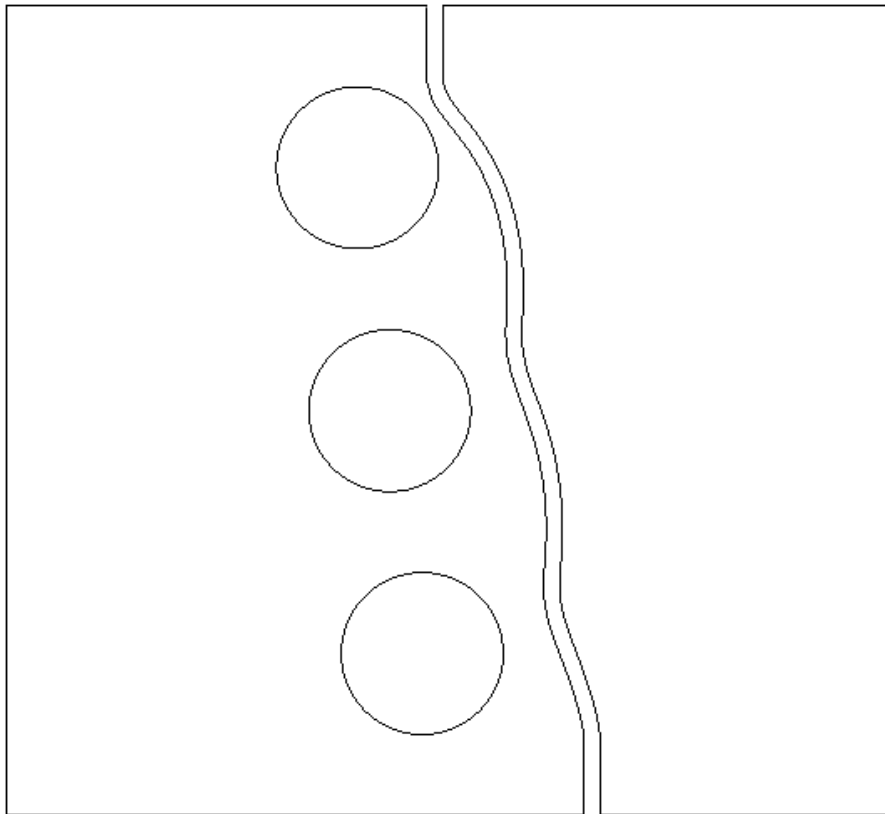


# Master Thesis

## Numerical Analysis of Crack Propagation and Lifetime Estimation

---

Fracture Mechanics and Numerical Programming



BM4-2

Bo Ernst Westergren Jensen

Aalborg University Esbjerg

16<sup>th</sup> of June 2015

Title: Numerical Analysis of Crack Propagation and Lifetime Estimation  
Theme: Fracture Mechanics and Numerical Programming  
Project type: M.Sc. Master Thesis  
Project period: 01-09-2014 to 16-06-2015  
Project group: BM4-2  
Supervisor: Lars Damkilde, Professor, Aalborg University Esbjerg  
Søren Heide Lambertsen, Assistant Professor, Aalborg University  
Esbjerg  
University: Aalborg University Esbjerg  
Institut for Byggeri og Anlæg  
Niels Bohrs Vej 8  
6700 Esbjerg  
Pages: 84  
Student:

---

*Bo Ernst Westergren Jensen*



**AALBORG UNIVERSITET**  
ESBJERG

### **Abstract**

This Master Thesis concerns crack propagation and lifetime estimation of a 2D structure subjected for given boundary condition. Stress intensity factors and energy release rate due to Linear Elastic Fracture Mechanic (LEFM) and crack growth models of Paris, Forman and NASGROW is taking into account.

ANSYS Mechanical APDL is used to programme a code to simulate the trajectory of a crack and determine the lifetime due to crack propagation.

Results from verification of the code indicate good agreement in order to simulate the trajectory of a crack, the estimation of lifetime show an error of 42%, if known sources of error is included an error of 17% is present.

# Preface

This Master Thesis is formulated by a M.Sc. engineer student at Aalborg University Esbjerg, as a long-term project, during 9. and 10. semester in the period of 1<sup>th</sup> of September 2014 to 16<sup>th</sup> of June 2015. The project consist of a main report and an attached DVD.

The topic of the Master Thesis is fracture mechanics, where the behaviour of linear elastic fracture mechanics (LEFM) is taking into account. The general theory of LEFM, criteria and models for simulate the crack trajectory due to crack propagation and lifetime estimation due to cyclic loading is described.

The finite element program Mechanical APDL 15.0 (ANSYS classic), called ANSYS in rest of the project, is used to programme a APDL code that simulate the crack trajectory and estimate the lifetime of a 2D structure subjected for a load case. In order to conduct the APDL code user-friendly it is implemented in the ANSYS user interface menu GUI, by the user interface design language (UIDL).

In order to verify the APDL code for crack trajectory and lifetime estimation, two external experimental results is used for benchmarking.

## Set-up in the project

Tables and figures is refer by: e.g. Figure 1 and Table 1.

In case of two figures beside each other, index: (R) = right and (L) = left, is used.

Equations: e.g. eq.(3.1).

Reference: e.g. [1] is referred it the bibliography in the end of the project.

## YouTube videos

Two YouTube Videos have been produced in order to demonstrate the use of the APDL code, this is only additional material, and is not necessary for the conception of the project.

		QR code
Video name:	Crack Propagation and Lifetime Estimation in ANSYS Mechanical APDL 1	
URL address:	<a href="https://www.youtube.com/watch?v=6ceGp-Wp6cc">https://www.youtube.com/watch?v=6ceGp-Wp6cc</a>	
Video name:	Crack Propagation and Lifetime Estimation in ANSYS Mechanical APDL 2	
URL address:	<a href="https://www.youtube.com/watch?v=mp_2P2T2KK4">https://www.youtube.com/watch?v=mp_2P2T2KK4</a>	

## Table of Content

Master Thesis.....	
1 Introduction.....	1
1.1 Scope of project.....	2
2 Linear Elastic Fracture Mechanics.....	3
2.1 Fatigue Crack Growth.....	3
2.2 Fracture Mechanics.....	4
3 Static load Crack-tip Condition.....	6
3.1 Griffith Energy Balance.....	6
3.2 Energy release rate.....	9
3.3 Resistance curve.....	9
3.4 Stress analysis of cracks.....	14
3.5 J Integral.....	19
3.6 Crack-tip plasticity.....	22
3.7 Plane stress vs. plane strain.....	24
4 Dynamics load Crack-Tip Condition.....	26
4.1 Crack branching.....	27
5 Fracture Toughness.....	29
5.1 Mixed-mode fracture toughness.....	31
6 Crack Trajectories.....	33
6.1 Direction for crack propagation.....	33
6.2 Mix-mode of Stress Intensity Factors.....	36
7 Lifetime Estimation.....	38
7.1 Fatigue Crack Growth Rate.....	39
7.2 Models for fatigue crack propagation.....	44
7.3 Modified crack growth models.....	48
8 Numerical condition.....	52
8.1 Domain Integral.....	52
8.2 Mesh configuration.....	55
8.3 Analysis of number of counters.....	57
8.4 Analysis of mesh size.....	60
9 Programming in ANSYS.....	64

9.1	Crack propagation configuration in APDL code.....	66
9.2	Configuration of ANSYS interface .....	69
10	Verification of APDL code .....	72
10.1	Trajectories .....	72
10.2	Discussion of results.....	75
10.3	Verification of lifetime estimation .....	76
10.4	Discussion of results.....	81
11	Conclusion.....	82
12	Bibliography.....	83
13	Appendix 1 .....	1

### **Content on attached DVD**

PDF fil of Master Thesis.

Folder with available papers from bibliography.

Folder with UIDL- and APDL files.

# 1 Introduction

Through the history a lot of disasters caused by fracture failure of structures have caused many injuries and financial loss. Annual cost of failure in U.S.A in 1978 was estimated to \$119 billion or 4% of the national product, the annual cost could be reduced by \$35 billion if current technology were applied and could be reduced additional by \$28 billion, if further reached was implemented [1].

During the World War II, the Liberty ships, see Figure 1, were produced with revolutionary procedure for fabricating ships quickly by an all-welded hull, where it normally was joined by riveted [1].



*Figure 1: Liberty ship exposed for fracture*

After some time a lot of the Liberty ships obtained fracture failures, where some of the ships broke completely in two. Investigation showed that the ships failures were caused by combination of three factors [1]:

- The welds, due to the poor quality of the welds, contained crack-like flaws.
- Most of the fractures caused local stress concentrations from the deck at square hatch corners.
- The steel had poor fracture toughness.

After these fracture failures, the mechanics of fracture became an engineering issue, standards and procedure for inspections were conducted. One of the leading researchers in this area was Dr. G.R. Irwin after studying the early works of Inglis, Griffith, Westergaard and other scientists, he explored some of today's tools for fracture mechanics. Today Irwin is called one of the “fathers” of fracture mechanics [2].

## 1.1 Scope of project

The history of the Liberty ships from above is an example of how important the understanding and knowledge of fracture failure has become. This Master Thesis is conducted in accordance to get an understanding of the phenomenon crack propagation through a structure, and to estimate a corresponding lifetime. For this purpose some of the fracture tool conducted of Dr. G.R Irwin is taking into account.

In Figure 2 a Work-Flow Chart of the Master Thesis is showed, the tasks is categorised into two groups the main tasks and sub tasks, where the bold tasks is the main tasks.

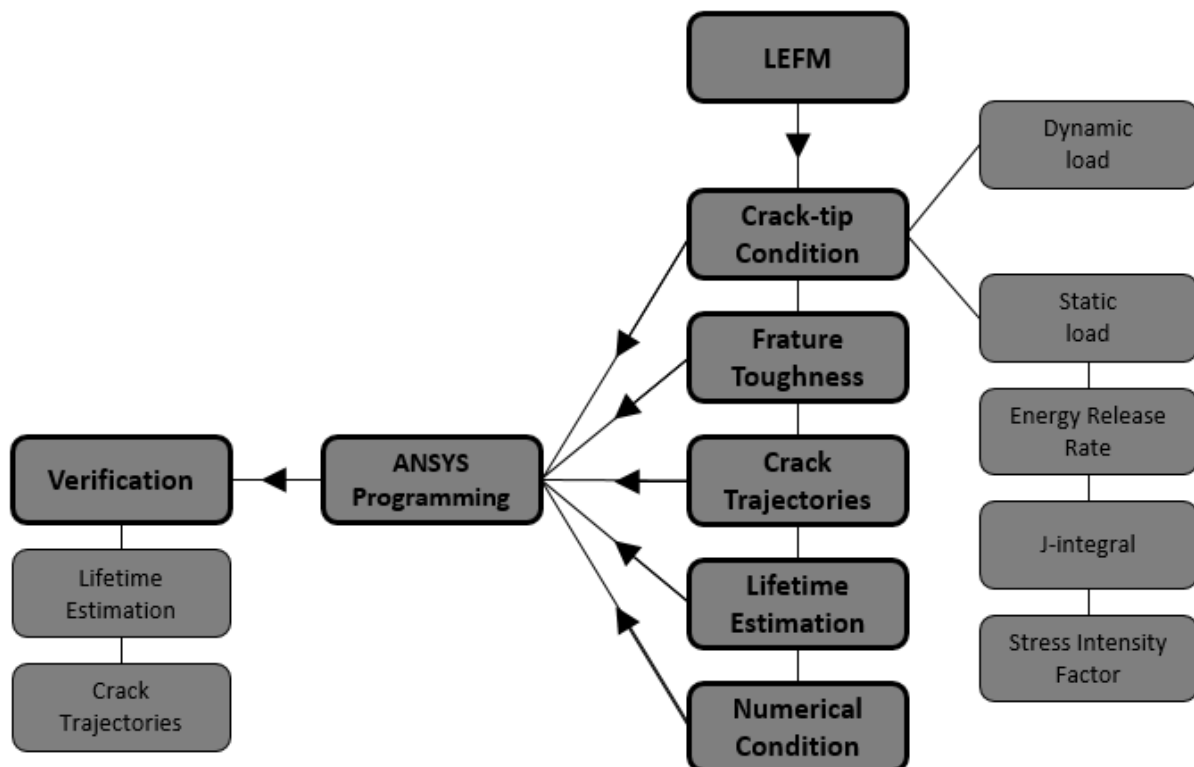


Figure 2: Work-Flow Chart of the Master Thesis

The Master Thesis start with general theory regarding the of determning crack behaviour due to propagation and lifetime estimation. Numerical solutions is conducted in ANSYS, and a process of programming due to obtain generals numerical solutions for crack trajectories and lifetime estaimations is accomplished. In order to verify the numerical solutions from ANSYS, experimental results is taking into account for benchmarking.

## 2 Linear Elastic Fracture Mechanics

The applications and limitations of linear elastic fracture mechanics (LEFM) is explained, and the corresponding relations to classical failure theory is performed. The behaviour of fatigue crack growth from the nucleation to the macro perspective of a crack is conducted in order to define the state of fracture mechanics.

### 2.1 Fatigue Crack Growth

Crack growth depends on different condition and materials behaviour, the crack growth is expressed in three stages, before final failure occur [2], schematic showed in Figure 3.

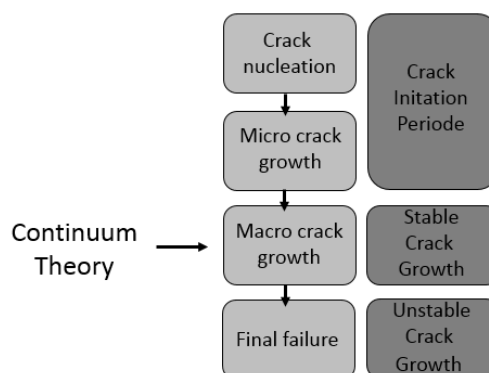


Figure 3: Different stages of crack fatigue crack growth life

- Crack-nucleation
  - In most loadings situations, the critical area due to stresses are at the surface, where the crack nucleation develop.
  - The crack nucleate along slip lines orientated in a plane of maximum shear stress
- Micro-crack growth
  - When the crack size reach typically 10 grain diameters it is called micro cracks.
  - The fatigue crack growth occur predominantly in a plane of maximum shear stress
- Macro-crack growth
  - When the micro-crack are present and cycling loading continues, the fatigue crack tend to grow in the plane of maximum tensile stress, and become a macro-crack.
  - In this stage the continuum theory is taking into account.

Crack growth in the three stages depends on stress levels of the structure, if the stress level is high the total fatigue life occur in the micro- and macro-crack stages. Otherwise if the stress level is low the fatigue life is present in the nucleation- and micro-crack stages [2].

In this Master Thesis the solid mechanics conditions is taking into account with corresponding continuum theory and LEFM approach, so the focus is at the macro crack growth stages to final failure.

## 2.2 Fracture Mechanics

In general two forms of failure in solids exist, permanent (plastic) deformation and breakage, the classical failure theory describe failure of a structure due to the relation between applied stress and yield or tensile strength, Figure 4(R)

For the fracture mechanics three important variables are pronounced, a combination between the applied stress, flaw size and the fracture toughness that replace the strength determine whether or not the structure leads to failure [3]. Figure 4(L)



Figure 4: (R) Relation of Classical failure theory, (L) Relation of Fracture mechanics

The classical failure theory assume that no defects exist in the material and for a plate affected by an uniform load a corresponding uniform stress variation is introduced, see Figure 5(R). During materials manufacturing, processing and service a flaw or crack is introduced and a local stress concentration is presented. In Figure 5(L) the plate is affected by a crack that produce a stress concentration or singular stress field [3]

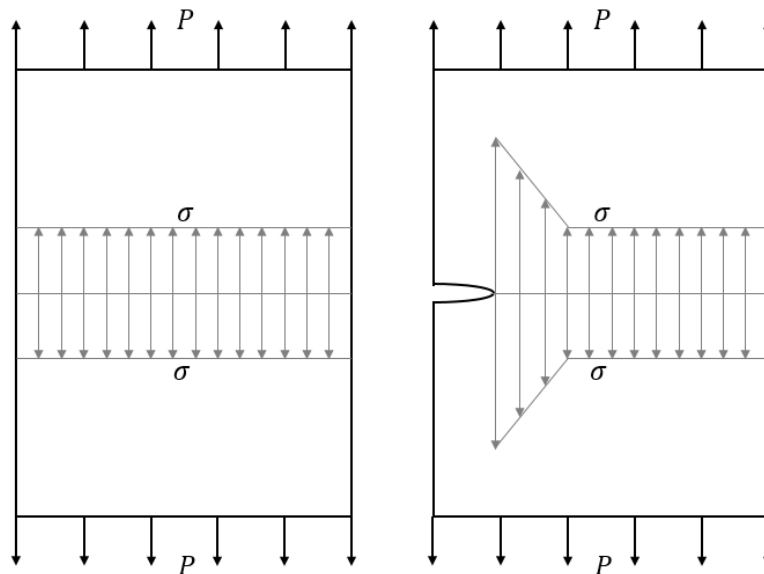


Figure 5: (L) Plate with uniform distributed stress, (R) Cracked plate with stress concentrations

The plate affected by a uniform stress field is described by criteria from e.g. Von Mises, and compared with the yield stress in order to see if failure occur. The local stress concentrations field in the cracked plate is varying by a singularity at the crack-tip. In order to determine this singular stress field the fracture mechanism is taking into account [3].

For the classical failure theory yield criterion is introduced in order to obtain failure behaviour, for fracture mechanical a corresponding value is taking into account, to determine when fracture occur, this value is the fracture toughness.

The fracture toughness vs. stress variation is showed in Figure 6, for brittle material with low toughness value the stress variation and fracture toughness varies linearly when  $\sigma < \sigma_y 0,8$ , and the linear-elastic fracture mechanism (LEFM) is taking into account. For a ductile material that obtain higher toughness value the LEFM approach is not adequate, and the elastic-plastic fracture mechanism (EPFM) cover this area. Materials that obtain very high toughness value the limit load analysis from classical failure theory must be taking into account, due to the fact that high stress level is insensitive to toughness [1].

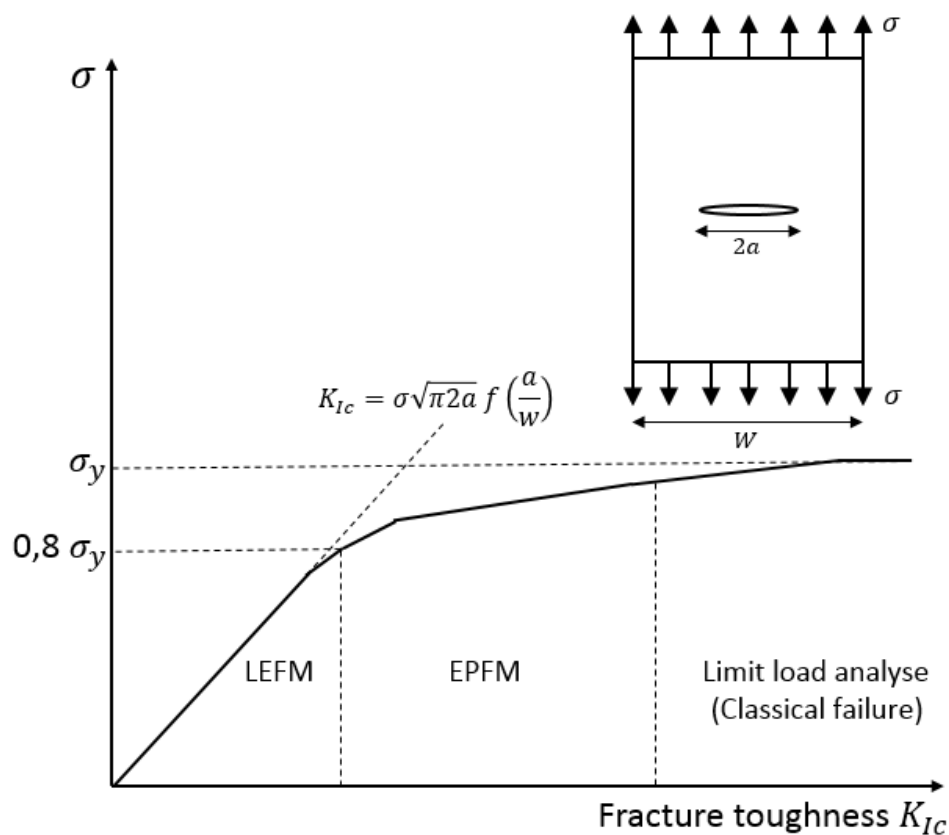


Figure 6: Effect of fracture toughness on the governing fracture mechanism

In this master thesis the LEFM approach is taking into account in order to determine the crack propagation trajectories, and lifetime determination, and it is assumed that the material obtain homogenous and isotopic behaviour.

### 3 Static load Crack-tip Condition

The condition that is taking place due to crack propagation for a static load relation is described in this section. From an energy point of view the theory from Griffith and Irwin is explained, from this the variation of stresses due to a crack-tip is described. The J-integral is introduced to determine this variation of stresses and is fundamental for the numerical analysis. In order to ensure the behaviour of LEFM due to plasticity, corrections is taking into account and the circumstance of plane stress and strain is described.

#### 3.1 Griffith Energy Balance

During fracture two new surfaces are created and the total energy of the system are either decreased or remain constant due to the loads that affects the system. Griffith advance an energy balance between the potential energy and work required to form a crack. Where an incremental increase in crack area under equilibrium condition are given by [1]:

$$\frac{dE}{dA} = \frac{dE_p}{dA} + \frac{dW_s}{dA} = 0 \tag{3.1}$$

Or

$$-\frac{dE_p}{dA} = \frac{dW_s}{dA} \tag{3.2}$$

Component	Description
$E$	Total energy
$E_p$	Potential energy from internal strain and external force
$W_s$	Work required to create two new surfaces
$dA$	Increase in crack area

This relation can be showed by a cracked plate, see Figure 7, subjected for an increase in crack area  $dA$  due to crack increment  $da$ , and create two new surfaces.

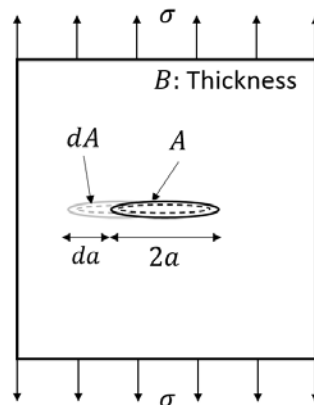


Figure 7: Through crack subjected for increase in crack area

The potential energy in terms of strain energy, is given by a solution from Inglis of stress distribution:

$$E_p = E_{p,0} - \frac{\pi\sigma^2 a^2 B}{E} \quad (3.3)$$

The work from surface energy is given by:

$$W_s = 4aB\gamma_s \quad (3.4)$$

Where  $4aB = 2 dA$ .

Component	Description
$E_{p,0}$	Potential energy of un-cracked plate
$E$	E-modulus
$\gamma_s$	Surface energy

A schematic plot of the energy variation with corresponding crack length is showed in Figure 8, where the total energy:  $E_{tot} = E_{pot} + W_s$ .

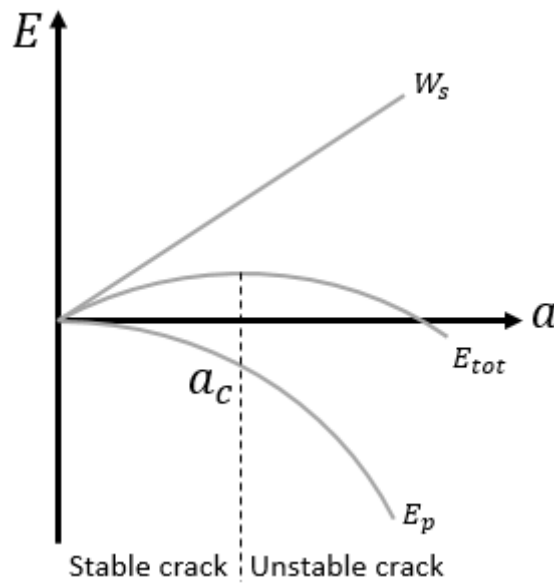


Figure 8: Energy variation with corresponding crack length

The work from surface energy behave linear and the potential energy is parabolic varying due to  $a^2$  in eq.(3.3). When the potential and surface energy is in equilibrium with a corresponding critical crack length  $a_c$ , where the slope of  $E_{tot}$  curve is 0, the crack become unstable and start propagating [4].

Similar a corresponding critical stress level is obtained by differentiating eq.(3.3) and eq.(3.4) with respect to increase in crack area from eq.(3.2).

$$-\frac{dE_p}{dA} = \frac{\pi\sigma^2 a}{E} \quad (3.5)$$

And

$$\frac{dW_s}{dA} = \gamma_s \quad (3.6)$$

Equating eq.(3.5) and (3.6) solving for critical stress  $\sigma_c$ :

$$\sigma_c = \sqrt{\frac{2\gamma_s E}{\pi a}} \quad (3.7)$$

The surface energy  $\gamma_s$  depends on material behaviour and are typical given for brittle materials, when the material become more ductile a factor  $\gamma_p$ , that ensure plastic behaviour, is introduced.

$$\sigma_c = \sqrt{\frac{2E(\gamma_s + \gamma_p)}{\pi a}} \quad (3.8)$$

An generalized expression for any type of energy dissipation is given by:

$$\sigma_c = \sqrt{\frac{2Ew_f}{\pi a}} \quad (3.9)$$

Where  $w_f$  is the fracture energy that include e.g. plastic behaviour depending on the material [1],  $w_f$  describe whether or not fracture occur, due to a given value of energy release rate.

### 3.2 Energy release rate

The Griffith energy balance was further improved by Irwin that defined the energy release rate. This is the rate of change in potential energy due to the crack area, given by:

$$G = -\frac{dE_p}{dA} \quad (3.10)$$

Where:

$$E_p = U - F \quad (3.11)$$

Component	Description
$U$	Strain Energy
$F$	Work by external forces

The energy release rate is compared to the fracture energy  $w_f$  required to generate two new surfaces, and a critical value of energy release rate become:

$$G_c = \frac{W_s}{dA} = 2w_f \quad (3.12)$$

And crack propagation occur when  $G \geq G_c$ , this behaviour is described by the resistance curve [1].

### 3.3 Resistance curve

From the fracture toughness values of a material see section 5, a resistance curve of the material is performed due to crack propagation called, R-curve. A corresponding curve to the R-curve is the driving force curve that is the change in energy release rate due to crack propagation. When the driving force curve exceeds the value of the R-curve fracture occur, and is given by followed expression:

$$\frac{dG}{da} \geq \frac{dR}{da} \quad (3.13)$$

The R-curve describe the material behaviour due to crack propagation. The R-curve exhibit different shapes for different material e.g. for ideal brittle material the R-curve is constant, and for a ductile material usually results in a rising R-curve. In Figure 9 two R-curves with four corresponding driving force curves ( $\sigma_1 - \sigma_4$ ) is showed [1].

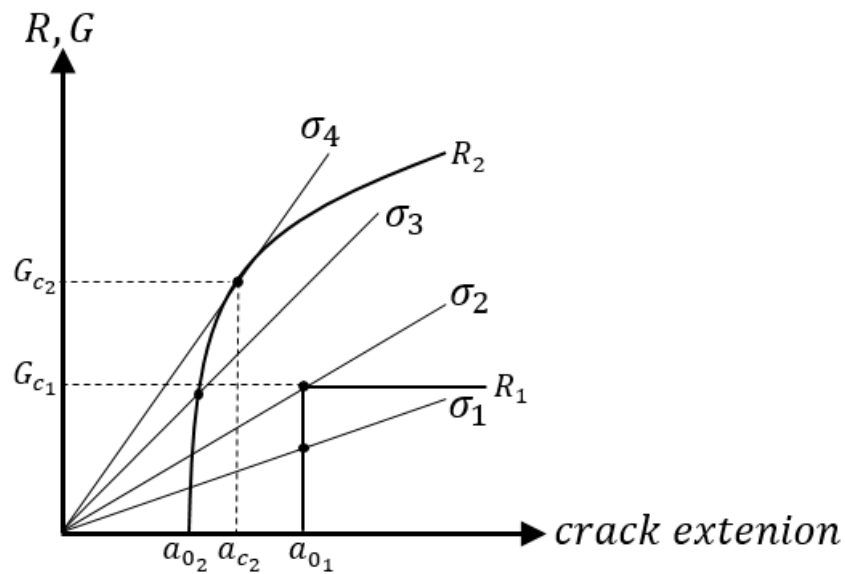


Figure 9: Two R-curve with corresponding four driving force curve 1-4

The first R-curve  $R_1$  is a flat curve with a critical energy release value  $G_{c1}$  if the driving force curve exceeds this value the crack become unstable, e.g.  $\sigma_1$  is stable, no crack propagation occur and  $\sigma_2$  is unstable and crack propagation occur. The second R-curve  $R_2$  is a rising curve, where  $\sigma_3$  is stable and  $\sigma_4$  is unstable but opposite the constant curve the crack is allowed to propagate to a critical value  $a_{c2}$  with a corresponding critical energy release rate  $G_{c2}$ .

The energy release rate distinguish between two load cases, constant load and constant displacement that is of major important due to the variation of the resistance curve [1].

### Constant load vs. constant displacement

Consider two double cantilever beams (DCB) specimen that is subjected to constant load and constant displacement respectively see Figure 10 [4]. The specimen are affected by a crack increment  $da$ .

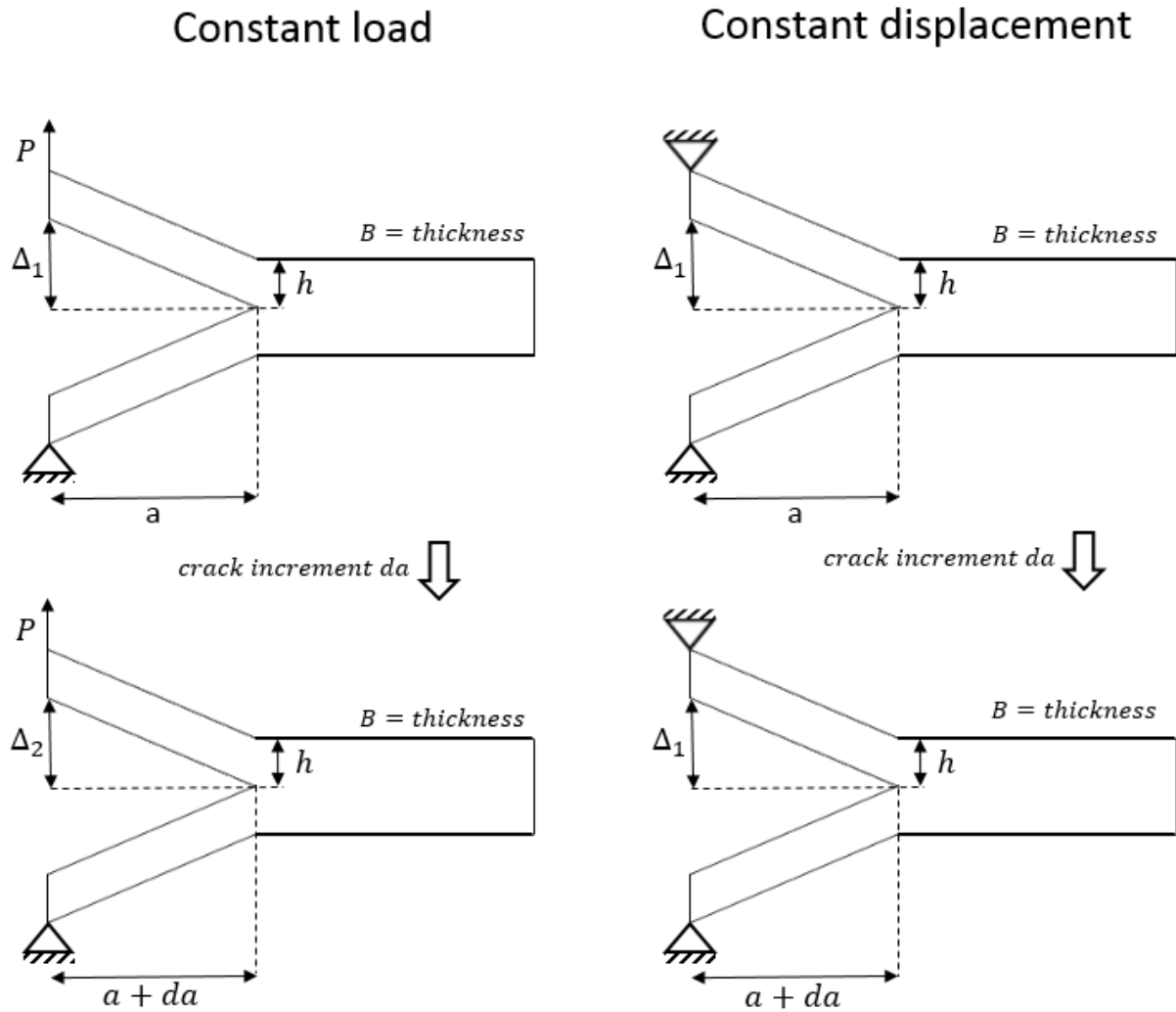


Figure 10: Two DCB specimen under constant load ( $R$ ), and constant displacement ( $L$ ) affected by a crack increment  $da$

The potential energy due to strain energy  $U$  and work from external force  $F$  the crack increment form the two load-cases are given by the two load-displacement diagrams in Figure 11.

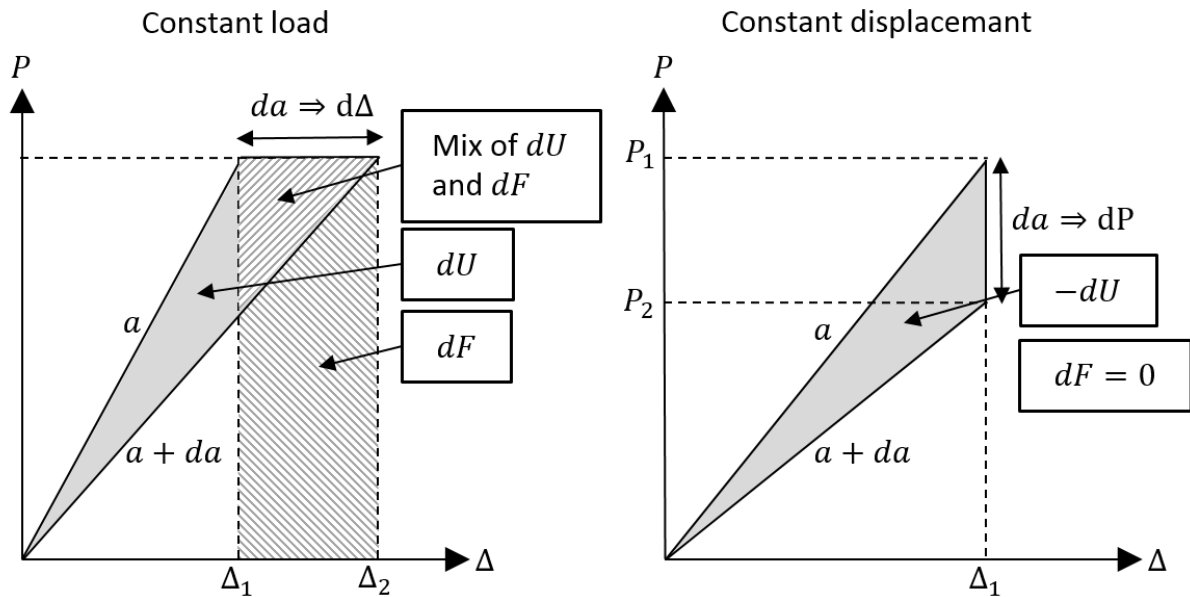


Figure 11: Load-displacement curves for a crack increment with constant load (R), and constant displacement (L)

For the specimen with constant load an increase in the displacement occur, and from the constant displacement a decrease in load occur. From eq.(3.11) the potential energy of the two systems become:

Constant load	Constant displacement
$dU = \frac{1}{2} P d\Delta$	$dU = \frac{1}{2} \Delta dP$
$dF = P d\Delta$	$dF = 0$
$dE_p = -\frac{1}{2} P d\Delta$	$dE_p = \frac{1}{2} \Delta dP$

(3.14)

The energy release rate from eq.(3.10), introduction of compliance  $C = \Delta/P$  and the area  $A = B da$ , the energy release rate for constant load and displacement become:

Constant load	Constant displacement
$G = \frac{1}{B} \frac{dU}{da} = \frac{P}{2B} \frac{dC}{da}$	$G = -\frac{1}{B} \frac{dU}{da} = -\frac{\Delta}{2B} \frac{dC}{da}$

(3.15)

Modifications of the expressions from eq.(3.15) by compliance:  $d\Delta = P dC$  and  $dP = -P \frac{dC}{C}$ , shows that:

$$G = \frac{P^2}{2B} \frac{dC}{da} \tag{3.16}$$

From the results above it is given that the energy release rate for constant load and constant displacement is the same, but with different variation of the resistance curve [4].

## Resistance curves for constant load vs. constant displacement

It is seen from eq.(3.16) that the energy release rate for constant load and constant displacement is the same. But when looking at driving force in eq.(3.16) and compare the expressions in eq.(3.15) the constant displacement gives a negative value and the constant load is positive. A schematic graph for the driving force for constant load and displacement [1].

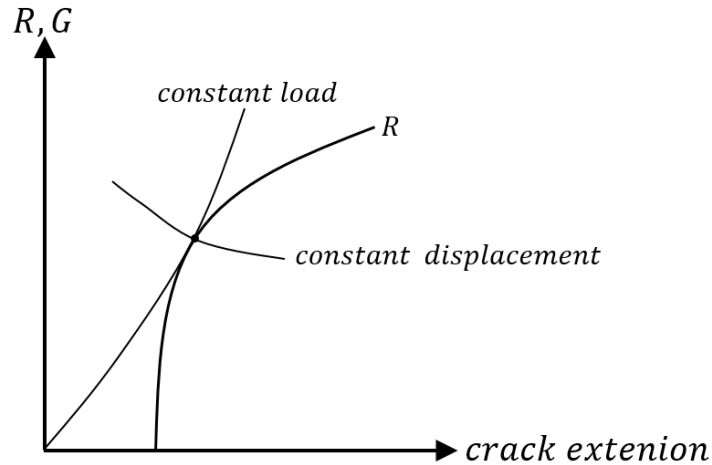


Figure 12: Schematic graph of R-curve with corresponding driving force curves for constant load and displacement

It is seen that the driving force curve for constant load is increasing and the curve for constant displacement are decreasing due to the operational sign in eq.(3.15). That is the displacement must be increased for further crack extension.

When the R-curve is determined experimentally the specimen are usually tested in constant displacement configuration close as possible. In real structure the load condition is somewhere between constant load and constant displacement [1]

### 3.4 Stress analysis of cracks

From Griffith's theory of energy balance, Irwin showed a relationship between the energy release rate and stress variation, given by the stress intensity factor  $K$ .

$$G = \frac{K_I^2}{E'} \quad (3.17)$$

Component	Description
$E' = E$	For plane stress
$E' = \frac{E}{1 - \nu^2}$	For plane strain

The subscript I denote the mode of loading a crack can experience in Figure 13 the three mode showed.

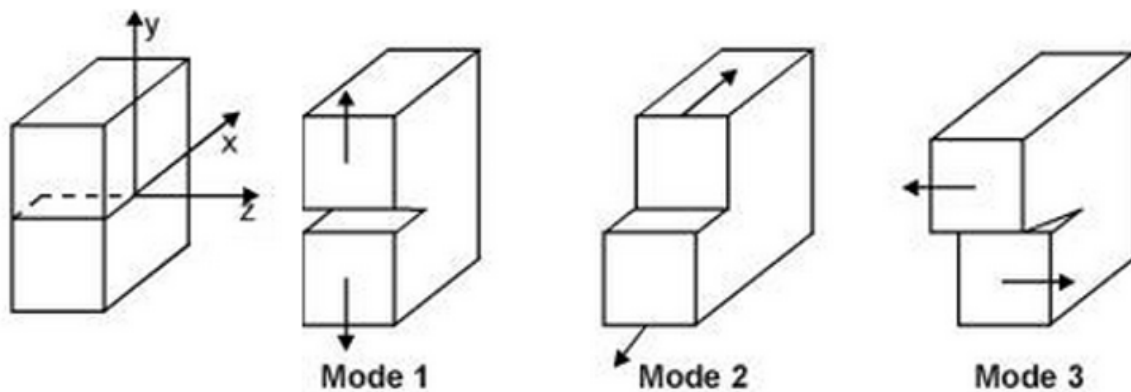


Figure 13: Three mode of loading with corresponding coordinate system [5]

Mode I: Load is applied normal to the crack plane called opening mode.

Mode II: In-plane shear load, tends to slide one crack face with respect to the other.

Mode III: Out-of-plane mode, shear load.

The stress distribution around a crack-tip is schematic sketch in Figure 14(R). Two stress component are assumed a singular and a non-singular stress component. Where the singular part is the stresses in the vicinity of the crack-tip and the non-singular part is the stresses away from the crack-tip [1].

Griffith found a relationship between the variations of the singular stresses and the distance from the crack-tip with  $1/\sqrt{r}$  singularity, when  $r \rightarrow 0$  the stress is going to be infinity. The singular stress fields was described by Irwin from modification of stress functions from e.g. Westergaard and Williams [1]. Irwin developed the stress intensity factor  $K$  that describe the crack-tip conditions relative to stress, strain and displacement near the crack tip. The stress intensity factor for each loading mode with subscript I-III are present. The symbol  $K$  is in honour of Irwin's assistance Kies.

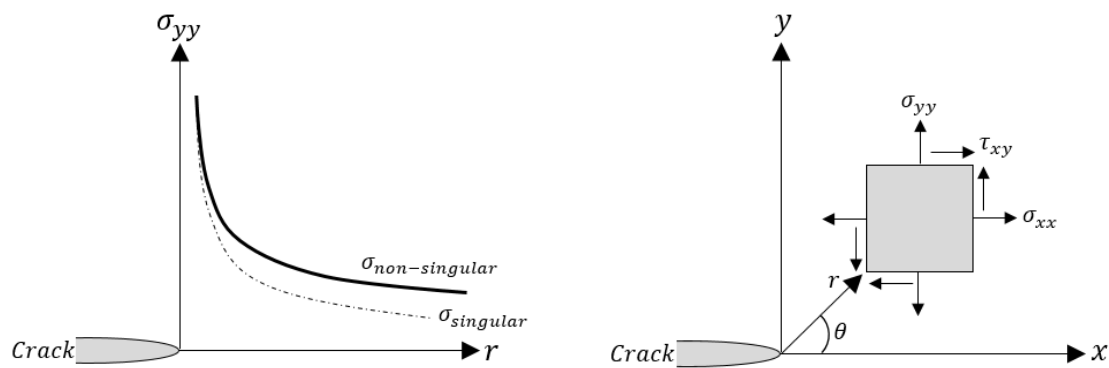


Figure 14: (R) Stress variation around crack tip, (L) Stress components in polar coordinates

From Figure 14(L) the coordinate system ahead of the crack-tip and the polar coordinate are defined. The singular stress fields are given as functions of the three modes of loading from the polar coordinate system  $r, \theta$  [1].

$$\begin{aligned}
 \sigma_{xx} &= \frac{K_I}{\sqrt{2\pi r}} \cos\left(\frac{\theta}{2}\right) \left[1 - \sin\left(\frac{\theta}{2}\right) \sin\left(\frac{3\theta}{2}\right)\right] - \frac{K_{II}}{\sqrt{2\pi r}} \sin\left(\frac{\theta}{2}\right) \left[2 + \cos\left(\frac{\theta}{2}\right) \cos\left(\frac{3\theta}{2}\right)\right] \\
 \sigma_{yy} &= \frac{K_I}{\sqrt{2\pi r}} \cos\left(\frac{\theta}{2}\right) \left[1 + \sin\left(\frac{\theta}{2}\right) \sin\left(\frac{3\theta}{2}\right)\right] + \frac{K_{II}}{\sqrt{2\pi r}} \sin\left(\frac{\theta}{2}\right) \cos\left(\frac{\theta}{2}\right) \cos\left(\frac{3\theta}{2}\right) \\
 \sigma_{xy} &= \frac{K_I}{\sqrt{2\pi r}} \cos\left(\frac{\theta}{2}\right) \sin\left(\frac{\theta}{2}\right) \cos\left(\frac{3\theta}{2}\right) + \frac{K_{II}}{\sqrt{2\pi r}} \sin\left(\frac{\theta}{2}\right) \left[1 - \sin\left(\frac{\theta}{2}\right) \sin\left(\frac{3\theta}{2}\right)\right]
 \end{aligned} \tag{3.18}$$

In Figure 15 the singular stress field of the crack-tip from eq.(3.18) is plotted in a polar coordinate system as function of  $\theta$ , for mode I, where  $K_{II} = 0$ . Similar plots of the three stress components is performed in ANSYS and is schematic showed. The variation of stresses around the crack-tip look similar for the normal stresses, where the schematic plots of shear stresses is not totally symmetric, because a little amount of mode II affect the analysis.

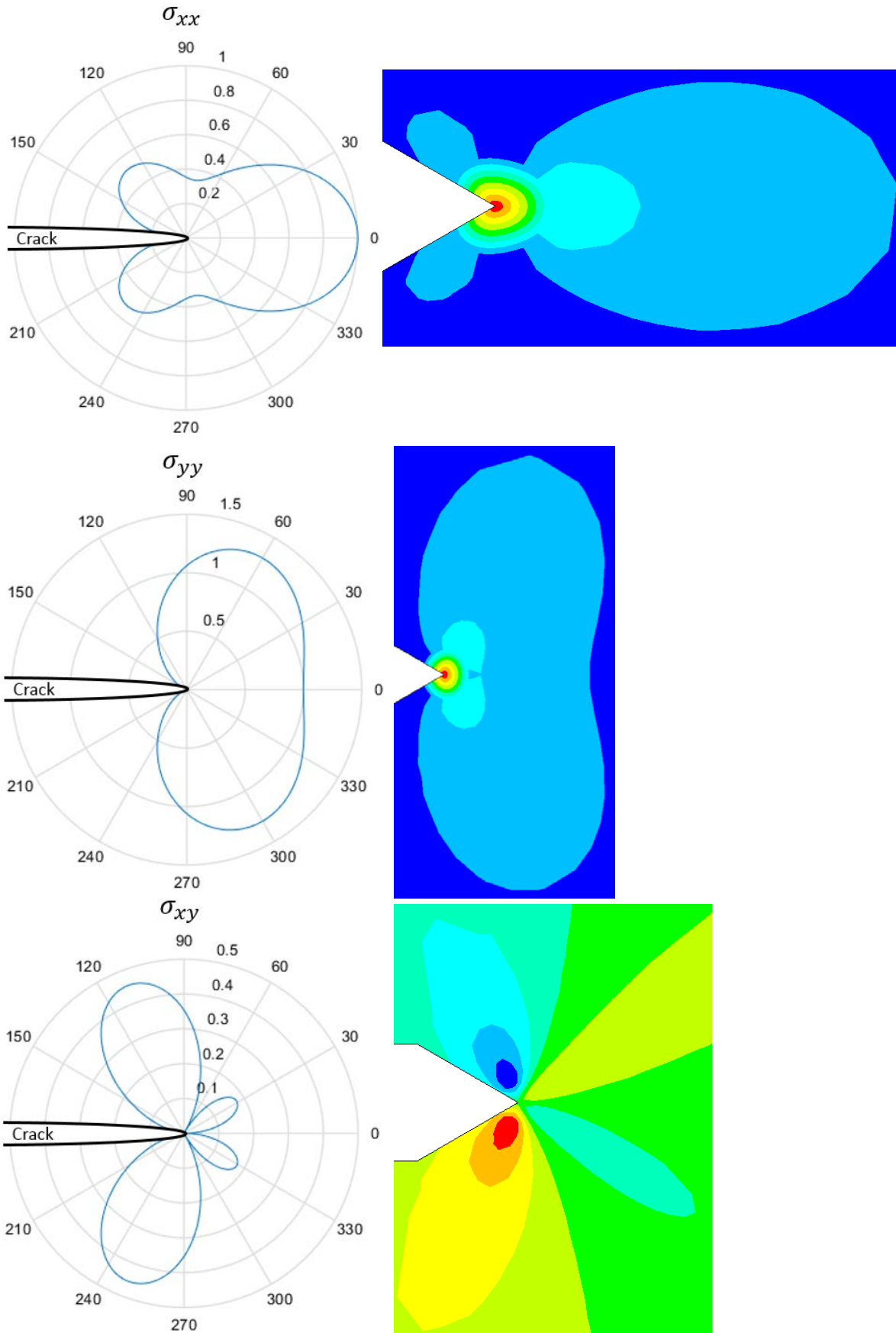


Figure 15: Variation of stress components from eq.(3.18) and mode I loading from ANSYS

The stress intensity factor for mode I, for a through crack in an infinity plate see, Figure 16, is given by:

$$K_I = \sigma\sqrt{\pi a} \quad (3.19)$$

This is the most simply solution of stress intensity factors, and only depend at the applied stress and crack length [1].

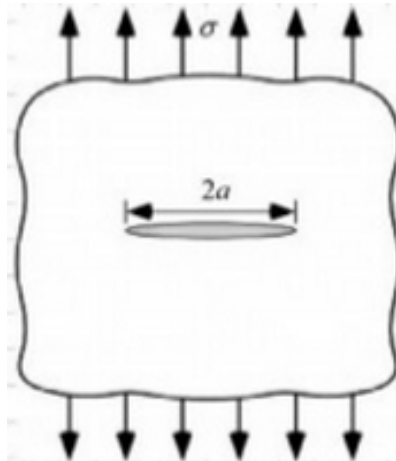


Figure 16: Through crack

A lot of closed forms solutions of the stress intensity factors is obtained, for all three mode of loading, a general solution is given in eq.(3.20).

$$K_{(I,II,III)} = \sigma\sqrt{\pi a} f(W, a) \quad (3.20)$$

Component	Description
$\sigma$	Characteristic stress
$f(W, a)$	Function of crack length and dimension of geometry

The variation in dimension of geometry is seen from a single edge crack specimen subjected for mode I and mode II loading, see Figure 17, where the load is applied normal to the crack front and as a shear load.

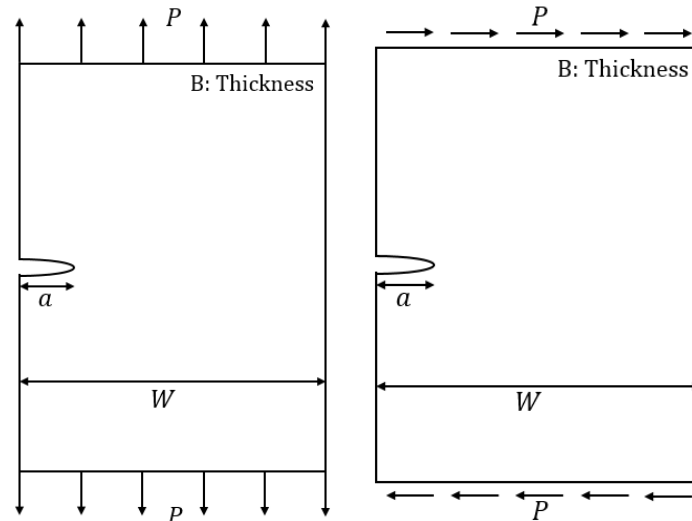


Figure 17: Single edge crack for mode I and II

Analytical solutions for the stress intensity factor for mode I and II is given by [6]:

$$K_I = \frac{P}{BW} \sqrt{\pi a} \left[ 1,12 - 0,231 \left(\frac{a}{W}\right) + 10,55 \left(\frac{a}{W}\right)^2 - 21,72 \left(\frac{a}{W}\right)^3 + 30,39 \left(\frac{a}{W}\right)^4 \right] \quad (3.21)$$

$$K_{II} = \frac{P}{BW} \sqrt{\pi a} \left[ 4,886 \left(\frac{a}{W}\right) - 11,383 \left(\frac{a}{W}\right)^2 + 28,198 \left(\frac{a}{W}\right)^3 - 38,563 \left(\frac{a}{W}\right)^4 + 20,555 \left(\frac{a}{W}\right)^5 \right] \quad (3.22)$$

From the equations above it is seen that the stresses relation between crack length  $a$  and width of specimen  $W$ , contribute significant to the value of the stress intensity factor, especially for mode I as seen in Figure 18.

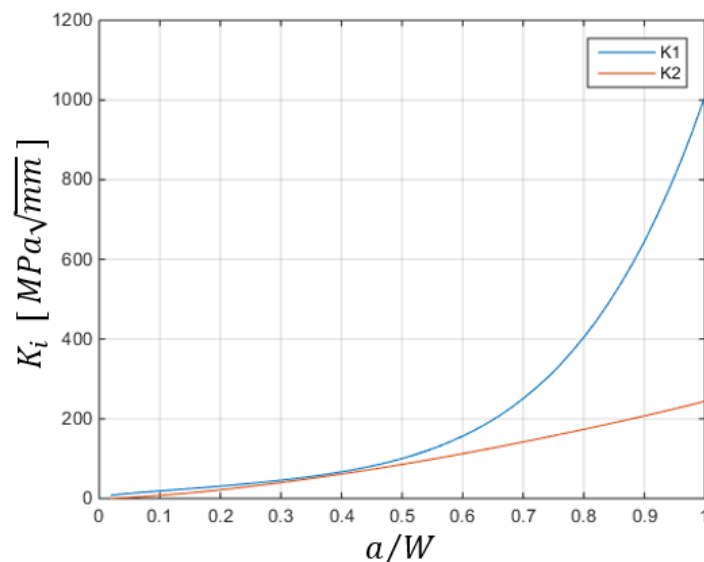


Figure 18: Stress intensity factor for mode I and II with corresponding ration of  $a/W$

### 3.5 J Integral

In section 3.2. the energy release rate is described, J. Rice obtained a path independent contour integral, the J-integral, from his first-name Jim, which describe the energy release rate in LEFM, and similar eq.(3.10) the J-integral are given by [1]:

$$J = G \tag{3.23}$$

The J-integral are also cable to describe the elastic-plastic (EPFM) behaviour which is not the case for energy release rate.

The J-integral can be described by a path around a crack tip given by followed expression see Figure 19.

$$J = \int_{\Gamma} \left( w \, dy - T_i \frac{\partial u_i}{\partial x} \, ds \right) \tag{3.24}$$

Where:

$$w = \int_0^{\varepsilon_{ij}} \sigma_{ij} \, d\varepsilon_{ij} \qquad T_i = \sigma_{ij} n_j$$

Component	Description
$w$	Strain energy density
$T_i$	Traction vector
$n_j$	Unit vector normal to $\Gamma$
$u_i$	Displacement vector
$ds$	Length increment along the contour $\Gamma$
$\Gamma$	Path around crack tip
$\sigma_{ij}, \varepsilon_{ij}$	Stress and strain tensor

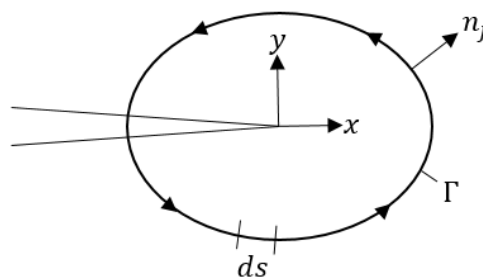


Figure 19: Contour around the crack-tip

## Example J-integral

Determination of the energy release rate by J-integral is performed for a double cantilever beam [4] see Figure 20, where the dotted line from  $B$  to  $G$  is the contour  $\Gamma$  of the J-integral from eq.(3.24).

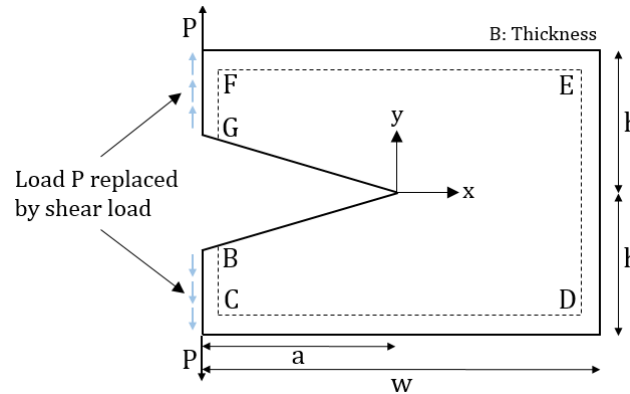


Figure 20: J-integral for a cantilever beam

Followed approximations is taking into account.

- The strain energy of the system is negligible.
- $CD, DE$  and  $EF$  is free surface, no traction is subject.
- $P$  is replaced by a shear load, become traction load at  $BC$  and  $FG$ .
- No displacement or traction in  $x$  direction.

Displacement and traction in  $y$  direction for  $BC$  and  $FG$ , the J-integral become:

$$J = -2 \int_0^h \left( T_y \frac{\partial u_y}{\partial x} \right) ds \quad (3.25)$$

The displacement in  $y$  direction is taking as the slope from a cantilever beam with a point mass in the end, where  $l$  is replaced by  $a$ , moment of inertia is  $I = Bh^3/12$ .

$$\theta = \frac{1}{2} \frac{Pa^2}{EI} \Rightarrow u_y = \frac{6Pa^2}{EBh^3} \quad (3.26)$$

The traction in  $y$  direction for  $BC$  and  $FG$  is given by  $T_y = P/B$ , and the J-integral become:

$$J = \frac{12P^2a^2}{B^2Eh^3} \quad (3.27)$$

The relation between J-integral, energy release rate and stress intensity factor, with a E-modulus of 210 GPa, become:

$$\begin{aligned} J &= G = \frac{K^2}{E} \text{ for plane stress} \\ \Rightarrow J &= \sqrt{KE} = 102 \text{ MPa}\sqrt{\text{mm}} \end{aligned} \quad (3.28)$$

Analytical solution for a double cantilever beam [3]:

$$\frac{P}{B\sqrt{h}} 2\sqrt{3} \left(\frac{a}{h}\right) + 0.64 = 107 \text{ MPa}\sqrt{\text{mm}} \quad (3.29)$$

It is seen that the solution of the J-integral and analytical solution is within an error of 5%.

Modification of the J-integral have been used in the numerical evaluation of the stress intensity factor, see section 8.

### 3.6 Crack-tip plasticity

As described in section 3.4, the singular stress variation for LEFM is given by eq.(3.18), and the stress at the crack tip is infinity. In real material behaviour the stress is finite and a plastic deformation will occur at the crack tip and the stress intensity factor will obtain a new value. It is possible to maintain LEFM behaviour if some correction is made and the plastic deformation is small compared to crack length and the geometry of the system.

Two approach has been provided due to this correction of the stress intensity factor, the first one is obtained by Irwin that is schematic sketch in Figure 21(R). Where elastic stress variation for a crack is showed [1].

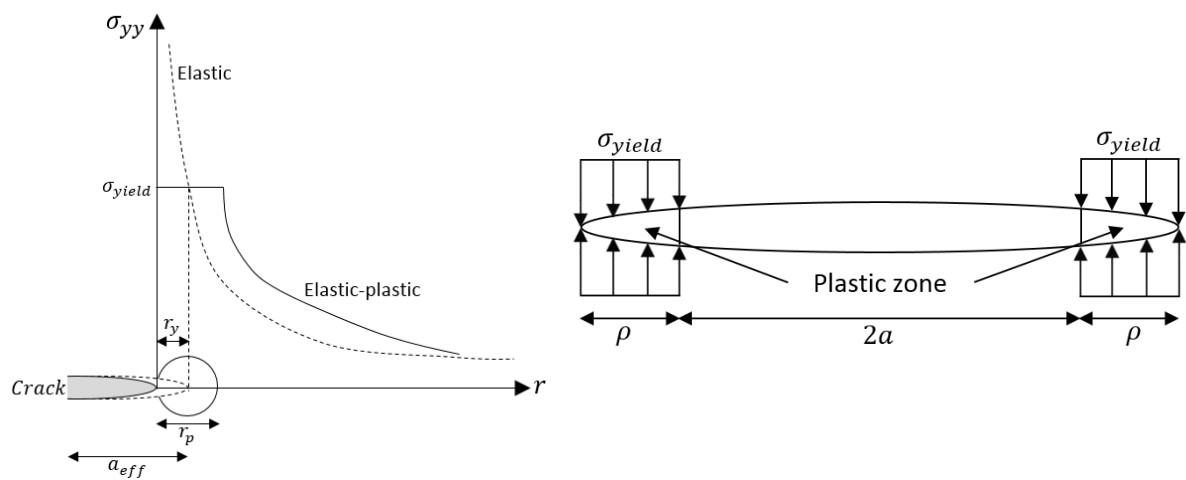


Figure 21: (R) Irwin approach to obtain a effective crack length, (L) Strip-yield model with compressive yield stress at the plastic zone

Irwin showed that the elastic stress component must be redistribute in order to satisfy equilibrium due to the plastic stress component, he found that the radius  $r_y$  of the plastic zone  $r_p$  is determined from yield stress:

$$\sigma_{yield} = \frac{K_I}{\sqrt{2\pi r_y}} \Rightarrow r_y = \frac{1}{2\pi} \left( \frac{K_I}{\sigma_{yield}} \right)^2 \Rightarrow r_p = 2r_y \quad (3.30)$$

To describe the stress variation from the stress intensity factor an effective crack tip length must been taking into account:

$$a_{eff} = a + r_y \quad (3.31)$$

From an iterative solution an effective stress intensity factor is determined, here a closed form solution for the though crack is given by:

$$K_{eff} = \frac{\sigma_{yy}\sqrt{\pi a}}{\sqrt{1 - \frac{1}{2}\left(\frac{\sigma_{yy}}{\sigma_{yield}}\right)^2}} \quad (3.32)$$

Dugdale and Barenblatt obtained the Strip-yield model showed in Figure 21(L). Where the plastic zone with a length of  $2\rho$ , for a crack in compression with a load corresponding to the yield stress. From this a stress intensity factor for closure stress is obtained, and a length of the plastic zone is given with a size that almost is the same obtained by Irwin from eq.(3.30).

$$\rho = \frac{\pi}{8}\left(\frac{K_I}{\sigma_{yield}}\right) \approx r_y \Rightarrow 2\left[\frac{1}{2\pi}\left(\frac{K_I}{\sigma_{yield}}\right)^2\right] \quad (3.33)$$

Burekin and Stone found that an effective crack length  $a_{eff}$  in the area between  $a - (a + \rho)$  and determined an expression for the effective stress intensity factor. A closed form solution for the through crack is given by:

$$K_{eff} = \sigma_{yield}\sqrt{\pi a}\left[\frac{8}{\pi^2}\ln\sec\left(\frac{\pi\sigma}{2\sigma_{yield}}\right)\right]^{\frac{1}{2}} \quad (3.34)$$

Variation of  $K_{eff}$  of Irwin and the strip-yield correction model in eq.(3.32) and eq.(3.34) is compared with the solution for a through crack from LEM in eq.(3.19) with respect to the normalized stress and nondimensionalized  $K_{eff}$ , [1] see Figure 22.

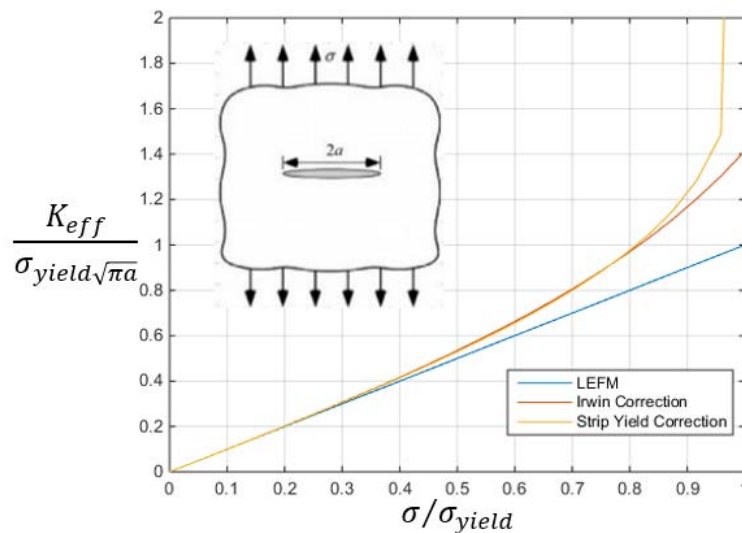


Figure 22: Comparison of plastic zone corrections for a through crack

The  $K_{eff}$  of Irwin and strip-yield model deviate from the LEFM solution at stresses greater than  $0,5 \sigma_{yield}$ , the two correction models agree with each other up to a value of approximated  $0,85 \sigma_{yield}$ , where the strip-yield model become infinity.

The LEFM approach is ensured if the plastic zone is small compared to the dimension of the geometry. Restriction due to crack size and stress variation have been suggested in order to ensure the LEFM approach [2].

Monotonic loading

$$r_y \leq \frac{a}{8}$$

Cyclic loading

$$r_y \leq \frac{a}{4}$$

Stresses

$$\sigma_{max} \leq 0,8 \cdot \sigma_y$$

The restrictions due to monotonic- and cyclic loading and correction from Irwin eq.(3.30) is taking into account for the analysis of trajectory and lifetime estimation in section 10. The is

### 3.7 Plane stress vs. plane strain

The definitions of plane stress and plane strain is given by:

$$\begin{aligned} \sigma_{zz} = \sigma_{xz} = \sigma_{yz} = 0 &\Rightarrow \text{plane stress} \\ \varepsilon_{zz} = \varepsilon_{xz} = \varepsilon_{yz} = 0 &\Rightarrow \text{plane strain} \end{aligned} \tag{3.35}$$

In Figure 23(R) a 3D edge crack are showed with two coordinate systems where subscribes  $i$  and  $s$  denotes the interior and the surface of the crack. When the crack are subjected to a load the material around the crack tip in the interior region tries to contract in the x and z directions, but is prevented from doing so by the surrounding material, the Poisson effect. That leads to very high triaxial stresses and a stage of plane strain is acting in this region. Near the surface the triaxial stresses are lower but only at the surface the stage of plane stress exists [1].

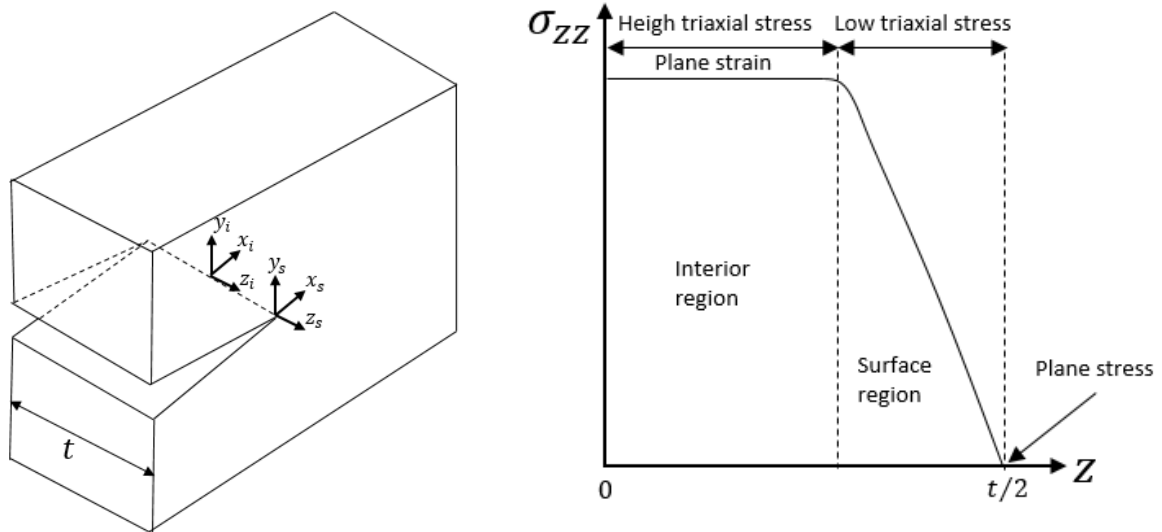


Figure 23: (R) 3D edge crack with interior and a surface coordinate system, (L) Stress variation along the z-axes in the 3D edge crack

The level of triaxial stresses is schematic plotted in Figure 23(L) with the corresponding normal stress in the z directions. It is seen that the level of triaxial stresses decrease due to  $\sigma_{zz}$  near the surface.

To illustrate the variation between plane strain and plan stress variation due to the Von Mises yield criteria. From eq.(3.18) stress variation of a crack-tip, setting  $\theta = 0$  gives followed results for x, y and z stress components [1]:

$$\begin{aligned} \sigma_{xx} &= \frac{K_I}{\sqrt{2\pi r}} & \sigma_{yy} &= \frac{K_I}{\sqrt{2\pi r}} & \sigma_{zz} &= 0 & \text{For plan stress} \\ \sigma_{zz} &= \frac{2\nu K_I}{\sqrt{2\pi r}} & & & & & \text{For plan strain} \end{aligned}$$

The Von Mises yield criteria and corresponding different in  $\sigma_{yy}$  are given by:

$$\begin{aligned} \sigma_{Von\ Mises} &= \frac{1}{\sqrt{2}} \left[ (\sigma_{xx} - \sigma_{yy})^2 + (\sigma_{xx} - \sigma_{zz})^2 + (\sigma_{yy} - \sigma_{zz})^2 \right]^{\frac{1}{2}} \\ \Rightarrow \sigma_{yy}(\text{at yield}) &= \begin{cases} \sigma_{yield} & \text{(Plane stress)} \\ 2,5\sigma_{yield} & \text{(Plane strain)} \end{cases} \end{aligned} \quad (3.36)$$

It is seen there exist a major different for plane stress and plane strain condition and it is important to distinguish between this two stages when talking fracture mechanics. Followed condition exist for plane stress and strain:

$$\begin{aligned} E' &= E & \text{For plane stress} \\ E' &= \frac{E}{1 - \nu^2} & \text{For plane strain} \end{aligned}$$

## 4 Dynamics load Crack-Tip Condition

If a structure is affected of rapid loading e.g. from an impact with a second structure or the material obtain high brittle behaviour, the scenario of “rapid crack propagation” occur. From section 3.1 the Griffith balance of energy for a propagating crack is performed for a static load-case where the potential energy introduced. If “rapid crack propagation” occur the velocity become essential and the kinetic energy also is taking into account.

Energy release rate from form eq.(3.1) is modified to a dynamic energy release rate to include the kinetic energy by followed [1]:

$$G(t) = \frac{dF}{dA} - \frac{dU}{dA} - \frac{dE_k}{dA} \quad (4.1)$$

Potential- and kinetic energy is given by:

$$E_p = U - F \quad E_k = \frac{1}{2} mV^2 \quad (4.2)$$

With followed parameters:

$$E_p = f(\sigma, E, a) \quad E_k = f(\sigma, E, a, m, V) \quad (4.3)$$

The fracture toughness for the energy release rate is equal to the fracture energy  $W_f$ , due to two surfaces, the static- and dynamic load-case is given by [1]:

$$G_{c,sta.} = E_p = 2W_f \quad G(t)_{c,dyn.} = \frac{1}{2} \frac{d}{da} [E_p - E_k] = 2W_f \quad (4.4)$$

It is seen that the dynamics fracture toughness is less than the static value. This behaviour occur since less energy is needed to maintain a propagating crack, than a stationary crack.

Relation between the energy release rate and the stress intensity factor for a static load-case is given by  $G = K_I^2/E'$ , from this a dynamic stress intensity factor is obtained [1]:

$$K(t)_I = K(V) K(0) \quad (4.5)$$

$K(0)$  representing te stress intensity factor for a static load-case, and  $K(V)$  is a parameter ranging from  $[0 - 1]$ , depended of the crack velocity, given by:

$$K(V) \approx \left(1 - \frac{V}{c_r}\right) \sqrt{1 - hV} \quad (4.6)$$

$h$  is a function of longitudinal- and transverse waves velocity, and  $c_r$  is the Rayleigh waves velocity.

The dynamic stress intensity factor in eq.(4.5) is valid as long as the length of crack propagation ( $a - a_0$ ) is small compared to the specimen dimension, because the reflecting stress waves will not had time to reach the crack-tip. Otherwise the reflecting stress waves can have a significant effect on the local crack-tip fields [1].

### Rayleigh waves velocity

Mechanical waves are waves which propagate trough a material at a wave speed which depends on the elastic and inertial properties of the material. There are two basic types of waves, longitudinal and transverse. The longitudinal travel have the fastest velocity, the transverse waves travel with a slower velocity. The Rayleigh waves travel through the material with both a longitudinal- and transverse direction, Rayleigh waves travel with slower velocity than transverse wave [7].

The case of dynamic crack propagation take place from “rapid loading” and the velocity is taking into account, this phenomenon occur due to crack branching.

## 4.1 Crack branching

In sections 3, it have been found that when a crack propagate a given amount of energy, the crack start propagating, due to dissipating the energy around the crack-tip. Recall the Griffith energy criterion and stress intensity factor from section 3.1 and 3.4,  $G = K_i^2/E'$  for plane stress.

From experiments [8] in high brittle materials such as Plexiglas (PMMA) or Soda-Lime glass, it have been showed that at a critical velocity:  $V_c$  the system chose to develop a new mode of dissipation, it diverts this energy not only to a single crack propagation, but to the formation of additional new cracks, called branches, typical two new cracks symmetric around the main crack.

This phenomenon is showed in Figure 24, where four different specimen of PMMA is subjected for only tensile displacement to ensure pure mode I loading, with different crack velocities. The critical crack velocity is  $V_c = 330 \text{ m/s}$  or  $0,39 C_r$ , where  $C_r$  is the Rayleigh wave speed.

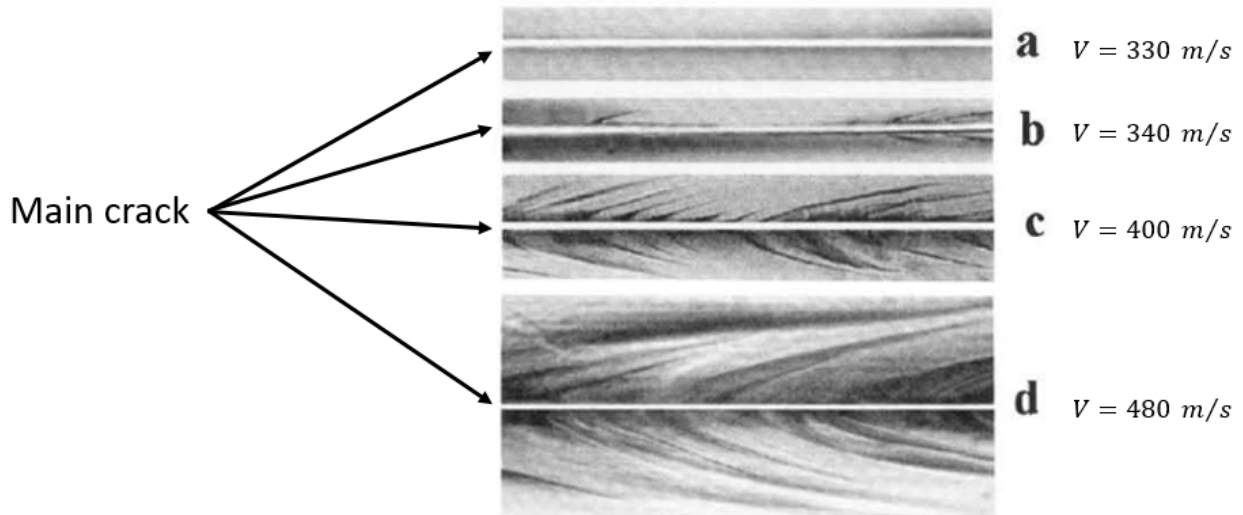


Figure 24: Experiment of crack branching in PMMA [8]

When the crack velocity increase the branching effect increase, generally the branching cracks do not extend throughout the entire thickness of the specimen, they only affects the surface area of the specimen. The branching length is depended of the velocity in the main crack as seen in Figure 24, where the length of the branching increase with increasing crack velocity.

Velocity of the main crack is changing during the process of branching due to loss of energy when a branching crack propagating. The branching crack stop propagating due to loss of energy to the main crack, and the main crack increases in velocity, see Figure 25.

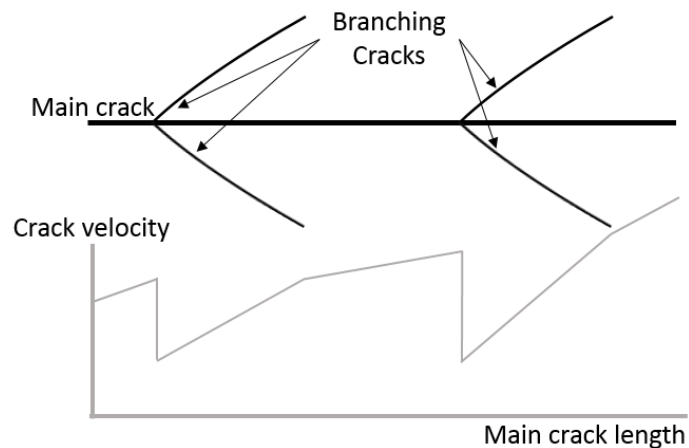


Figure 25: Varying Main crack velocity due to branching

The phenomenon of crack branching is included for structure that is exposed for dynamic condition, where “rapid crack propagation” or high brittle behaviour is obtained. In this Master Thesis the dynamic condition is not taking into account, due to the fact that the loading condition for verification, see section 10, is assumed to be static or quasi-static.

## 5 Fracture Toughness

The fracture toughness is a property of the material that describe the resistance due to crack fracture or failure. The fracture toughness of a material is dependent on temperature, corrosive environment also the stress variation and crack length influence the fracture toughness [1].

Stress intensity factor from eq.(3.19) for mode I, is substituted with the fracture toughness  $K_{Ic}$ , the influence of crack length and stress variation is seen:

$$K_{Ic} = \sigma\sqrt{\pi a}f(W, a) \Rightarrow \sigma = \frac{K_{Ic}}{\sqrt{\pi a}}f(W, a) \Rightarrow a = \frac{K_{Ic}^2}{2\pi\sigma}f(W, a) \quad (5.1)$$

From the expressions above it is seen that the crack length influence the fracture toughness more than the stress variation.

The fracture toughness value is estimated from test results that is described in different standards. The most common one is the standard from American Society for Testing and Materials (ASTM), where the procedure for testing of fracture toughness and resistance curves is described. The fracture toughness value is a single value, where the resistance curve is various values of the fracture toughness.

### Measurement of fracture toughness for mode I from ASTM E399

The principle of evaluating the fracture toughness  $K_{Ic}$ , for mode I, according to ASTM E399 standard is given below. Different specimen configuration are permitted in evaluation of  $K_{Ic}$ , here a compact specimen in evaluated see Figure 26. Plane strain and LEFM is assumed, that the plastic zone must be small compared to the specimen dimension and constant displacement is taking into account [1].

Requirements for the length of initial crack lengths:  $0,45 \leq \frac{a_0}{W} \leq 0,55$ .

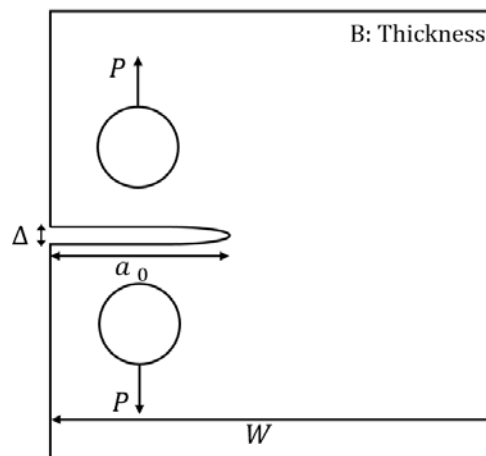


Figure 26: Compact specimen for evaluation of fracture toughness

Testing of the specimen is conducted by applying a load  $P$ , the load is increased with a speed that ensure quasi-static condition, finally the specimen reach fracture and is broken. During the test measurements of the load  $P$  and displacement of the crack moud opening displacement (CMOD)  $\Delta$  is conducted. I order to ensure the right value of the load to determine the fracture toughness, a corresponding load  $P_Q$  is used. In Figure 27 three different behaviour of a  $P - \Delta$  diagram is showed.

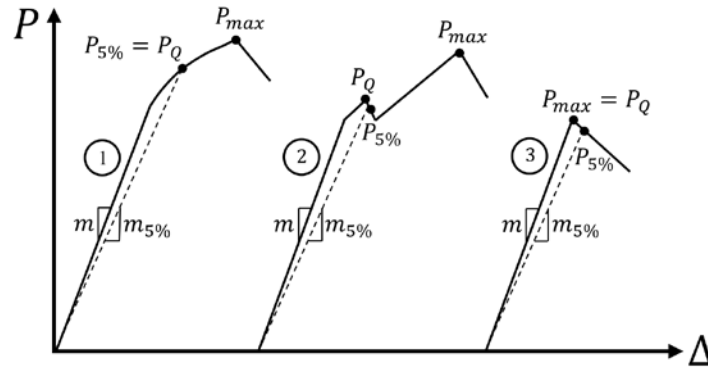


Figure 27: Different behaviour of  $P - \Delta$  diagram

Component	Description
$P_{max}$	Maximum measured load from test
$P_Q$	The corresponding load for determining $K_{IC}$
$m$	Initial elastic loading slope
$m_{5\%}$	95% slope of $m$ -slope
$P_{5\%}$	Load where $m_{5\%}$ intersect with $P - \Delta$ curve

Description of the three  $P - \Delta$  curve [1]:

1. Smooth in elastic region, and it deviates slightly when reach nonlinearity caused by plasticity.
2. Unstable crack growth (e.g. flaws) occurs before deviates from linearity by 5%.
3. Fails completely before achieving 5% nonlinearity.

When the value of  $P_Q$  is estimated a corresponding stress intensity factor is obtained with a function of specimen dimensions:

$$K_Q = \frac{P_Q}{B\sqrt{W}} f(a, W)$$

In order to valid  $K_Q$  followed condition must be satisfied:

$$B, a \geq 2,5 \left( \frac{K_Q}{\sigma_y} \right)^2$$

$$P_{max} \leq 1,10 P_Q$$

If the above conditions is satisfied the  $K_Q = K_{Ic}$

## 5.1 Mixed-mode fracture toughness

Fracture toughness for mode I is described in the section above, where the mode I loading is taking into account. In many cases a structure is affected by more than mode I loading, where the mode II loading also play an essential role. Then the fracture toughness must consider mode I and II, for the mixed-mode fracture toughness.

The relations between the mixed-mode toughness is schematic showed in Figure 28, a field below the toughness value of mode I and II define the zone where no fracture occur.

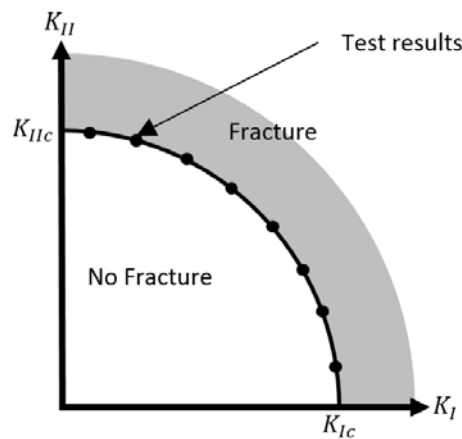


Figure 28: Illustrations of mix-mode fracture toughness

Fracture toughness for mix-mode is determined from test results with different ratio of mode I and II, a corresponding fit of the test results define the field where no fracture occur.

### Measurement of fracture toughness for mix-mode from ASTM D6671

Determination of the mix-mode fracture toughness from test results, is performed by the ASTM D6671 standard, where the main principle is outlined here.

The standard is used for composite material e.g. unidirectional carbon fiber tape laminates and glass-fiber, which contain brittle behavior. Specimen used for testing is the double cantilever beam (DCB) which is subjected for opening mode and shear mode by bending, by use of mixed-mode bending apparatus schematics showed in Figure 29.

The apparatus contain a Lever which is subjected to a load  $P$  that produce bend and opening of the specimen that is fixed to a hinge at both size to ensure a continuous opening with no bending. The position of load  $P$  is varying by the length  $c$  for different test results in order to ensure varying ratio of the mode I and II. A large value of  $c$  produce a large opening (mode I) and

small bending (mode II) and vice versa. Displacement  $\Delta$  of the crack is a mixture of the bending and opening. The apparatus operate in constant displacement mode.

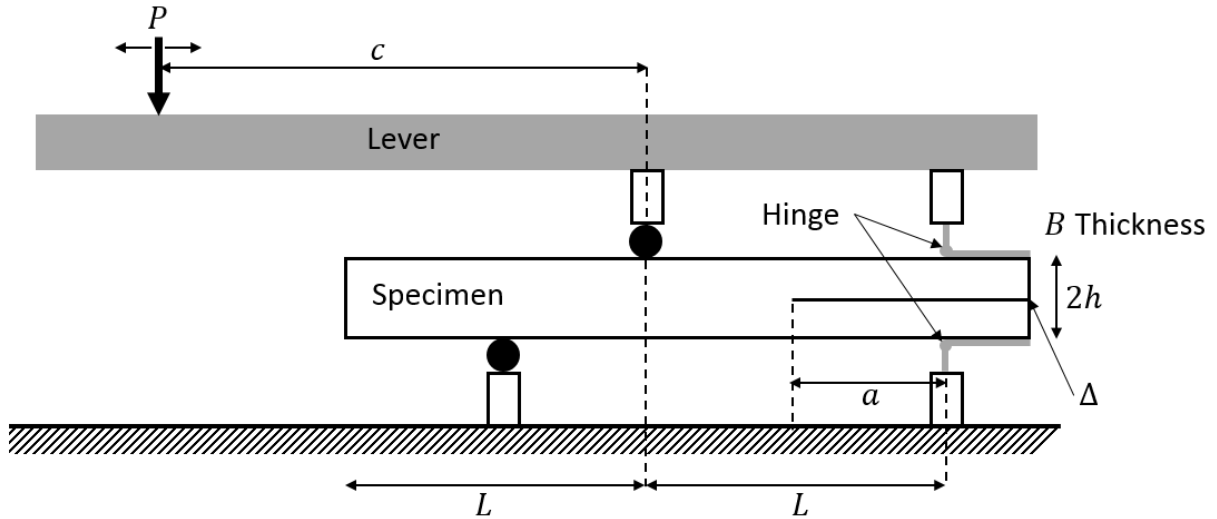


Figure 29: Mixed-mode Bending apparatus with DCB specimen

From each test a load-displacement curve is performed similar as in Figure 27, where a load  $P_Q$  and slope  $m$  is determined.

The fracture toughness is determined from the energy release rate, where the relation to stress intensity factor is given by:  $G = K_I^2/E$  for plane stress. The toughness value for mode I and II is given by followed expressions:

$$G_{I,c} = \frac{12P_Q^2(3c - L)^2}{16B^2h^3L^2E_{if}} (a + \chi h)^2 \quad (5.2)$$

$$G_{II,c} = \frac{9P_Q^2(c - L)^2}{16B^2h^3L^2E_{if}} (a + 0.42\chi h)^2 \quad (5.3)$$

Component	Description
$P_Q$	The corresponding load for determining $K_{Ic}$
$\chi$	Correction parameter for longitude and transverse modulus (orthotropic material)
$E_{if}$	E-modulus in fibre direction, include the slope $m$ (orthotropic material)

The number of test and ratio of mode I- and II toughness value depends on the structure and corresponding load cases, which typically is described in standards.

## 6 Crack Trajectories

In order to determine the trajectories of a propagating crack through a structure, conditions for the direction of the crack and the correlation of stress intensity factors for mode I and II is described in this section.

### 6.1 Direction for crack propagation

Determination of the direction of crack propagation in mixed-mode loading where an opening and in-plan shear mode occur have been performed by Erdogan and Sih [9]. Where it is assumed that the crack propagate in a direction equal to the maximum tangential stresses  $\sigma_{\theta\theta}$  and the shear stress is equal zero. The tangential and shear stress components in polar coordinates are given by:

$$\sigma_{\theta\theta} = \frac{K_I}{4\sqrt{2\pi r}} \left[ 3 \cos\left(\frac{\theta}{2}\right) + \cos\left(\frac{3\theta}{2}\right) \right] - \frac{K_{II}}{4\sqrt{2\pi r}} \left[ 3 \sin\left(\frac{\theta}{2}\right) + \sin\left(\frac{3\theta}{2}\right) \right] \quad (6.1)$$

$$\sigma_{r\theta} = \frac{K_I}{4\sqrt{2\pi r}} \left[ \sin\left(\frac{\theta}{2}\right) + \sin\left(\frac{3\theta}{2}\right) \right] + \frac{K_{II}}{4\sqrt{2\pi r}} \left[ 3 \cos\left(\frac{\theta}{2}\right) + 3 \cos\left(\frac{3\theta}{2}\right) \right] \quad (6.2)$$

The radial stress component is not taking into account since it do not contribute to the direction of the crack.

The normalized tangential and shear stress variation is showed in Figure 30, where the first plot(R) show the stresses for the opening mode where  $K_{II} = 0$ , and similar for the second plot(L) that show the stresses for the in-plane shear mode  $K_I = 0$ .

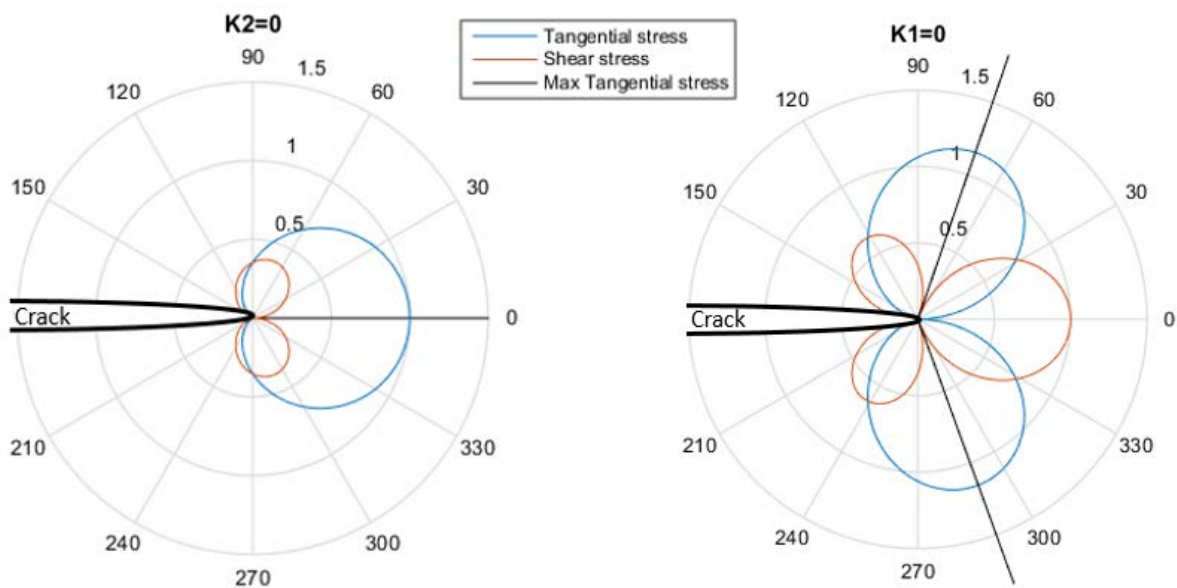


Figure 30: Tangential and shear stress variation (R) for  $K_{II} = 0$  and (L) for  $K_I = 0$

It is seen that the maximum tangential stress occur where the shear stresses is zero and the angle of maximum tangential stress is:

$$\begin{aligned} K_{II} = 0 &\Rightarrow \sigma_{\theta\theta,max} \Rightarrow 0^\circ \\ K_I = 0 &\Rightarrow \sigma_{\theta\theta,max} \Rightarrow 70,5^\circ \end{aligned} \quad (6.3)$$

Erdogan and Sih showed the followed relationship:

$$\frac{\partial \sigma_{\theta\theta}}{\partial \theta} = -\frac{3}{2} \sigma_{r\theta} \quad (6.4)$$

When  $\sigma_{\theta\theta}$  reach maximum at a given angle  $\theta_0 \Rightarrow \sigma_{r\theta} = 0$ , the crack direction angle  $\theta_0$  satisfies the following equation:

$$\begin{aligned} \cos\left(\frac{\theta_0}{2}\right) [K_I \sin(\theta_0) + K_{II}(3 \cos(\theta_0 - 1))] &= 0 \\ \Rightarrow \theta_0 = -\arccos\left(\frac{3K_{II}^2 + K_I^2 \sqrt{K_I^2 + 8K_{II}^2}}{K_I^2 + 9K_{II}^2}\right) \end{aligned} \quad (6.5)$$

The relationship of Erdogan and Sih is called Maximum tangential stress (MTS).

Another criterion for direction of a crack is performed by Richard [10], from a large number of experiments he found followed empirical solution of crack direction:

$$\theta_0 = \mp \left[ 155,5^\circ \frac{|K_{II}|}{|K_I| + |K_{II}|} \right] - 83,4^\circ \left[ \frac{|K_{II}|}{|K_I| + |K_{II}|} \right]^2 \quad (6.6)$$

From equation above the maximum angle of crack direction is:

$$\begin{aligned} K_{II} = 0 &\Rightarrow 0^\circ \\ K_I = 0 &\Rightarrow 72,1^\circ \end{aligned} \quad (6.7)$$

From both criterion the value of  $K_I$  is always positive or zero, that the normal loading always is tension or zero. The shear-load from mode II achieve both positive and negative values with corresponding sign of the angle of crack direction see Figure 31 [10].

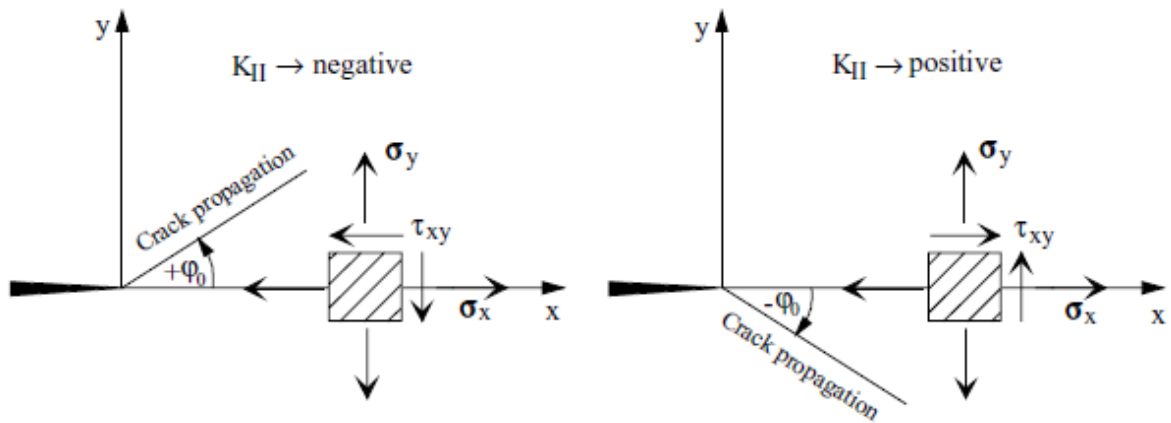


Figure 31: Sign of crack angles with corresponding sign of  $K_{II}$  [10]

Followed relationship of shear-load,  $K_{II}$  value and angle of crack direction is obtained:

$$\begin{aligned} \tau > 0 &\Rightarrow K_{II} > 0 \Rightarrow \theta_0 < 0 \\ \tau < 0 &\Rightarrow K_{II} < 0 \Rightarrow \theta_0 > 0 \end{aligned} \quad (6.8)$$

The two criteria of Erdogan/Sih and Richard with varying  $K_{II}$  values and a fixed value of  $K_I = 10 \text{ MPa}\sqrt{\text{m}}$  is showed Figure 32.

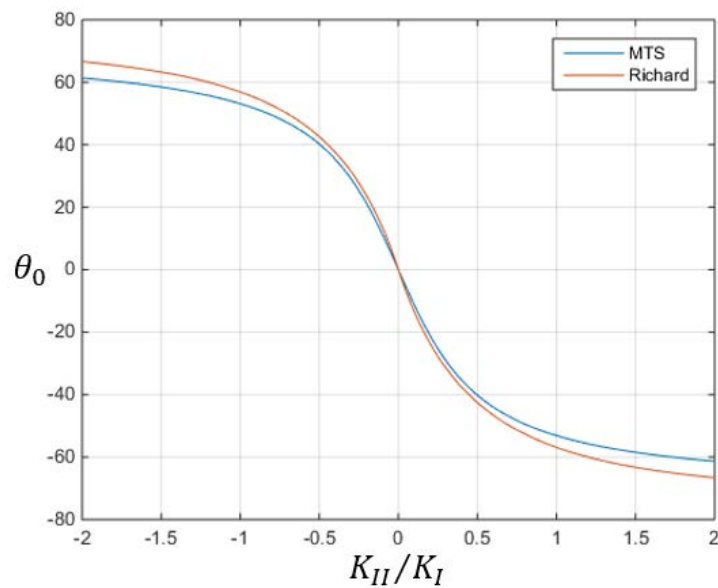


Figure 32: Crack direction criteria MTS and Richard

The two criteria looks similar, when they reach the extrema values of  $K_{II}/K_I$  the criteria of Richard exceed a higher value of  $\theta_0$ .

## 6.2 Mix-mode of Stress Intensity Factors

If more than one loading condition is applied two or three mode is activated, only 2D problem is taking into account here, so only mode I and II is consider.

Numerous of criteria have been proposed to determine an equivalent stress intensity factor for mode I and II. From experiments explicit expression have been made to “weighted” the different value of mode I and II into an equivalent stress intensity factor.

Three different criteria for mix-mode is considered for material that is isotropic and homogeneous and the value of mode I always obtain positive value,  $K_I > 0$ , that no crack propagation occur when a load of compression is considered.

- Tanaka’s criteria [11]:

$$K_{eq,T} = (K_I^4 + 8K_{II}^4)^{\frac{1}{4}} \quad (6.9)$$

- Richard’s criteria [10]:

$$K_{eq,R} = \frac{K_I}{2} + \frac{1}{2} \sqrt{K_I^2 + 4(\alpha K_{II})^2} \quad (6.10)$$

Where:

$$\alpha = 1,155$$

- Irwin’s criteria [12]:

$$K_{eq,I} = \sqrt{K_I^2 + K_{II}^2} \quad (6.11)$$

From the three criteria it is seen that when  $K_{II} = 0$ , the equivalent stress intensity factor  $K_{eq} = K_I$ .

Comparison of the three criteria due to variation of  $K_{II}$ , with a fixed value of  $K_I = 10 \text{ MPa}\sqrt{\text{m}}$  is seen in Figure 33

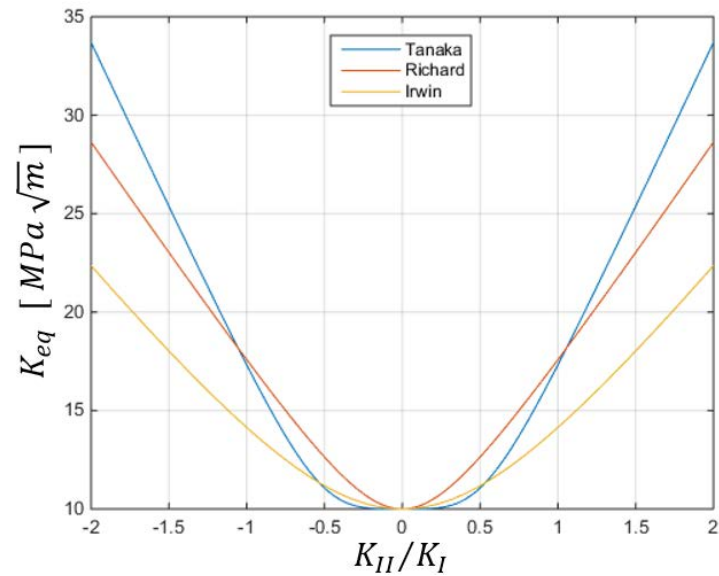


Figure 33: Three criteria of equivalent stress intensity factor with varying  $K_{II}$  value

Tanaka is the most conservative in the area  $K_{II}/K_I < \pm 0,5$ , when  $K_{II}/K_I > \pm 1$  it become non-conservative, Richard and Irwin variety similar but with a steeper slope for Richard.

The criterion from Richard and MTS of crack direction and the mix-mode criteria is taking into account in the numerical analysis.

## 7 Lifetime Estimation

During a load-case subjected to a structure, crack will start propagating and with the circumstance that small-scale yielding occur, than LEFM is taking into account, the lifetime for failure can be estimated from the stress intensity factor and the corresponding load-case.

In this section the estimation of lifetime due to crack propagation is evaluated for different empirical models with the influence of various load-cases, and the factors of range in stress intensity and crack closure effect is investigated.

### Load-cases

The load-case is categorised in two main groups, constant-amplitude loading and variable-amplitude loading, in Figure 34 three different load-cases is illustrated with the minimum and maximum value of stress intensity factor  $K_{min}$  and  $K_{max}$  for a corresponding time series.

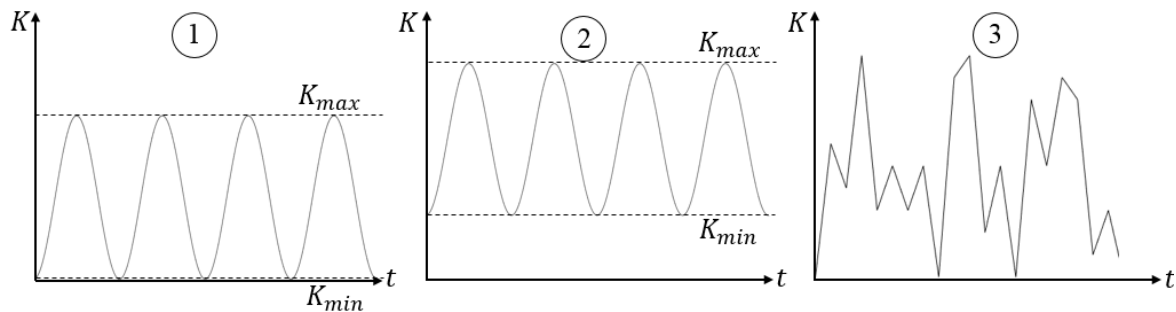


Figure 34: Three load-cases 1-3

Load-case 1 and 2 is defined as constant amplitude loading, and number 3 is variable amplitude loading. Load-case 2 is constant amplitude loading with mean stress effect or R-ratio. The constant amplitude loading is well described in literature and research due to fracture failure, where the variable amplitude loading are more complex and due to the history dependence from e.g. prior occasional of over- or under-loads [1].

In this project the constant amplitude loading is investigated, for load-cases with positive values of  $K_{min} \geq 0$  and  $K_{max} > 0$ , that only tensile load is taking into account, and no compression.

## 7.1 Fatigue Crack Growth Rate

In order to estimate the lifetime of a structure subjected to a load-case, research have showed an correlation, between the crack propagation and number of load cycles called fatigue crack growth rate, and properties that influence the crack propagation.

For constant amplitude loading crack growth rate can be described by followed relationship [1]:

$$\frac{da}{dN} = f(R, \Delta K) \tag{7.1}$$

Where:

$$\Delta K = K_{max} - K_{min} \qquad R = \frac{K_{min}}{K_{max}}$$

Component	Description
$\Delta K$	Range in stress intensity
$R$	Mean stress effect or R-ratio
$da$	Different in crack length: $a_{i+1} - a_i$
$dN$	Different in number of cycles: $N_{i+1} - N_i$

The mean stress effect  $R$  is seen for load-case 2 in Figure 34, where the value of  $K_{min}$  exceed 0. The value of  $R$  only obtain 0 or  $R > 0$  in this project because only tensile loads is taking into account.

Crack growth rate behaviour for constant amplitude loading is described by a sigmoidal curve, see Figure 35, where a log-log plot of  $da/dN$  and  $\Delta K$  is showed.

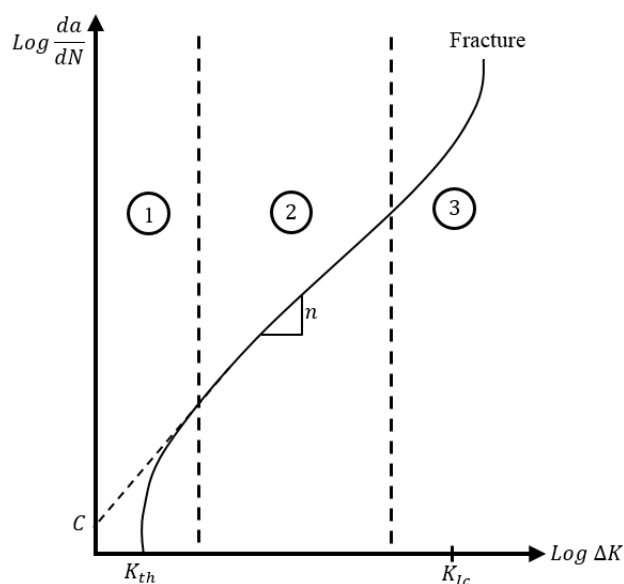


Figure 35: Fatigue crack propagation behaviour

Component	Description
$K_{th}$	Threshold value, minimum value of $\Delta K$ for crack propagation
$K_{Ic}$	Fracture toughness, maximum value of $\Delta K$ for fracture
$n$	Slope of the fatigue crack growth curve in region 2
$C$	Intercept of sigmoidal curve in region 2

The material parameters  $C$  and  $n$  is estimated form experimental testing, it is noted that the crack growth rate only obtain positives values, due to the logarithmic scales of the plot.

The crack starts to growth at a given threshold value, that is minimum value of the stress intensity factor where the crack start propagate, this is defined as region 1. The crack continue to propagate in a linear way with increase in stress intensity and crack growth, this step is called region 2. The final end of the crack propagation is fracture where the stress intensity reach the fracture toughness value described in section 5, and a corresponding crack growth value that leads to fracture of the system, this region define the region 3. Here a short description of the 3 region [1]:

Region 1: The threshold value is a very complex case and a lot of research have been done during the time to describe this value. The value contain of two parts, a material property, and as a function of the loading, the threshold is typical defined from experiments similar as for the fracture toughness.

Region 2: In this region the crack propagation is linear and stable, this region is the most common for a crack during its lifetime.

Region 3: The crack growth rate accelerates in this region and lead to fracture, researchers have during the time reached two explanations for this behaviour. The first one is due to microscopic fracture from e.g. flaws due discontinuity. A other explanations is that the crack growth rate  $da/dN$  is not real due to larger plastic zone with an larger value of crack driving force.

### Mean stress effect

The mean stress effect or R-ratio is given as the ratio between minimum and maximum stress intensity factor for a given load case:  $R = K_{min}/K_{max}$ .

Illustration of the mean stress effect is schematic showed in the next two figures. In Figure 36 four different load-cases here defined as blocks with followed conditions:

- Constant R-ratio for each block.
- Identical increase in the value of  $K_{max}$ .
- Different increase in the values of  $K_{min}$ .

This gives an increase in range of stress  $\Delta K$  in the block, but a generally decrease through all the blocks.

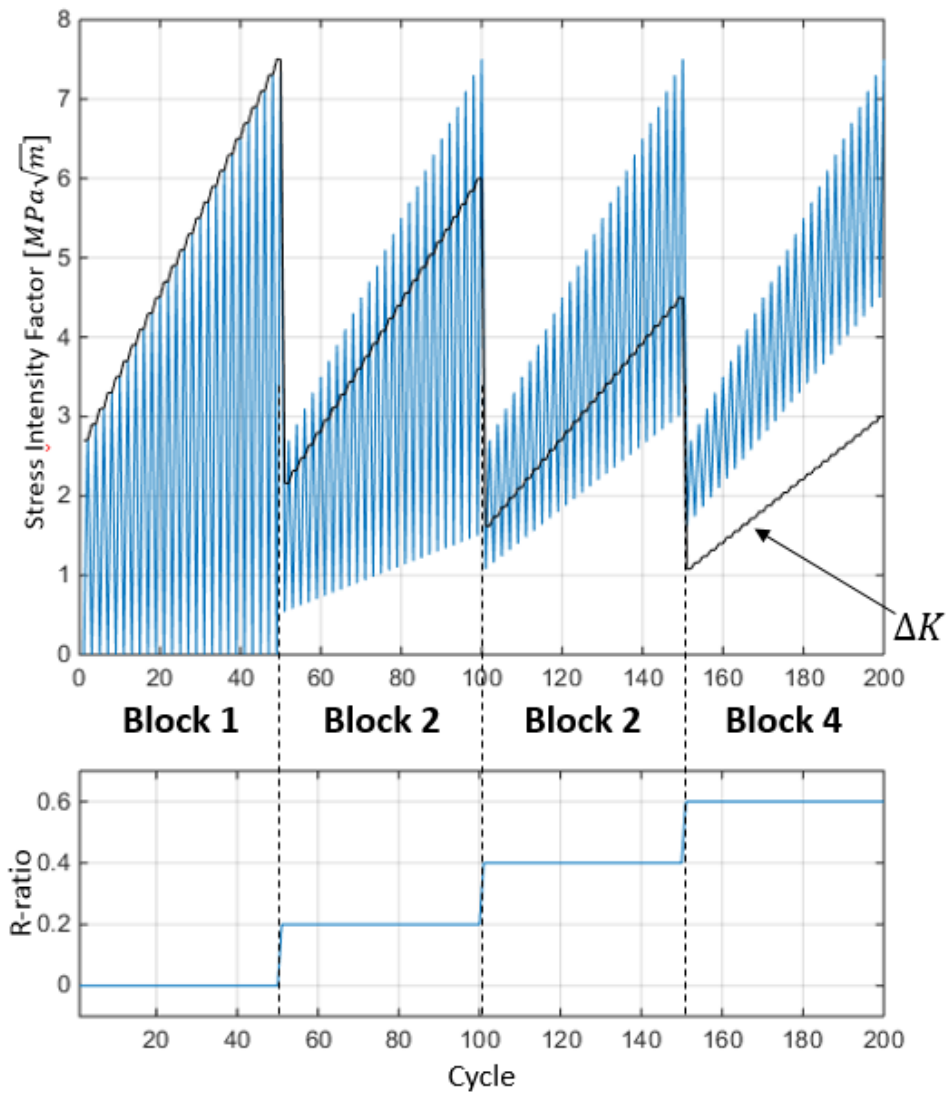


Figure 36: Four different blocks of loads with varying range of stress intensity and different R-ratio

The first block is subjected for an increase in  $K_{max}$  but with a constant  $K_{min}$  with a value of zero from which follows  $K_{max} = \Delta K$ , for the three existing blocks an increase in  $K_{min}$ ,  $K_{max}$  and  $\Delta K$  is showed.

In Figure 37 the variation of the sigmoidal curve is showed due to the four blocks with different R-ratio. Implemented of the curves is performed by the NASGROW model, see section 7.2.

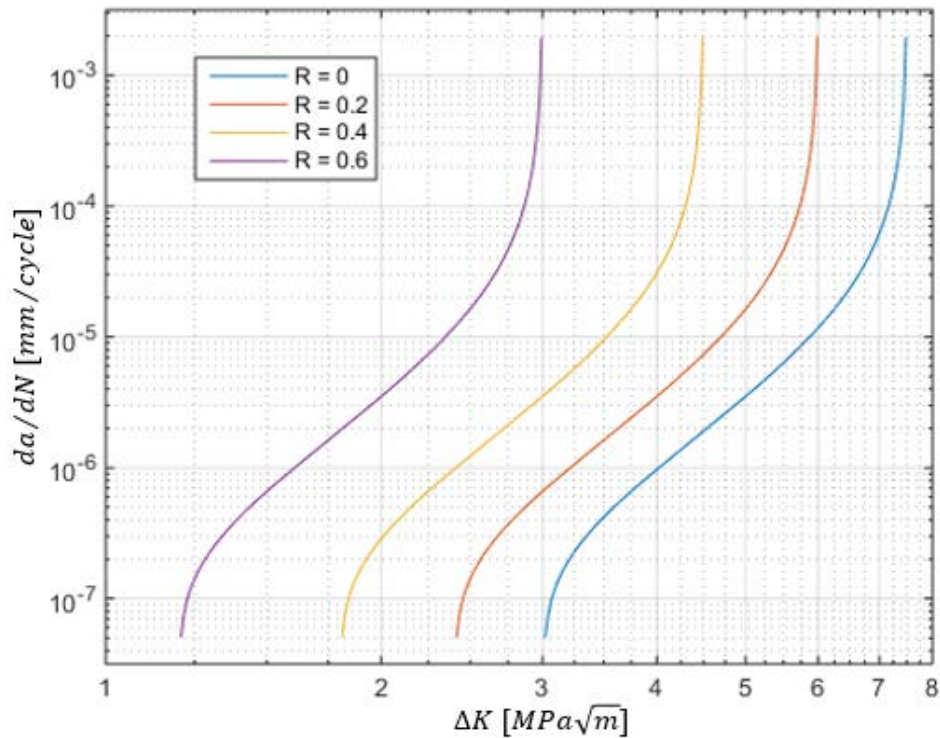


Figure 37: Crack growth rate for four blocks of loads with varying stress intensity factor, and different R-ratio

It is obvious that different values of R-ratio affects the lifetime or crack growth of the material. The increase in R-ratio gives an increase in the crack growth and obtain a less conservative value of the threshold in region 1 and the fracture toughness in region 3. This is an important factor to take into account when determining the threshold- and fracture toughness values, where the load-case for testing procedure and the “real” structure have to be similar.

## Crack closure

During experimental test, Elber [1] discover the phenomenon crack closure, when a crack is subjected to low loads the crack opening of the material become the same or even less from a uncracked material. During a load cycle, see Figure 38, the crack start to close before it reach the  $K_{min}$  value, due to contact between the crack surfaces. It is seen that the crack stop closing at the  $K_{OP}$  value, the stress intensity at which the crack opens [1].

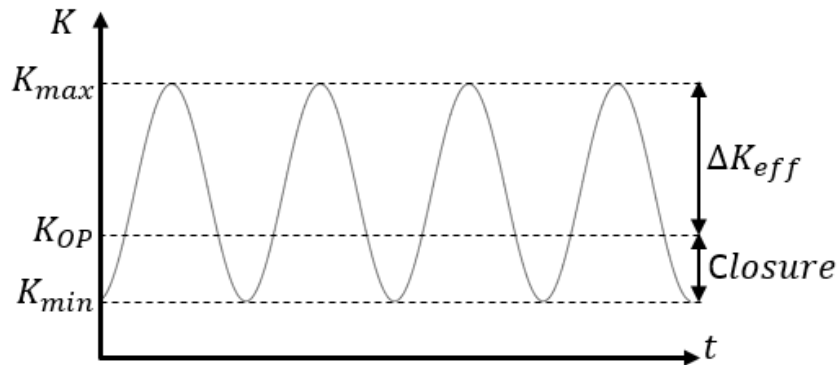


Figure 38: Load cycles with crack closure

Elber assume that the portion of the cycle below  $K_{OP}$  does not contribute to fatigue crack growth due to closure effect, and defined an effective stress intensity range:

$$\Delta K_{eff} = K_{max} - K_{OP} \quad (7.2)$$

Substituting  $\Delta K$  with  $\Delta K_{eff}$  in eq.(7.1) an expression for the crack grow rate is obtained by introducing the crack closure effect. The crack opening stress intensity from Elber [1] is given by:

$$K_{op} = \Delta K \left( \frac{1}{(1 - R)} - 0,5 - 0,4R \right) \quad (7.3)$$

It is seen that when the mean stress level effect  $R \rightarrow 0$  the value of opening stress intensity factor  $K_{op} = \Delta K$ .

The closure effect occur for different reasoned, Suresh and Ritchie [1] identified five mechanisms for closure effect [1].

- Plasticity
  - Compressive residual stresses in the wake zone of the crack tip cause the crack faces to close.
- Roughness
  - Coarse grain size of the material can cause deflection between crack surfaces, due to microstructural heterogeneity and lead to mix-mode, cause mismatch between the crack faces.

- Corrosion
  - Corrosion become wedged between crack faces, prevent crack faces to close.
- Viscous fluid
  - Become wedged between crack faces, prevent crack faces to close.
- Martensitic transformation
  - Martensitic transformation in the wake zone of crack tip, cause residual stresses.

## 7.2 Models for fatigue crack propagation

Fatigue crack growth rate for constant amplitude loading is well described, and different crack growth models have been obtained during the time. Here four different models is introduced that cover different regions of the sigmoidal curve and loads effects see Table 1.

Table 1: Crack growth models with corresponding regions and loads effects

Model	Region 1 ( $K_{th}$ )	Region 2	Region 3 ( $K_{Ic}$ )	Mean stress effect ( $R$ )	Crack closure ( $f$ )
Klesnil and Lukas	X				
Paris		X			
Forman		X	X	X	
NASGROW	X	X	X	X	X

### Klesnil and Lukas

Describe the crack growth rate and corresponding range in stress intensity for region 1 [1]:

$$\frac{da}{dN} = C(\Delta K^n - \Delta K_{th}^n) \quad (7.4)$$

It is seen that the crack growth only obtain a value when  $\Delta K > K_{th}$ , and afterwards become linear in region 2 and 3.

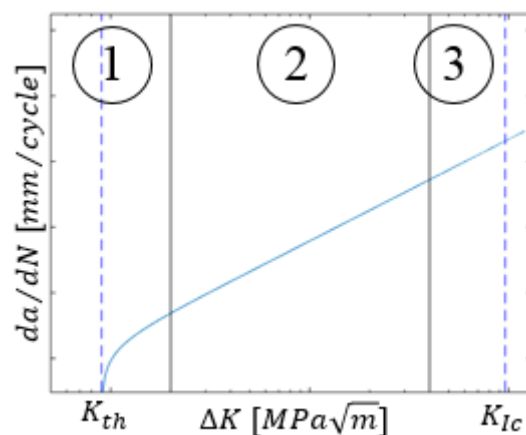


Figure 39: Schematic crack growth behaviour for Klesnil and Lukas, with random values.

**Paris**

This was the first relation that describe the crack growth behaviour, here only region 2 is taking into account [1].

$$\frac{da}{dN} = C\Delta K^n \tag{7.5}$$

It is seen that the crack growth only obtain linear behaviour, and do not include  $K_{th}$  or  $K_{Ic}$ .

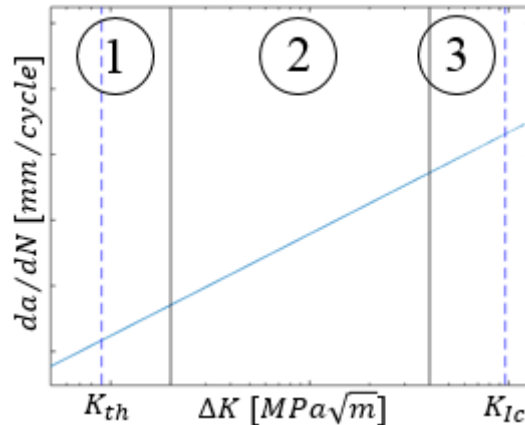


Figure 40: Schematic crack growth behaviour for Paris, with random values.

**Forman**

This model describe the region 2 and 3, where the fracture toughness and R-ratio is taking into account [1].

$$\frac{da}{dN} = \frac{C\Delta K^n}{(1 - R)K_{Ic} - \Delta K} \tag{7.6}$$

It is seen that when  $(1 - R)K_{Ic}$  exceeds the value of  $\Delta K$ , crack growth going to infinity.

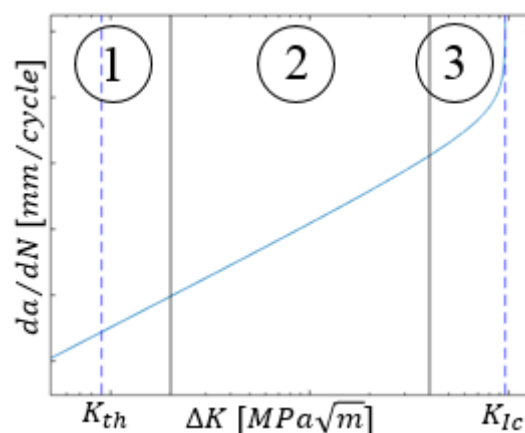


Figure 41: Schematic crack growth behaviour for Forman, with random values.

## NASGRO

Developed at National Aeronautics and Space Administration (NASA) and published by Forman and Mettu [13] and [1], describe the crack growth in all the three regions.

$$\frac{da}{dN} = C \left[ \left( \frac{1-f}{1-R} \right) \Delta K \right]^n \frac{\left( 1 - \frac{K_{th}}{\Delta K} \right)^p}{\left( 1 - \frac{K_{max}}{K_{Ic}} \right)^q} \quad (7.7)$$

Materials constants  $p$  and  $q$  is estimated form experimental testing. The function  $f$  define the ratio between opening stress intensity  $K_{Op}$  from eq.(7.4) and  $K_{max}$ .

$$f = \frac{K_{Op}}{K_{max}} \quad (7.8)$$

It is seen from eq.(7.7) when  $K_{th}$  exceed  $\Delta K$  or  $K_{max}$  exceed  $K_{Ic}$  crack growth value is going to infinity.

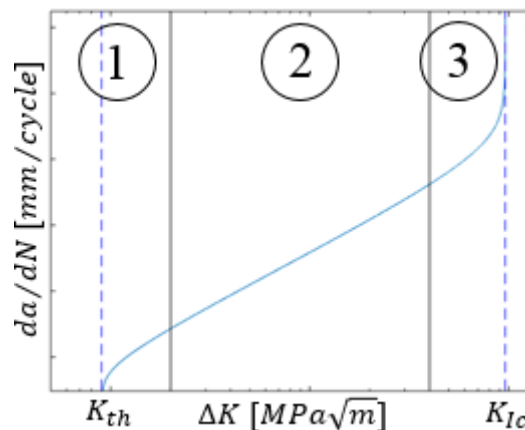


Figure 42: Schematic crack growth behaviour for NASGROW, with random values.

In order to visualize the variation of the four crack growth models from above, a load-case with a value of  $K_{min} = 0$  and an increasing value of  $K_{max}$  in the interval  $0 - 120 \text{ MPa}\sqrt{\text{m}}$ , that indicate a value of range in stress intensity of  $R = 0$ , see Figure 43.

The value of threshold and fracture toughness is given as,  $K_{th} = 0,9 \text{ MPa}\sqrt{\text{m}}$  and  $K_{Ic} = 96 \text{ MPa}\sqrt{\text{m}}$ . Material constants  $C, n, p, q$  is chosen values (only for visualize the variation).

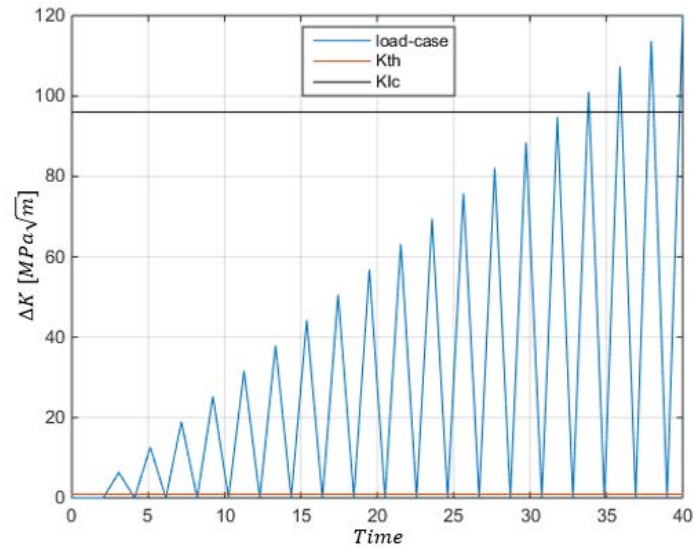


Figure 43: Load-case for visualize variation of crack growth models

The variation of the four crack growth models is schematic showed in Figure 44. It is seen clear that the four models covers different regions of the  $da/dN$  vs.  $\Delta K$  plot.

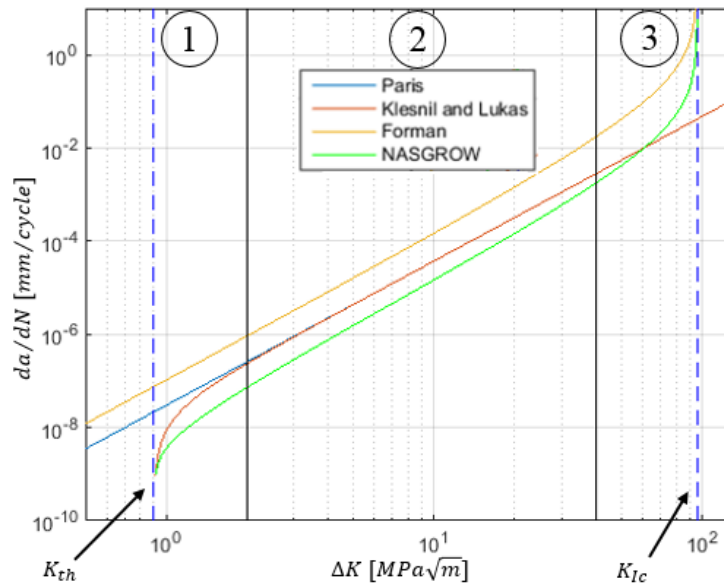


Figure 44: Variation of the four crack growth models

Region 1:

Klesnil and Lukas together with NASGROW cover this region, as seen they first obtain a value at the threshold value. The models of Paris and Forman do not cover this region, and the value of range in stress intensity  $\Delta K$  cannot be taking into account.

Region 2:

Paris, Forman and NASGROW cover this region and behave uniformly, Klesnil and Lukas behave as Paris' model but do not cover this region.

### Region 3

Forman and NASGROW cover this region, they obtain a value that going to infinity at the fracture toughness value, Paris together with Klesnil and Lukas obtain linear behaviour as they do not cover this region.

The model of Klesnil and Lukas only cover the region 1, in that case the model is not applicable for determining the lifetime of a structure, and for further work only the models of Paris, Forman and NASGROW is taking into account.

## 7.3 Modified crack growth models

In the former section the crack growth rate is described from the relation of change in crack length  $da$  and change in number of cycles  $dN$ . In case of determining the lifetime of a structure subjected to a constant amplitude load-case, modification of the crack growth models from above is implemented.

From eq.(7.1) the crack growth is given as  $da/dN = f(\Delta K, R)$ ,  $N$  is an integer and it is considered as a real number because the crack growth is assumed only to advance for at least a real number of cycles [14]. The crack growth rate is modified to only consider the number of cycles as followed:

$$N = f(da, \Delta K, R) \quad (7.9)$$

The crack growth models of Paris, Forman and NASGROW have been modified as followed:

#### Paris:

$$N = \frac{da}{C \cdot \Delta K^n} \quad (7.10)$$

#### Forman:

$$N = \frac{da[(1 - R)K_{Ic} - \Delta K]}{C \cdot \Delta K^n} \quad (7.11)$$

#### NASGROW:

$$N = \frac{da}{C \left[ \Delta K \frac{(f-1)}{(R-1)} \right]^n} \frac{\left( 1 - \frac{K_{max}}{K_{Ic}} \right)^q}{\left( 1 - \frac{K_{th}}{\Delta K} \right)^p} \quad (7.12)$$

In Figure 45 the three modified crack growth models is schematic showed, with the load-case from Figure 43 and value of threshold and fracture toughness is given as,  $K_{th} = 0,9 \text{ MPa}\sqrt{\text{m}}$  and  $K_{Ic} = 96 \text{ MPa}\sqrt{\text{m}}$ . Material constants  $C, n, p, q$  obtain a chosen value (only for visualize the variation).

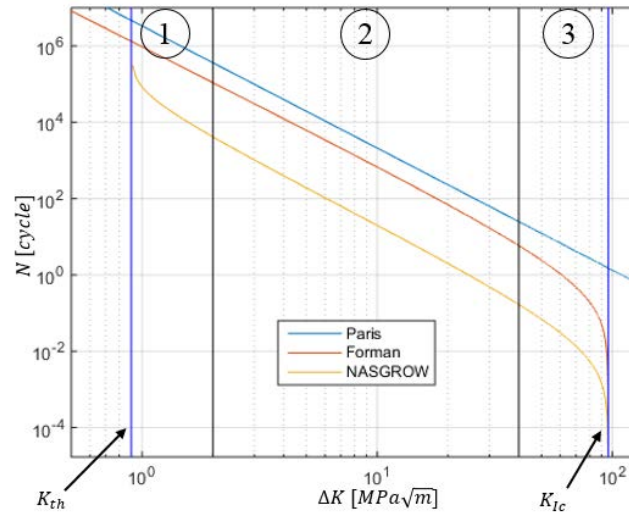


Figure 45: Variation of the three modified crack growth models

It is seen that the curves of the modified crack growth obtain a “mirror” configuration compared with the original crack growth curves in Figure 44. It also make sense that the number of cycles decrease when the range in stress intensity  $\Delta K$  increase and visa versa. From this modified crack growth models, the lifetime can be estimated due to number of cycle, this is implemented and verified in the section of numerical crack propagation.

### Estimation of the constants for growth models

Material constants  $C$  and  $n$  from the crack growth models in last section, is estimated from experimental data where the number of cycles and crack length is measured due to crack propagation of a specimen, with a corresponding analytical solution for the stress intensity factor for the specimen.

In Figure 46 a compact specimen and corresponding plot of the measured number of cycle and crack length is showed, the crack growth rate is estimated by followed:

$$\frac{da}{dN} = \frac{a_{i+1} - a_i}{N_{i+1} - N_i} \quad (7.13)$$

The range in stress intensity  $\Delta K = K_{max} - K_{min}$  is determined from an analytical solution of the stress intensity of the specimen due to crack length, given by:

$$K_{I,max} = \frac{P_{max}}{B\sqrt{W}} f\left(\frac{a_i}{W}\right) \quad (7.14)$$

From the relation of mean stress effect:  $R = K_{min}/K_{max}$  the range in stress intensity is given by:

$$\Delta K = K_{I,max} - (K_{I,max} \cdot R) \quad (7.15)$$

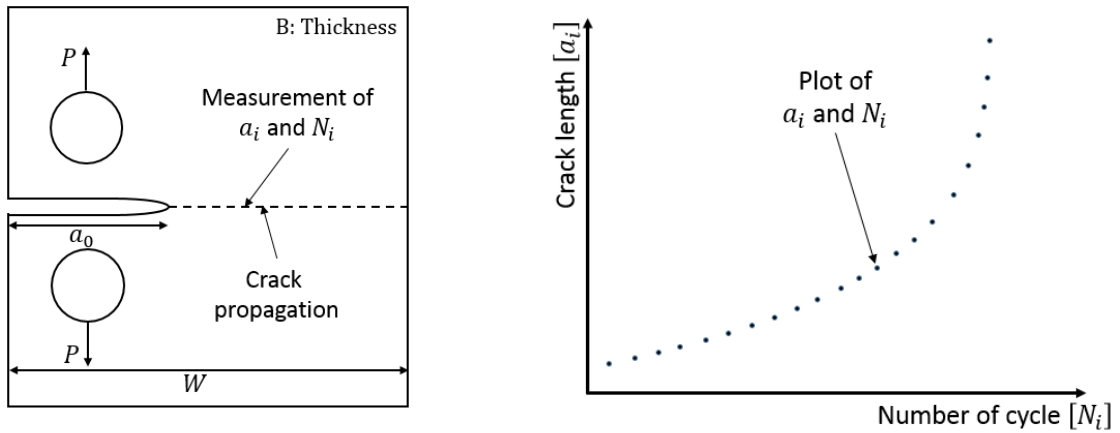


Figure 46: (R) Compact specimen, (L) measurement of numbers of cycles and crack length.

From the relation of crack growth rate and range in stress intensity from eq.(7.13) and (7.15) a logarithmic plot of the data can be performed as the sigmoidal curve in Figure 35.

The intercept and slope  $C$  and  $n$  is fitted from the method of least square of a power function that is given of the form [15]:

$$y = ax^b \quad (7.16)$$

The best fit is found from the total squared error, where  $N$  is the number of observations  $i$ :

$$E^2 = \sum_{i=1}^N \varepsilon_i^2 = \sum_{i=1}^N [y_i - f(x_i)]^2 = \sum_{i=1}^N [y_i - ax_i^b]^2 \quad (7.17)$$

Differentiate the total error with respect to  $a$  and  $b$ :

$$\frac{\partial E^2}{\partial a} = 0 \text{ and } \frac{\partial E^2}{\partial b} = 0 \quad (7.18)$$

Solving for  $a$  and  $b$  gives:

$$b = \frac{\sum \ln x_i \ln y_i - \frac{1}{N} \sum \ln x_i \sum \ln y_i}{\sum \ln x_i^2 - \frac{1}{N} \sum \ln x_i^2} \quad (7.19)$$

$$a = \exp\left(\frac{1}{N} \sum \ln y_i - b \frac{\sum \ln x_i}{N}\right) \quad (7.20)$$

The correlation coefficient, which obtain a value of 1 for perfect fit, and 0 for poor fit is given by:

$$r^2 = \frac{\left[ \sum \ln x_i \ln y_i - \frac{1}{N} \sum \ln x_i \sum \ln y_i \right]^2}{\left[ \sum \ln x_i^2 - \frac{\sum \ln x_i^2}{N} \right] \left[ \sum \ln x_i^2 - \frac{\sum \ln x_i^2}{N} \right]} \quad (7.21)$$

From this the material constants  $C$  and  $n$  is determined, from data of experiments and a corresponding analytical solution of the stress intensity factor. This have been used for lifetime estimation in the section of numerical analyses.

## 8 Numerical condition

In order to implement the determination of stress intensity factors due to crack propagation the numerical finite element program ANSYS is used. In this section a brief overview of numerical tools that is used in ANSYS is described. A study of mesh and contours configurations is carried out in order to define the optimal numerical condition for determining the stress intensity factor.

### 8.1 Domain Integral

The Domain Integral is a numerical solution of the J-integral from section 3.5, it determine different problems and different types of load e.g. Elastic, plastic and thermal loading, in the followed a quasi-static problem with elastic loading is assumed.

A closed contour containing an inner  $\Gamma_0$  and outer  $\Gamma_1$  contours is used where the inner is vanishingly small and the outer is finite see Figure 47. Divergence theorem can be applied and instead of integrating around a path of the crack tip, integration over the area between the paths is used to evaluate the J-Integration. Where the second integral is the components of traction [1].

$$J = \int_{A^*} \left[ \sigma_{ij} \frac{\partial u_j}{\partial x_1} - w \delta_{1i} \right] \frac{\partial q}{\partial x_i} dA - \int_{\Gamma_+ + \Gamma_-} \sigma_{2j} \frac{\partial u_j}{\partial x_1} q d\Gamma \quad (8.1)$$

Component	Description
$w$	Strain energy density
$q$	Weight function in $A^*$ , by $\Gamma_0 \rightarrow q = 1$ and $\Gamma_1 \rightarrow q = 0$
$u_j$	Displacement vector components
$\delta_{1i}$	Kronecker delta
$\Gamma_0, \Gamma_1$	Inner and outer contours
$\Gamma_+, \Gamma_-$	Upper and lower crack face
$\sigma_{ij}$	Stress tensor

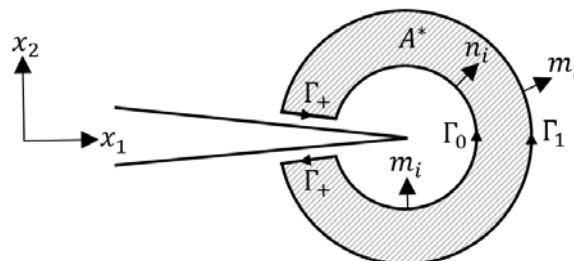


Figure 47: Inner and outer contours, which form a closed contour around crack tip

The Domain integral is equal to the energy release rate  $J = G$  with followed relationship to the stress intensity factors, where  $E'$  is for plane strain or plane stress condition:

$$J(s) = \frac{K_I^2 + K_{II}^2}{E'} + \frac{1 + \nu}{E} K_{III}^2 \quad (8.2)$$

### Interaction integral

A more convenient way to determine the mixed-mode SIF values compared to the domain integral is the interaction integral which gives a more robust and actual results [16]. A description of the main fields of the interaction integral are given and a briefly evaluation of the numerical approach which are the tools ANSYS use to determine the SIF values are given.

The interaction integral in a 3D domain is a contribution of the domain integral in eq.(8.2) called actual field, an auxiliary field and an interacting field between the actual and auxiliary field. Defined as:

$$\bar{J}^S = \bar{J}(s) + \bar{J}^{aux}(s) + \bar{I}(s) \quad (8.3)$$

$\bar{J}(s)$ : Actual field from the domain integral eq.(8.2)

$\bar{J}^{aux}(s)$ : Auxiliary field in the vicinity of a crack, containing the auxiliary stress, strain and displacement  $\sigma_{ij}^{aux}, \varepsilon_{ij}^{aux}, u_j^{aux}$ , that is functions of the auxiliary  $K_I^{aux}, K_{II}^{aux}, K_{III}^{aux}$  with their corresponding polar coordinates  $r, \theta$ .

$\bar{I}(s)$ : Interaction integral, that interacting the auxiliary and actual field are given by, without the components of traction:

$$\bar{I}(s) = \int_V \left( \sigma_{ij} \frac{\partial u_j^{aux}}{\partial x_i} + \sigma_{ij}^{aux} \frac{\partial u_j}{\partial x_i} - \sigma_{jk} \varepsilon_{jk}^{aux} \delta_{1i} \right) \frac{\partial q}{\partial x_i} dV \quad (8.4)$$

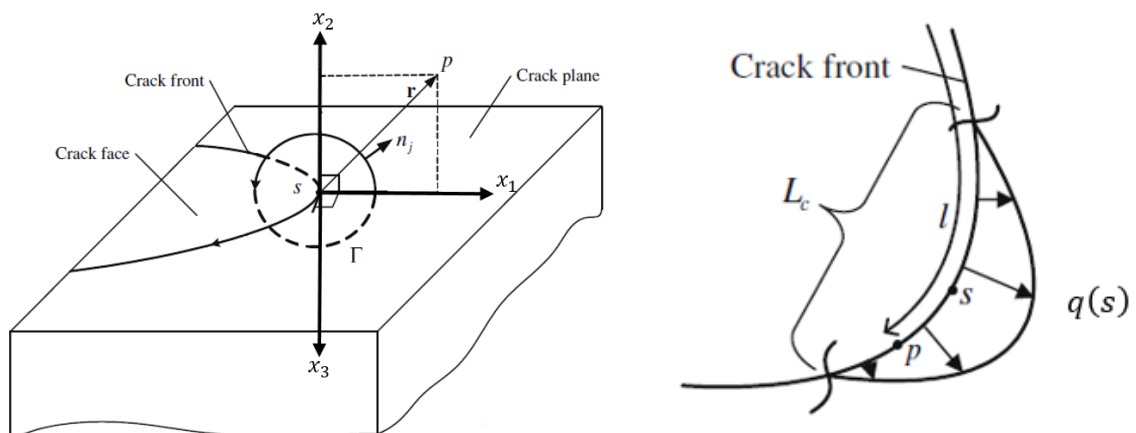


Figure 48: (R) 3D crack front (L) crack front in plane [17].

From this expression a pointwise value of the interaction integral at a given location  $s$ , along a 3D crack front see Figure 48, is given by:

$$I(s) = \frac{\bar{I}(s)}{\int_{L_c} q(s) ds} \quad (8.5)$$

To obtain SIF values appropriated values of the auxiliary SIF values must be taken into account, here an numerical evaluation by use of FE formulations is performed.

### Numerical evaluation of interaction integral

The numerical evaluation of interaction integral is performed in a finite-element framework by an isoparametric formulation with use of the Gauss-quadrature. Evaluation of integral in eq.(8.5) is given by [18]:

$$I(s) = \sum_V^{ele.} \sum_P^{gpts.} \left[ \left( \sigma_{ij} \frac{\partial u_j^{aux}}{\partial x_1} + \sigma_{ij}^{aux} \frac{\partial u_j}{\partial x_1} - \sigma_{jk} \varepsilon_{jk}^{aux} \delta_{1i} \right) \frac{\partial q}{\partial x_i} \det J \right]_p w_p \quad (8.6)$$

Component	Description
$ele.$	Elements in the domain
$gpts.$	Gauss points
$V$	Volume includes all elements
$P$	Points in the domain
$\delta_{1i}$	Kronecker delta
$\sigma_{ij}^{aux}, \varepsilon_{ij}^{aux}, u_j^{aux}$	Stress, strain and displacement of the auxiliary field
$\sigma_{ij}, u_j$	Stress and displacement of the actual field
$J$	Jacobian matrix
$q$	Weight function
$w_p$	Gauss integration weight factor for point $P$

Both the domain integral and interaction integral are numerical methods that are supported by ANSYS. But for mixed-mode problems the interaction integral gives the best and most robust results [17].

## 8.2 Mesh configuration

Determination of stress intensity factors in ANSYS is performed, in order to ensure accuracy of result, a study of the mesh is accomplished. Distinguish between two mesh configuration the near crack-tip mesh and global mesh for the remaining structure. Number of contours for the Domain Integral is also examined in this section.

### Near crack-tip mesh

Stress field in the vicinity of the crack tip is affected by the  $1/\sqrt{r}$  singularity and conventional elements cannot represent this singularity. A singular element have been introduced by taking an triangular isoperimetric element with mid-sides nodes and remove this nodes to a quarter points see Figure 49 which gives an more accurate results [19].

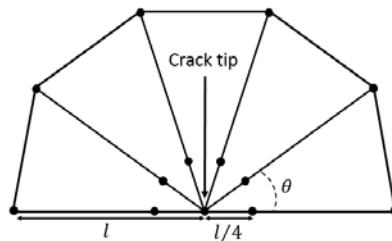


Figure 49: Singular element

To obtain the best results followed is recommended [18]:

- The singular triangle element have to be straight-sided
- Dimension correspond to crack tip:  $l < a/8$

### Global Mesh

ANSYS recommended [18] the PLANE183 elements for global meshing for 2D structure. PLANE183 is a higher order 8-node quadric- or 6-node triangular shaped element with mid-side nodes Figure 50, where nodes K,L,M contract and forms the triangular elements.

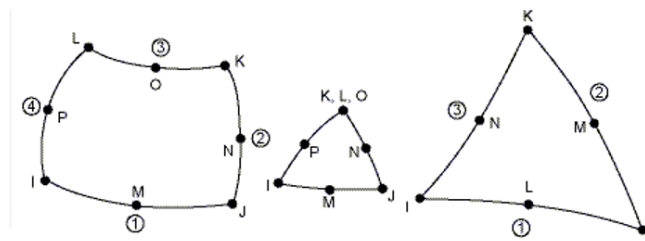


Figure 50: PLANE183 element, for quadric- and triangular shaped elements

Behaviour of PLANE183 elements:

- 2 degree of freedom in x- and y-direction per nodes.
- Plane stress or plane strain behaviour.

## Contours

The Domain Integral in eq.(8.1) take a different numbers of domains around the crack-tip due to accurately in ANSYS this is named contours, in Figure 51(R) a crack-tip with five  $n_1 - n_5$  contours, and mesh is illustrated.

Mesh is implemented by singular elements in the first contours, and quadric PLANE183 elements in rest of the contours, this mesh is recommended by [20].

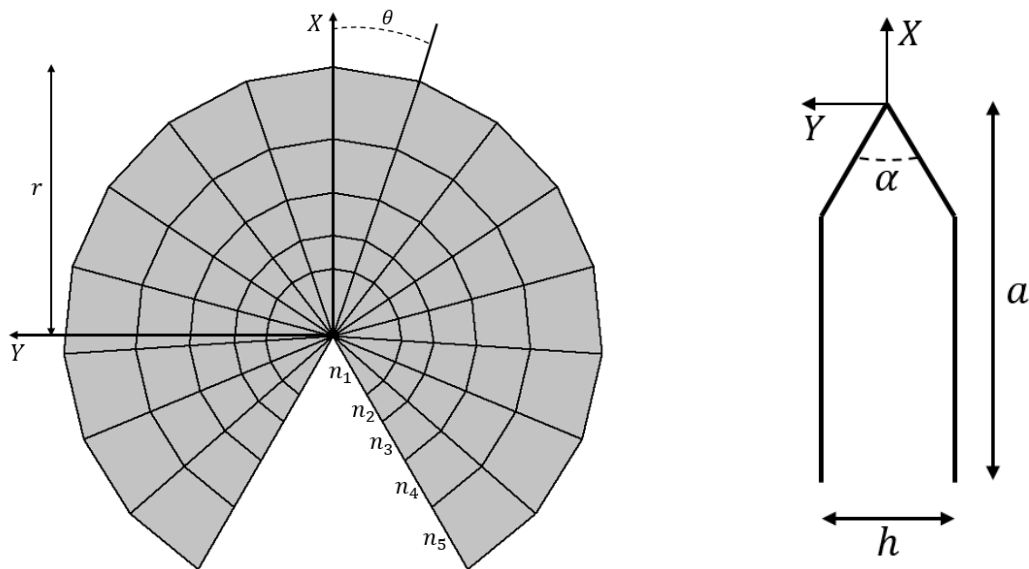


Figure 51: (R) Contours and mesh around crack-tip, (L) dimension of crack-tip

Mesh configuration due to the crack-tip dimension, Figure 51(L), is implemented by followed restrictions:

- Length of singular elements, see Figure 49:  $l = l/4$
- Radius of crack-tip mesh:  $r = h/2$
- Crack-tip angle:  $\alpha = 60^\circ$
- 16 division of crack-tip mesh:  $\theta = 18,75^\circ$

### 8.3 Analysis of number of counters

In order to ensure accurate number of contours for determining the stress intensity factors, the specimen from section 3.4 are determined from analytical solutions [6] eq.(3.21) and eq.(3.22), and numerical solution from ANSYS, with dimension, boundary conditions and material parameters in Figure 52 and Table 2. The solution in ANSYS is conducted for plane strain.

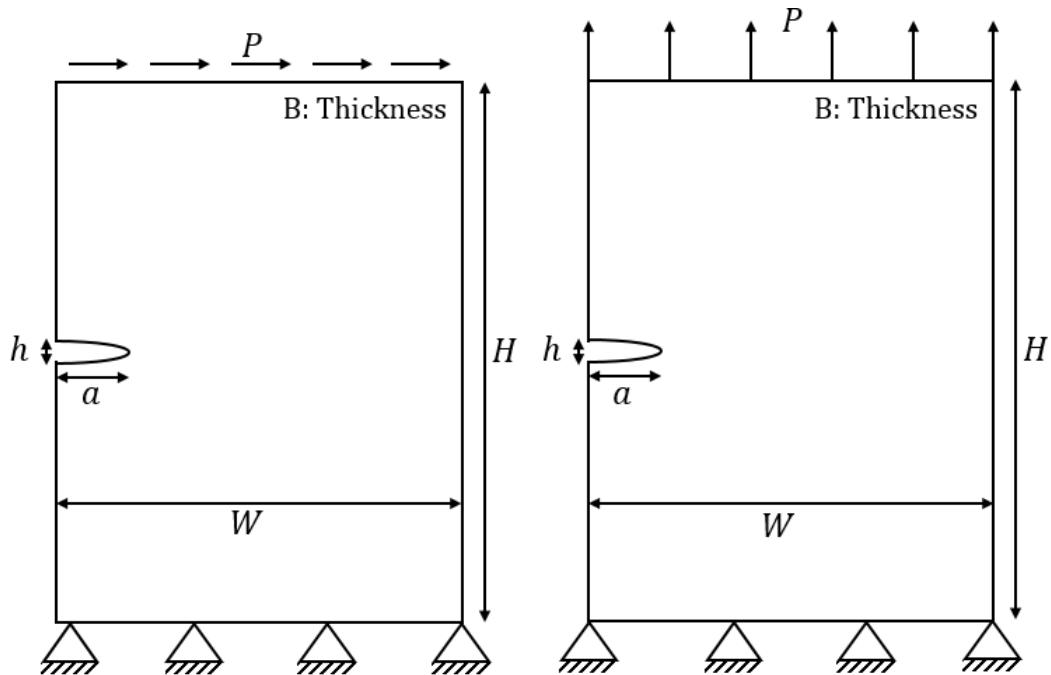


Figure 52: Single edge crack for mode I and II with corresponding boundary condition

Table 2: Dimension and material parameters for solution in ANSYS

Component	Description
$a$	5 mm
$W$	50 mm
$h$	1 mm
$H$	75 mm
$P$	600 N
E-modulus	173.000 MPa
$\nu$	0.3

Analytical solutions:  $K_I = 112,6 \text{ MPa} \sqrt{\text{mm}}$  and  $K_{II} = 46,4 \text{ MPa} \sqrt{\text{mm}}$ .

The mesh configuration from ANSYS for numerical determination for stress intensity factors is showed in Figure 53. The element size is 0,60 mm, and the total number of elements is 12.824.

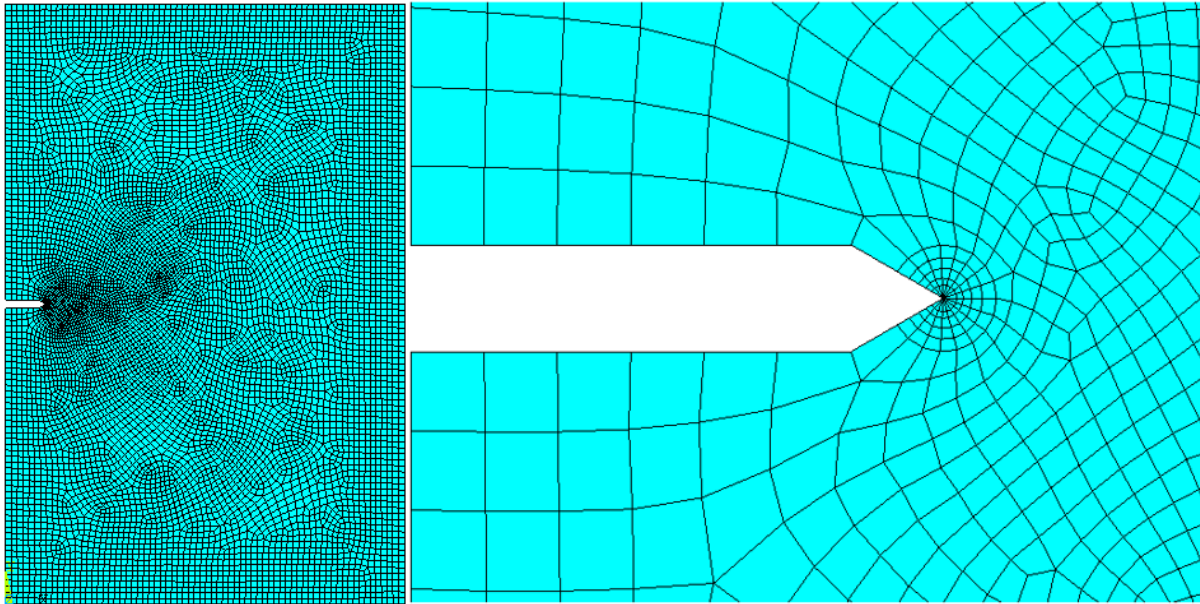


Figure 53: (R) Meshed specimen in ANSYS, (L) Close-up near by crack-tip

Stress intensity factors is extract from 9 contours due to the crack-tip, where the contours 1-5 is showed in Figure 51. The values from the 9 contours form mode I and II, is plotted in Figure 54, with corresponding value of the analytical solution.

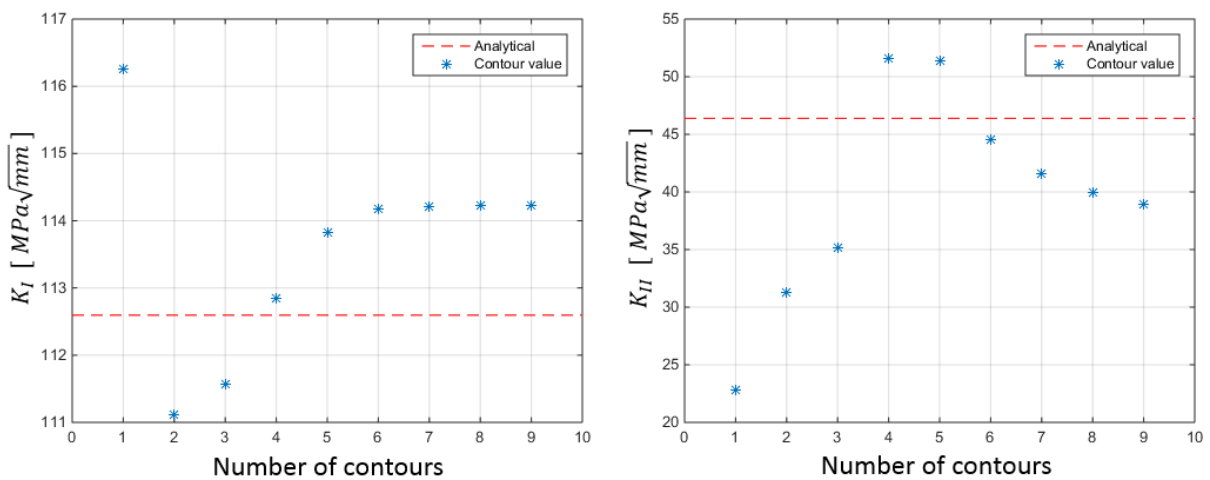


Figure 54: Numerical solution from ANSYS, with 9 different contours for mode I (R), and II (L).

Values for contours 1 and 2 is far from the analytical solution for both mode I and II, contours 6-9 is converging for mode I, in mode II the values become less accurate.

It is decided for further numerical analysis to average the value of contours 3-5 to obtain a effective stress intensity factor for mode I and II:

$$\text{Effective stress intensity factor: } \frac{n_3+n_4+n_5}{3} \Rightarrow \begin{cases} K_{I,eff} \\ K_{II,eff} \end{cases} \quad (8.7)$$

The effective stress intensity factor for mode I and II, and equivalent stress intensity factor from section 6.2 for different criteria get followed relationship:

$$K_{eq} = f(K_{I,eff}, K_{II,eff}) \quad (8.8)$$

Effective stress intensity factor (ESIF) and corresponding analytical solution:

Mode	Analytical $MPa\sqrt{mm}$	ESIF $MPa\sqrt{mm}$	Errors [%]
<i>I</i>	112,60	112,72	0,11
<i>II</i>	46,39	46,63	0,52

From the analytical solution [6], the accuracy of mode I and II is respective 0,5 % and 2 %.

## 8.4 Analysis of mesh size

Study of the influence from different size of the global mesh around the crack-tip is performed in order to analysis the flexibility of the near crack-tip mesh. The specimen from Figure 52, have been analysed for mode I and II with different mesh sizes, varying from 0,10 mm to 1,50 mm. In Figure 55 and Table 3 the results are plotted. The solution in ANSYS is conducted for plane strain.

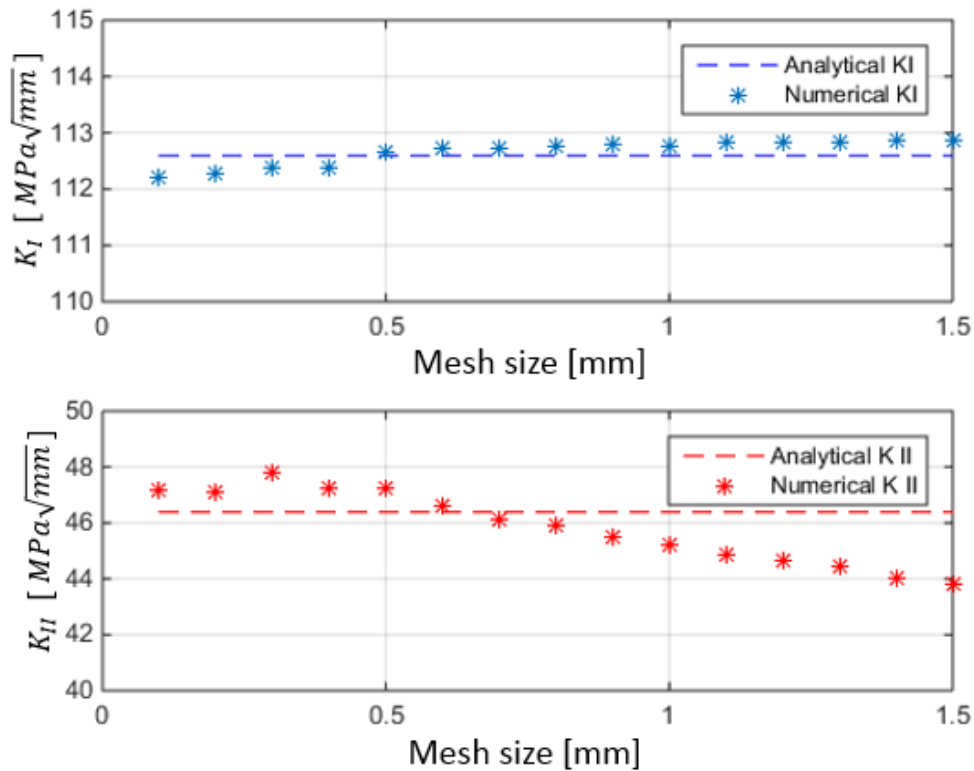


Figure 55: Different mesh size of global mesh for mode I and II with corresponding analytical solution

It is seen that the global mesh size varying from 0,10 to 0,80 (marked with red) maintain the accuracy of stress intensity factor with respect to the analytical solution, where the accuracy of mode I and II is respective 0,5 % and 2 %. In Table 3 the value from Figure 55 is summarize.

Table 3: Global mesh size with corresponding numbers of elements and Error compared with analytical solution

Meshsize [%]	0,10	0,20	0,40	0,60	0,80	1,00	1,20	1,40	1,50
Num. of Elements	238604	67739	24653	12824	7786	4934	4053	2819	2508
Error $K_I$ [%]	0,35	0,28	0,19	0,11	0,14	0,15	0,21	0,23	0,25
Error $K_{II}$ [%]	1,70	1,58	1,81	0,52	1,04	2,56	3,91	5,30	5,90

From the results above is seen that the global mesh size is relative flexible compared to the analytical solution. In Figure 56 the mesh for sizes of 0,10 mm and 0,80 mm is presented.

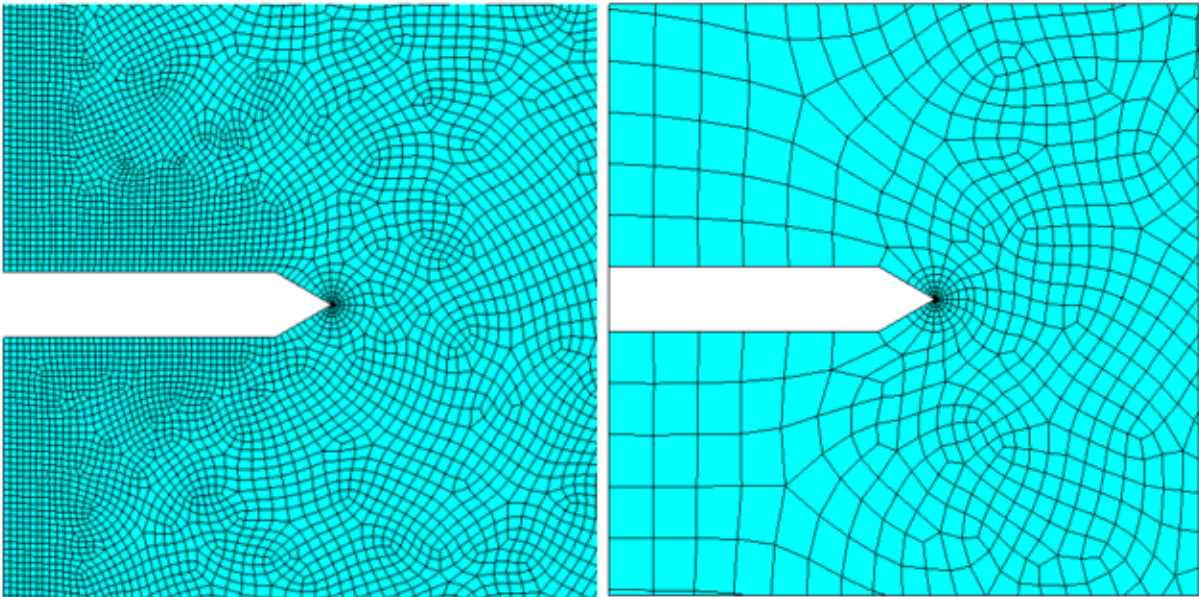


Figure 56: Different mesh sizes of 0,10 mm and 0,80 mm

To verify the flexibility of the mesh size, further three analyses of mesh size is conducted where the geometry of the specimen from Figure 52 is changed in dimension by a factor of 1/2, 1/4 and 1/8, with the same boundary condition and loads, see Table 4.

Table 4: Dimensions of four specimens

Component	Original [mm]	1/2 size [mm]	1/4 size [mm]	1/8 size [mm]
<i>a</i>	5	2,5	1,25	0,63
<i>W</i>	50	25	12,50	6,25
<i>H</i>	75	37,5	18,75	9,375
<i>h</i>	1,00	0,50	0,25	0,125

Results of the analyses for the four specimens is showed in Table 5, where the red marked numbers is the mesh sizes that maintain the accuracy of stress intensity factor with respect to the analytical solution. The mesh size varies for the different specimen due to a limit of allowed elements in ANSYS.

Table 5: Results of mesh size analyses of four specimen

Dimension factor	Mesh size [mm]	Num. of Elements	Error K I [%]	Error K II [%]
Original	0,10	238604	0,35	1,70
	0,20	67739	0,28	1,58
	0,40	24653	0,19	1,81
	0,60	12824	0,11	0,52
	0,80	7786	0,14	1,04
	1,00	4934	0,15	2,56
	1,20	4053	0,21	3,91
	1,40	2819	0,23	5,30
	1,50	2508	0,25	5,90
	1/2 size	0,05	262958	0,36
0,10		70409	0,28	1,52
0,20		24566	0,19	1,76
0,30		12783	0,11	0,40
0,40		7930	0,14	1,14
0,50		4872	0,14	2,61
0,60		4047	0,20	3,95
0,70		2812	0,22	5,39
1/4 size		0,025	353614	0,36
	0,05	88718	0,28	1,47
	0,10	24713	0,19	1,72
	0,15	12929	0,11	0,37
	0,20	7565	0,13	1,18
	0,25	4971	0,15	2,61
	0,30	3739	0,20	3,87
	0,35	2914	0,25	5,43
	1/8 size	0,025	106650	0,28
0,050		30420	0,19	1,68
0,10		7760	0,14	1,13
0,15		3983	0,19	4,043
0,20		2386	0,26	5,91
0,25		1502	0,27	7,04
0,30		1276	0,43	8,68
0,35		812	0,41	9,85

Relationship between the max value of allowed mesh size and the height of the crack  $h$  see Figure 51(L), can be written as:

$$\frac{mesh\ size_{max}}{h} = \frac{0,8}{1} = \frac{0,4}{0,5} = \frac{0,2}{0,25} = \frac{0,1}{0,125} = 0,8 \Rightarrow$$
$$Mesh\ size = 0,8 \cdot h \quad (8.9)$$

As a results of the global mesh size analysis, to ensure the accuracy of stress intensity factor with respect to the analytical solution and the least number of elements due to computations time, the mesh size for further analysis must follow the relationship from (8.9).

## 9 Programming in ANSYS

Numerical analysis of crack propagation is carried out in ANSYS, where a code have been programmed in ANSYS Parametric Design Language (APDL), determining the trajectories of the crack and calculating the number of cycles during a load series of constant amplitude load. In Figure 57 a schematic diagram for the code is showed.

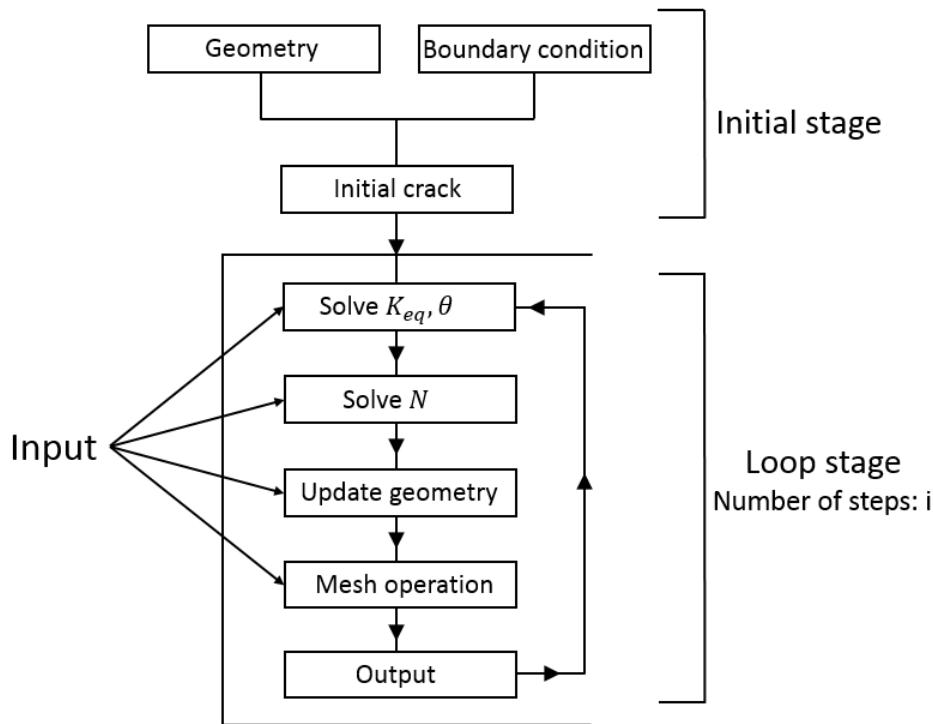


Figure 57: Schematic diagram for APDL code in ANSYS

The general procedure of the APDL code is categorised in two stages, an initial- and loop stage. In the initial stage a 2D geometry with boundary condition is defined, with the position and dimension of an initial crack. In the loop stage the crack is propagating with a given increment and a direction determined from the stress intensity factors, the crack stop propagating when the crack reach an edge in the crack material or the user defined number of steps is obtained. Further description of the APDL code is carried out in next section.

The required input for determination of crack trajectories and number of cycles is given by:

- Solve operation for  $K_{eq}$  and  $\theta$ 
  - Equivalent stress intensity factor from mode I and II with three different choices of criteria's from section 6.2.
    - Tanaka's criteria
    - Richard's criteria
    - Irwin's criteria
  - Direction of crack propagation, see section 6.1. with two different choices of criteria's.
    - Maximum tangential stress of Erdogan and Sih.
    - Richard's criteria

Criteria of equivalent stress intensity factor and direction of crack propagation, is chosen in accordance with the results from the verifications in section 10.

- Solve operation for numbers of cycles  $N$ .
  - Modified crack growth models, see section 7.3, with three different choices of models.
    - Paris
      - 2 inputs, values of materials constants  $C$  and  $n$
    - Forman
      - 4 inputs, values of materials constants  $C$  and  $n$ , range in stress intensity  $R$ , and fracture toughness  $K_{Ic}$ .
    - NASGROW
      - 7 inputs, values of materials constants  $C$ ,  $n$  and  $p, q$ , range in stress intensity  $R$ , threshold value  $K_{th}$ , fracture toughness  $K_{Ic}$ .
- Crack increment  $da$  for the updated geometry.
  - The value of  $da$  is chosen by the user.
- Mesh operation, see section 8.2, for the optimal mesh configuration.
  - Mesh size is recommended to  $0,8 \cdot h$ , but can be chosen by the user.
- Number of steps the analysis have to conduct

The output is written to an output-file for every step  $i$ , with followed outputs.

- Crack-tip coordinates with corresponding values of two crack angle.
  - 4 outputs,  $x_{tip}$ ,  $y_{tip}$  and  $\theta_{tip}$ ,  $\Delta\theta_{tip}$  (see next section).
- Stress intensity factors
  - 4 outputs, effective stress intensity  $K_I$  and  $K_{II}$ ,  $K_{eq}$ , and  $\Delta K$ .
- Accumulated crack length.
  - 1 output,  $a_{acc}$ .
- Number of cycles from the three modified crack growth models.
  - 4 outputs,  $N_{Par}$ ,  $N_{For}$  and  $N_{NAS}$  with closure function  $f$ .

## 9.1 Crack propagation configuration in APDL code

Here the function in the APDL code of the crack and the procedure of determining the crack trajectories is described. First the inputs for an initial crack is defined, from this the current crack configuration is determined see Figure 58.

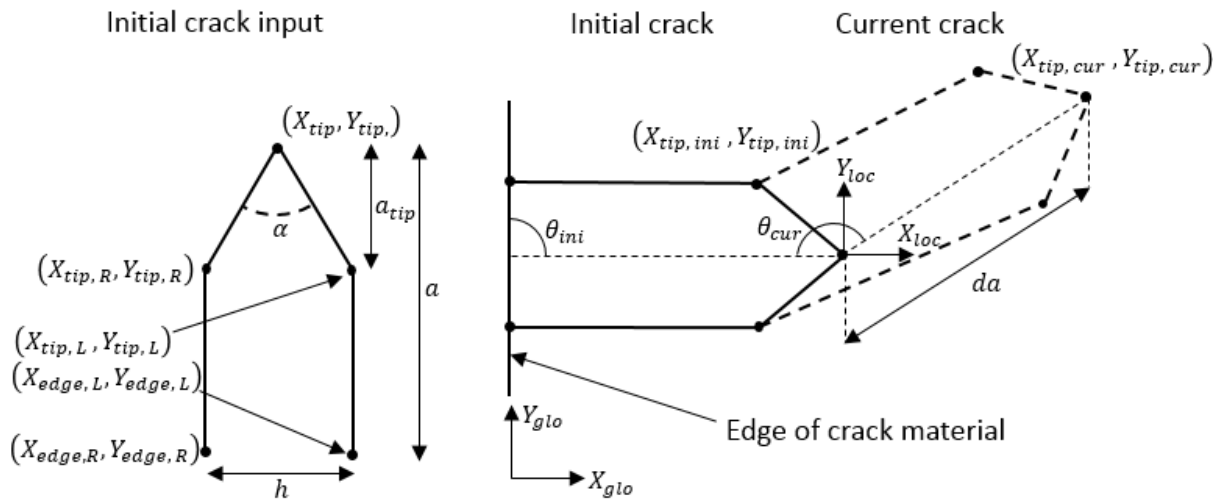


Figure 58: Definition of inputs for determining crack trajectories

Component	Description
$(X_{edge,R}, Y_{edge,R}), (X_{edge,L}, Y_{edge,L})$	X and Y coordinate for right and left edge of the crack
$(X_{tip,R}, Y_{tip,R}), (X_{tip,L}, Y_{tip,L})$	X and Y coordinate for right and left side of the crack-tip
$(X_{tip}, Y_{tip})$	X and Y coordinate for crack-tip
$a$	Crack length
$a_{tip} = h$	Length of crack-tip
$h = a_{tip}$	Width of crack
$\alpha$	Angle of crack-tip, $60^\circ$
$\theta_{ini}$	Initial crack angle, with respect to global coordinate system
$\theta_{cur}$	Current crack angle
$X_{loc}, Y_{loc}$	Local coordinate system by crack-tip
$X_{glo}, Y_{glo}$	Global coordinate system
$(X_{tip,ini}, Y_{tip,ini})$	X and Y coordinate for initial crack-tip
$(X_{tip,cur}, Y_{tip,cur})$	X and Y coordinate for current crack-tip

The initial crack is defined from coordinate of right and left edge and the crack-tip coordinate with a corresponding initial crack angle  $\theta_{ini}$ , from this the value of  $h$  and  $a_{tip}$  is calculated and the coordinate of right and left tip is determined with an angle of 30 deg. from the crack-tip.

The current crack is defined from the right and left tip coordinate, and the crack-tip is calculated from crack increment  $da$  and the current crack angle  $\theta_{cur}$ . This current crack angle is calculated from the initial angle  $\theta_{ini}$  and the angle determined from directions criteria  $\Delta\theta$ , from Erdogan and Sih or Richard from section 6.1, which gives  $\theta_{cur} = \theta_{ini} + \Delta\theta$ .

This procedure from the current crack is repeated in the loop stage, for the user defined number of steps or until the crack reach an edge in the crack material.

**Initial crack angle**

In order to determine the stress intensity factors in ANSYS a local coordinate system at the crack-tip is needed, in that case the initial crack angle  $\theta_{ini}$  is defined from the global coordinate system as showed in Figure 59,

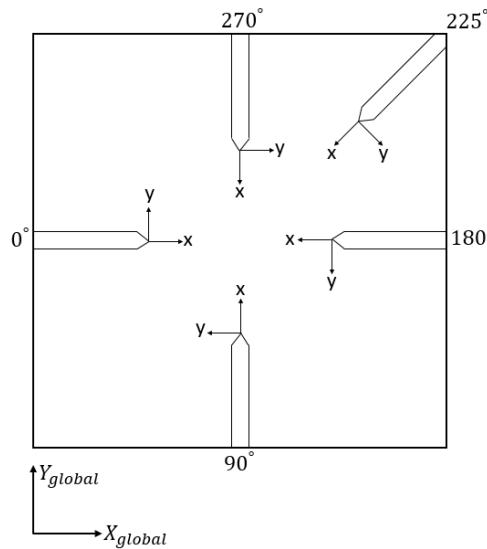


Figure 59: Definition of initial crack angle

**Determining the numbers of cycles in APDL code**

In accordance with the three modified crack growth models from section 7.3, and the equivalent stress intensity factor  $K_{eq}$  for mode I and II, see section 6.2 with effective stress intensity factor see section 8.3, a function of determining the numbers of cycles in the APDL code is defined.

For every step the maximum equivalent stress intensity  $K_{eq,max}$  is calculated and range in stress intensity is defined as:

$$\begin{aligned} \Delta K &= K_{eq,max} - K_{eq,min} \\ K_{eq,min} &= R \cdot K_{eq,max} \end{aligned} \tag{9.1}$$

The modified crack grow models contains different limitations from the threshold value  $K_{th}$  and fracture toughness  $K_{Ic}$ . Here a description of how the APDL code handle these limitations from the three modified crack growth models.

### **Paris**

No limitations is the model of Paris, in that case for every step a number of cycle is calculated.

### **Forman**

The fracture toughness is taking into account for the model of Forman, and the number of cycle is calculated with followed limitations.

$$N_i = \begin{cases} 0 & \text{if } \Delta K > K_{Ic} \\ N_i & \text{if } \Delta K < K_{Ic} \end{cases} \quad (9.2)$$

### **NASGROW**

For the NASGROW model the threshold and fracture toughness is taking into account, and the number of cycle is calculated with followed limitations.

$$N_i = \begin{cases} 0 & \text{if } \Delta K < K_{th} \\ N_i & \text{if } K_{th} < \Delta K < K_{Ic} \\ 0 & \text{if } \Delta K > K_{Ic} \end{cases} \quad (9.3)$$

It is important to mention that the function of crack propagation and determining the number of cycle is independent. That the crack propagation is carried out in accordance to the chosen increment  $da$ , and the determined angle of direction  $\Delta\theta$  from each step. The crack increment  $da$  is also used for determining number of cycle, but no further correlation between the two functions is used.

## 9.2 Configuration of ANSYS interface

In ANSYS the interface menu from where the program is controlled during a picking operations is called the GUI (Graphical User Interface), see Figure 60(R). From this menu all the functions available in ANSYS can be selected in order to implement analyses. All the functions is defined from a function block, see

Figure 60(L), where a function block for creating a rectangle is showed, these function blocks is programmed to call APDL codes to conduct the function.

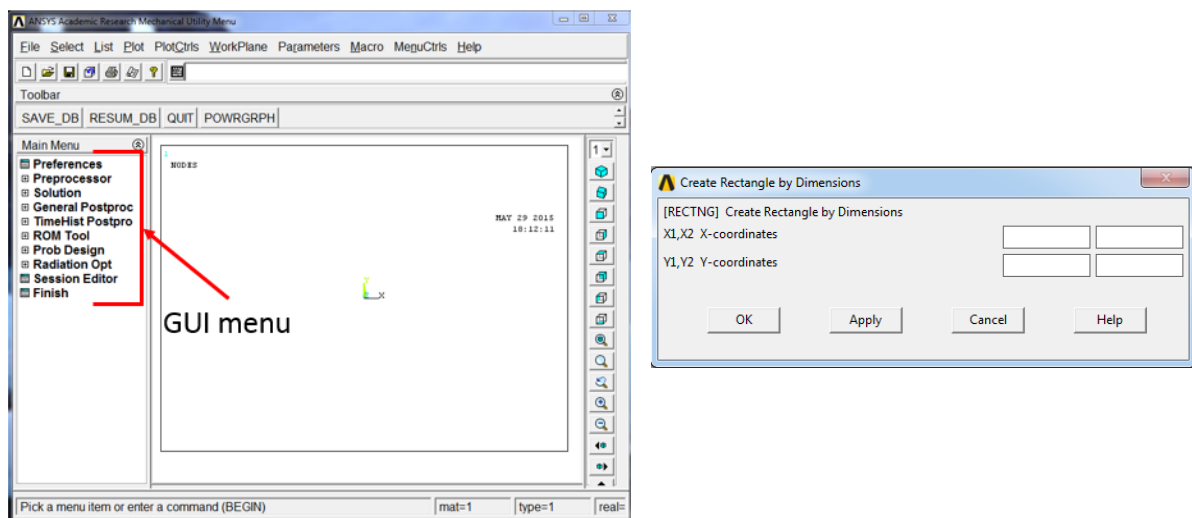


Figure 60: (R) GUI menu in ANSYS Mechanical, (L) function block for creating a rectangle

The function blocks is made by UIDL codes (User interface design language) that define the options for the function block. In order to arrange the functions blocks in the GUI menu a menu block can be used to ensure the correct placement of the function block. This menu- and function blocks is programmed into a control file from where the UIDL codes is conducted [21].

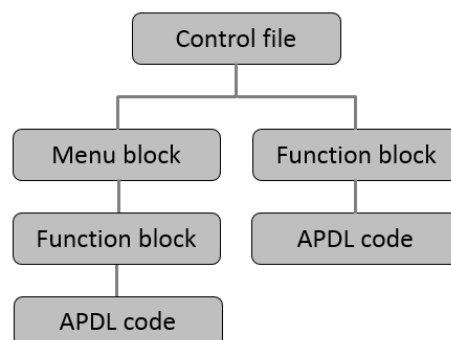


Figure 61: Example of the construction for menu- and function blocks

In Figure 61 an example of construct a control file with two function blocks, where the first is arranged by a menu file, and the second conducted directly from the control file.

## Implementing APDL code in ANSYS GUI

In ANSYS three control files arrange the menu- and functions files for the whole GUI menu. In order to implementing the APDL code from section 9.1. in the GUI, a user defined control file have been created to modify the GUI menu. In Figure 62 a diagram showed the configuration of this file, with the use of control file, menu- and function blocks, and the APDL codes.

The block bracket [ ] is used for file names and APDL codes, the parenthesis ( ) is used for names of the menu- and function blocks.

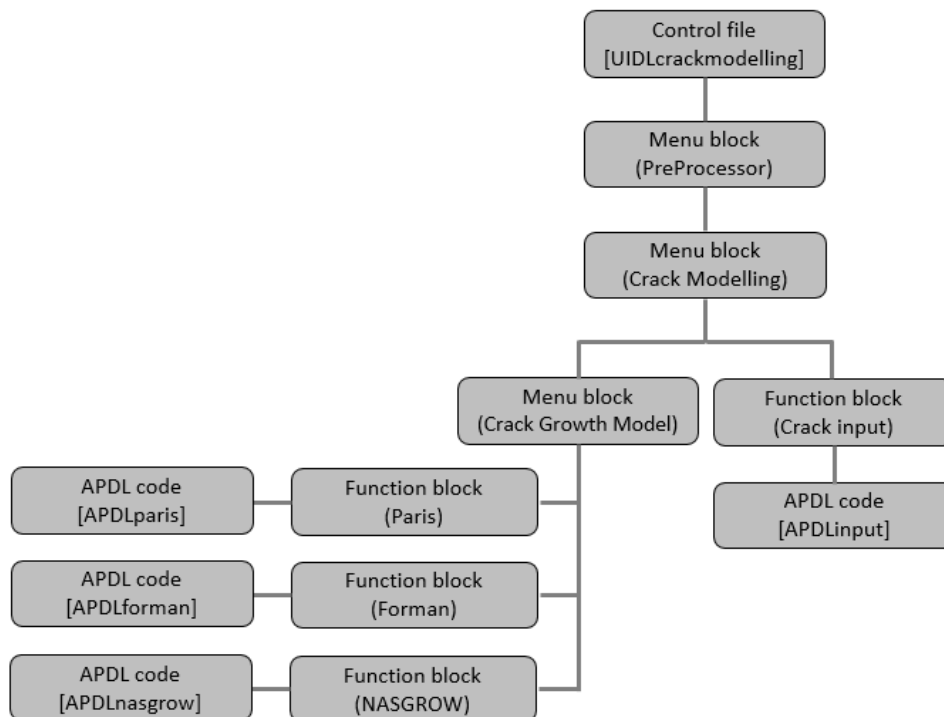


Figure 62: Schematic diagram for implementing the APDL code in ANSYS GUI

In order to implement the APDL codes in the GUI menu 5 files is used, one control file and 4 APDL codes. Implementing of this files in ANSYS is showed in appendix 1.

In Figure 63 the modified GUI menu is showed with corresponding menu- and function blocks.

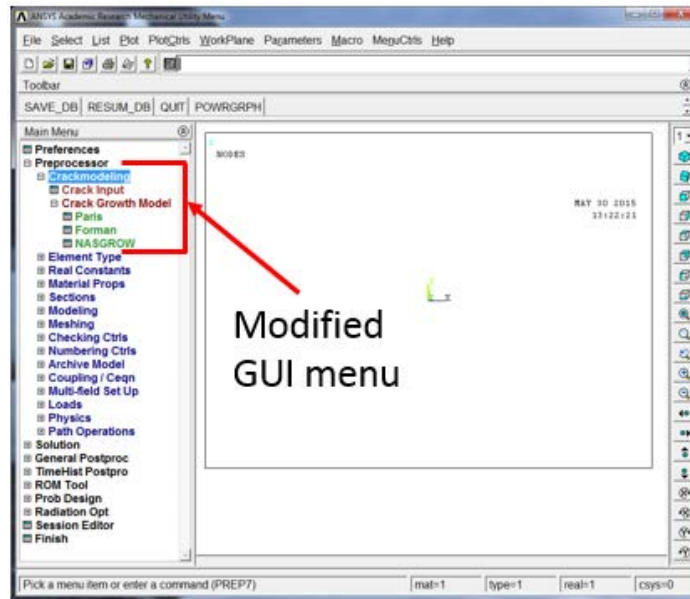


Figure 63: Modified GUI menu with implemented APDL codes for crack propagation

In Figure 64 the function block for the crack growth model of NASGROW is showed, where the inputs parameters and outputs parameters is described in section 9.1.

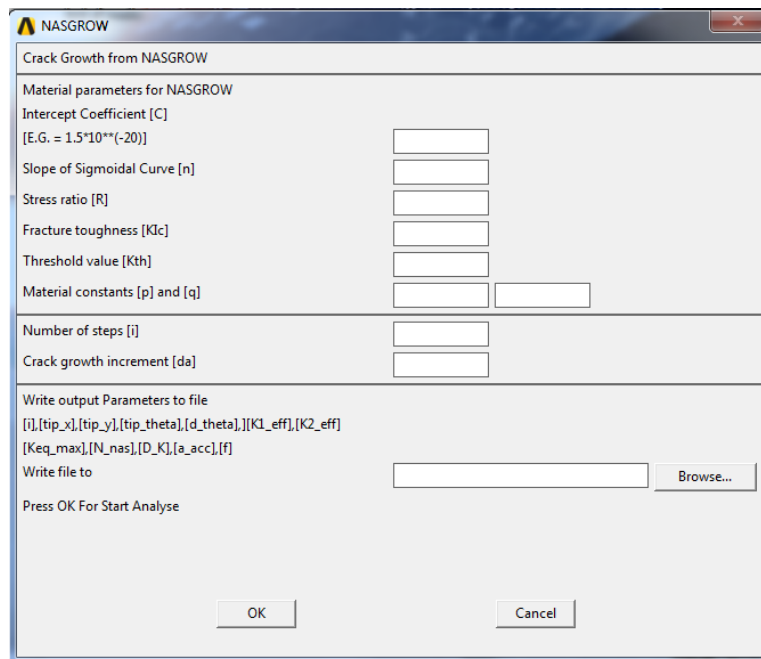


Figure 64: Function block for inputs for the crack growth from NASGROW

## 10 Verification of APDL code

In order to verify the APDL code described above with respect to the crack trajectories and the estimation of lifetime two experimental analyses is benchmarked with the result from the APDL code. The mix-mode criteria is compared and the plastic zone size is evaluated in order to ensure that LEFM behaviour is obtained.

### 10.1 Trajectories

The crack direction criterion, maximum tangential stress (MTS) and criterion of Richard from eq.(6.5) and eq.(6.6) is verify by external experimental data of a specimen with dimension and boundary condition [22], Figure 65(R).

Modified boundary condition is carried out in order to run a numerical analysis Figure 65(L). All dimension are in US customary units due to comparison of results.

The crack increment  $da$  for this analysis is 0,1 [in] and mesh configuration due to mesh size is implemented from section 8.2.

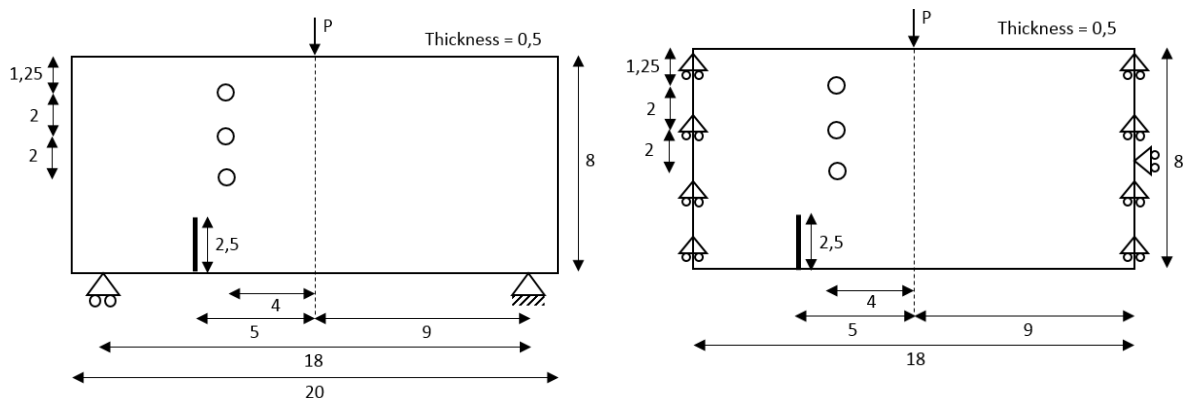


Figure 65: (R) Dimension and boundary condition of plate specimen, (L) Dimension and boundary condition of plate for numerical analysis in APDL, all dimension in inches

Component	Value
$E$	474.000 psi
$\nu$	0,3
$P$	1326 lb
$\sigma_{yield}$	10.000 psi

All dimension in US customary

Results of the numerical crack trajectories is showed in Figure 66 for a specimen with and without holes, note it is only for the specimen with holes where experimental results exists. The solution in ANSYS is conducted for plane strain.

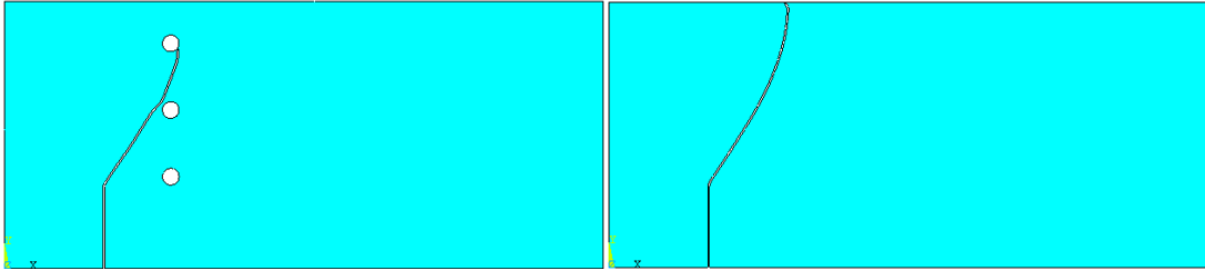


Figure 66: Numerical results in ANSYS of the crack trajectories

Comparison of numerical and experimental results is showed in Figure 67. The two criterion for numerical analysis MTS and Richard (RICH) practically follows the crack trajectories from experimental results.

The two criterion of MTSs and Richard look similar and for further studies the MTS criterion is taking into account.

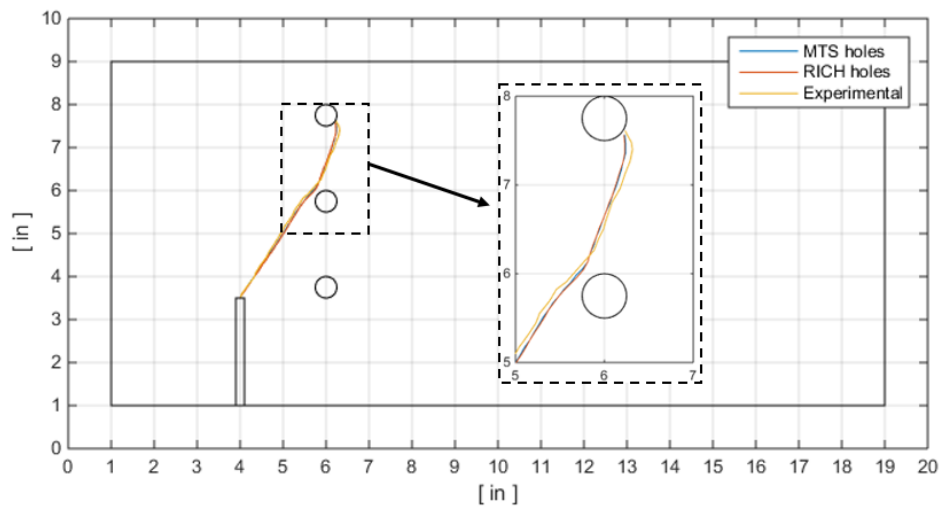


Figure 67: Experimental and two numerical crack trajectories for specimen with holes

Difference between the numerical crack trajectories for a specimen with and without holes is showed in Figure 68, and with the experimental results for comparison.

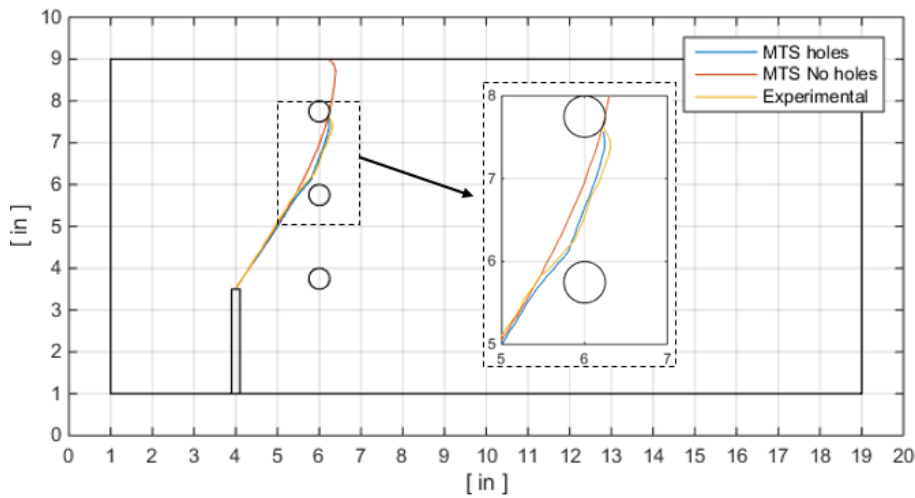


Figure 68: Crack trajectories for a specimen with and without holes

The hole in the middle affect the original trajectories by the Poisson effect, where stress concentrations around the hole produce shear stresses, and due to the MTS criterion from section 6.1, the crack direction is affected by shear stresses.

### Test of mix-mode criteria

In order to see the different of mix-mode criteria from section 6.2, the three criterion have been compared through analysis of the plate with three holes from above.

In Figure 69 the equivalent stress intensity factor  $K_{eq}$  from criterion of Tanaka, Richard and Irwin is showed with the corresponding crack length of the trajectories.

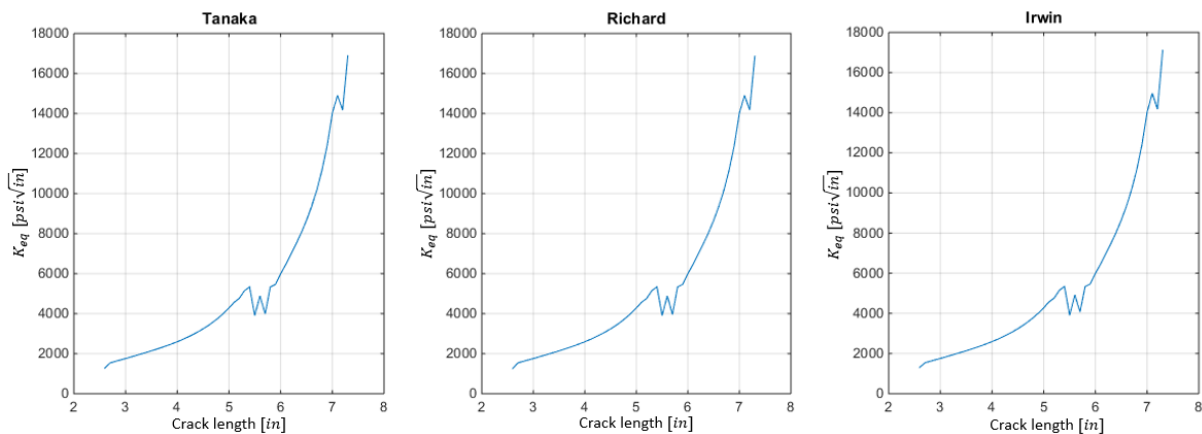


Figure 69: Equivalent stress intensity factor from three different criterion.

It is seen that the three criterion obtain almost the same value of  $K_{eq}$ , only with a difference in the decimal place. Note the unit is US customary due the input unite.

## Plastic zone radius

From section 3.6 the plastic zone around a crack-tip is described with corresponding criteria for approximation of the plastic zone to still obtain LEFM behavior. The criteria of the radius of the plastic zone from Irwin from eq.(3.30), with a varying of  $K_{eq}$  through the crack trajectories and a corresponding  $\sigma_{yield}$ . In Figure 70 the criteria of Irwin is showed, with a corresponding max value of plastic zone radius  $r_y \leq a/8$  for monotonic loading.

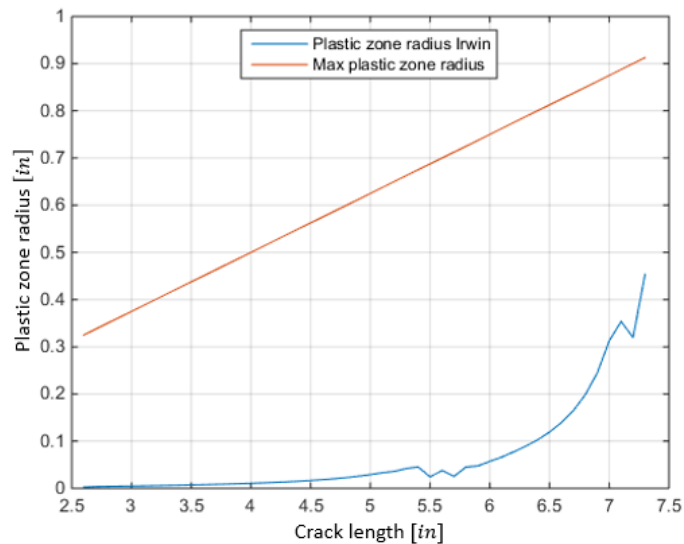


Figure 70: Radius of plastic zone from criteria of Irwin, and corresponding max value from monotonic loading

It is seen that the plastic zone radius from Irwin do not exceeds the max radius from monotonic loading that is a conservative approximation due to the fact the max radius for cyclic loading is  $r_y \leq 4$ .

## 10.2 Discussion of results

The crack trajectories from experimental and numerical results are almost identical and the two criteria of Richard, and Erdogan and Sih shows identical behaviour, and from this the maximum tangential stress criteria of Erdogan and Sih is used for further analysis. The analysis of mix-mode criteria showed almost no difference, so for further numerical analysis the criteria of Tanaka is chosen to determine the equivalent stress intensity factor.

### 10.3 Verification of lifetime estimation

In section 7.3, the prediction of lifetime for a structure subjected for cycle loading is described. Due to modified crack growth models the number of cycle can be obtained from material parameters, crack length and the stress intensity factor.

In this section a test specimen is evaluated from extrnal experimental data [23], where the material constants  $C$  and  $n$  is estimated, a comparison of the predicted number of cycle from the experiment and numerical analyses from ANSYS is performed, for plane strain.

In Figure 71(R) a modified compact test specimen subjected to a constant load series is showed, with a corresponding plot of the measured number of cycles and crack length, it is seen that the specimen is subjected for fracture for approximated 58.000 cycles and a crack length of 25 mm. Note that the initial crack length  $a_0$  is 10,5 mm.

The load is subjected by a test machine in constant load, the tensile load is 4.000 N with a stress ratio of  $R = 0,05$  that is neglect in the analysis.

Material data:

Component	Value
$E$	71,7GPa
$K_{th}$	0,9 MPa $\sqrt{m}$
$K_{Ic}$	96 MPa $\sqrt{m}$
$\sigma_{yield}$	470 MPa

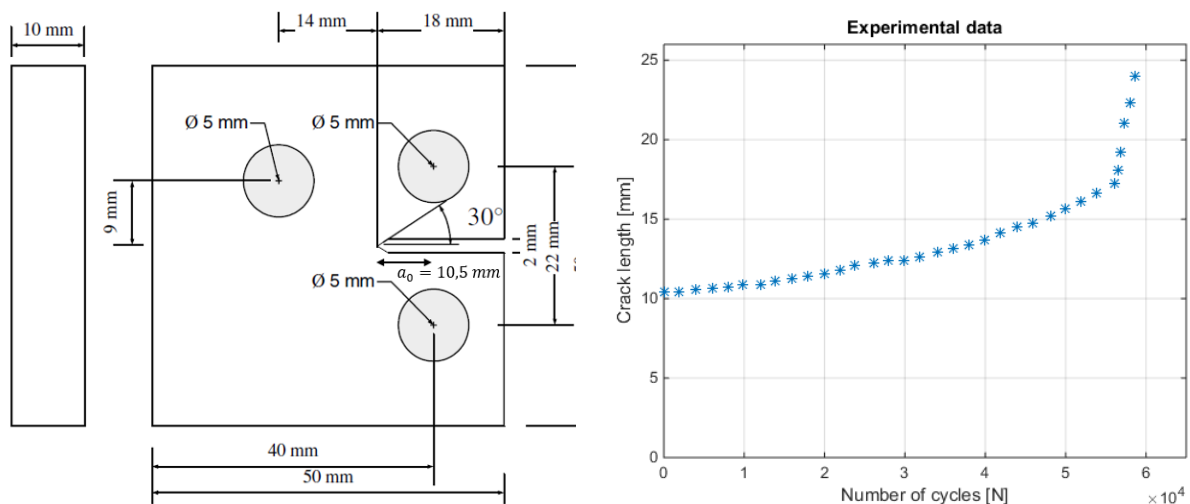


Figure 71: (R) Test specimen for lifetime estimation [23], (L) plot of measured number of cycles and crack length.

A numerical analyses is conducted in ANSYS in order to benchmark the results from the experimental and numerical analyses. The boundary conditions for the specimen is showed in Figure 72, the tensile loads  $P_1 - P_3$  obtain a value of 4000/3 respective, and the crack increment  $da = 0,2 \text{ mm}$ .

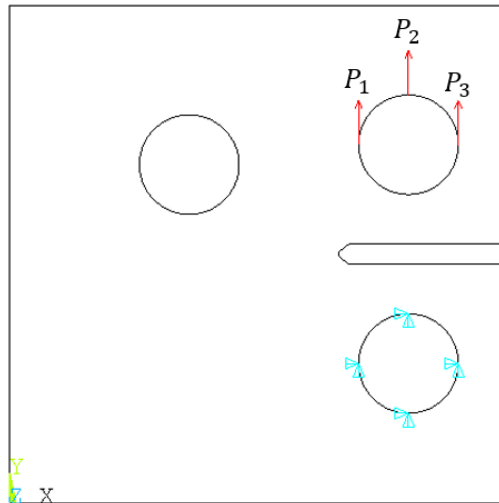


Figure 72: Boundary condition of modified compact specimen

The crack trajectories of the experimental and numerical analyses from ANSYS is showed in Figure 73. It is seen that the two crack paths almost look similar.

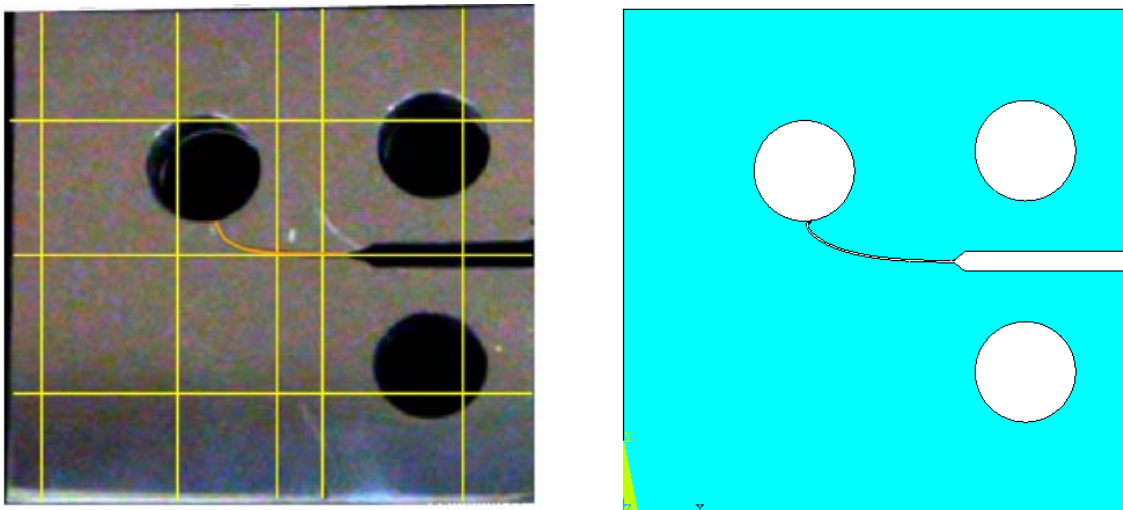


Figure 73: Crack trajectories, (R) for experimental specimen [23], (L) for numerical specimen from ANSYS

In order to estimate the number of cycles from the crack growth models of Paris law eq.(7.5) in ANSYS, the material constants  $C$  and  $n$  have to be estimated.

This is conducted in accordance with the description in section 7.2, first the range in stress intensity  $\Delta K$  is found from an analytical solution with corresponding crack length  $a_i$  and the

crack growth rate  $da/dN$  is determined from eq.(7.13). Then finally the intercept and slope of the  $da/dN$  vs.  $\Delta K$  curve is estimated from the method of least square from eq.(7.16) to (7.21).

The analytical solution for mode I of the modified compact specimen (normally the specimen only have two holes, besides the crack), is given by [6]:

$$K_I = \frac{P}{B\sqrt{W}} \frac{(2 + \alpha)(0,886 + 4,64 \cdot \alpha - 13,32 \cdot \alpha^2 + 14,72 \cdot \alpha^3 - 5,60 \cdot \alpha^4)}{(1 - \alpha)^{3/2}} \quad (10.1)$$

Where  $\alpha = \frac{a_i}{W}$ , the width:  $W = 40 \text{ mm}$  and thickness:  $B = 10 \text{ mm}$ , see Figure 71(R).

The stress ratio  $R = 0,05$  was neglect, therefore the value of  $\Delta K$  is equal to  $K_I$  in the further analyses.

The results of the analytical solution and the numerical results from ANSYS for mode I and II is showed in Figure 74, with a crack length varying from 10,5 mm to 25 mm in order to cover the same crack path length as the experimental.

It is seen that the mode II from ANSYS is zero for most of the analysis and first affect the mode I at the last part of the analysis. The analytical solution and mode I from ANSYS follow each other through the crack trajectories with a different for approximated 10%. Due to neglect of stress ratio  $R$ , the  $\Delta K$  is equal to  $K_{eq}$  from eq.(9.1) for results in ANSYS.

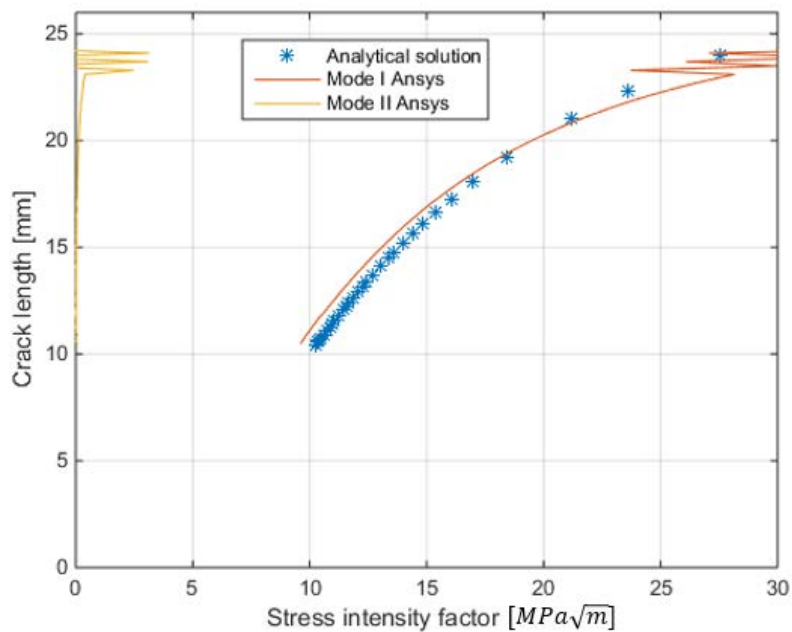


Figure 74: Analytical solution for modified compact specimen

In order to estimate a power function by the method of least square from section 7.2, 7 values is selected from the experimental data in Figure 71(L). The selected value is chosen in order to get the best fit for a power function due to lack of accurate data. In Figure 75(R) the 7 selected values is indicated with others experimental data.

The crack growth rate:  $\frac{da}{dN} = \frac{a_{i+1}-a_i}{N_{i+1}-N_i}$ , is determined for the experimental data and the 7 fit data values, that become 6 values for the crack growth rate, this is showed in Figure 75. From the method of least square the constants for intercept and slope of the power function is determined:

$$y = 3 \cdot 10^{-9} \cdot x^{4,1295} \tag{10.2}$$

Or

$$\frac{da}{dN} = 3 \cdot 10^{-9} \cdot \Delta K^{4,1295} \tag{10.3}$$

This power function or curve fit is showed in Figure 75(L), where it fits the corresponding data values. The correlation coefficient eq.(7.21) for this curve fit:  $R^2 = 0,9857$ , that is a reasonable value.

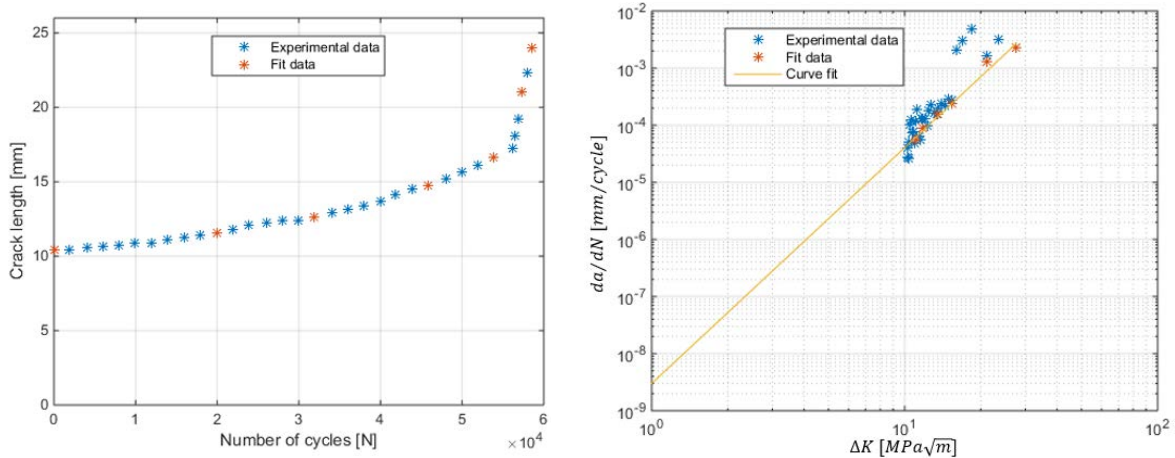


Figure 75: (R) Experimental data with 7 selected data set for curve fit, (L) log-log plot of data with corresponding curve fit.

The values from eq.(10.2) and (10.3) are the materials constants  $C = 3 \cdot 10^{-9}$  and  $n = 4,1295$  from Paris law.

In order to validate the determination of cycles through crack propagation in ANSYS the material constants for Paris estimated above have been used.

In Figure 76 a comparison of the experimental solution and the results from ANSYS is showed. As seen in Figure 74 the different between the stress intensity factor for mode I for analytical solution and the results from ANSYS was approximated 10%. If this lag of accuracy is taking into account the results is near by the results from the experiment seen by the yellow graph in the figure, where the range in stress intensity  $\Delta K$  have been increased by 10%.

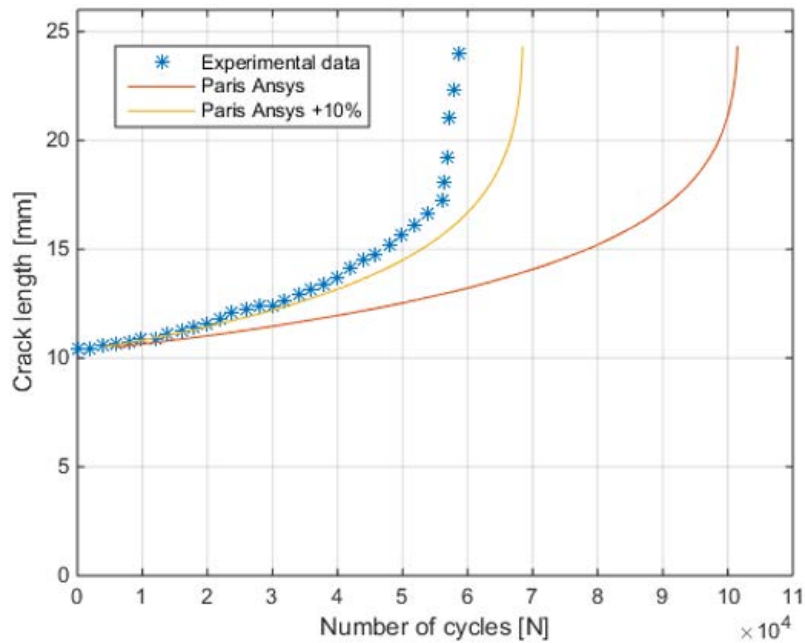


Figure 76: Comparison of experimental data and numerical data from ANSYS

## Plastic zone radius

The criteria of the radius of the plastic zone of Irwin from eq.(3.30), with a varying of  $K_{eq}$  through the crack trajectories and a corresponding  $\sigma_{yield}$ . In Figure 77 the criteria of Irwin is showed, with a corresponding max value of plastic zone radius  $r_y \leq a/8$  for monotonic loading.

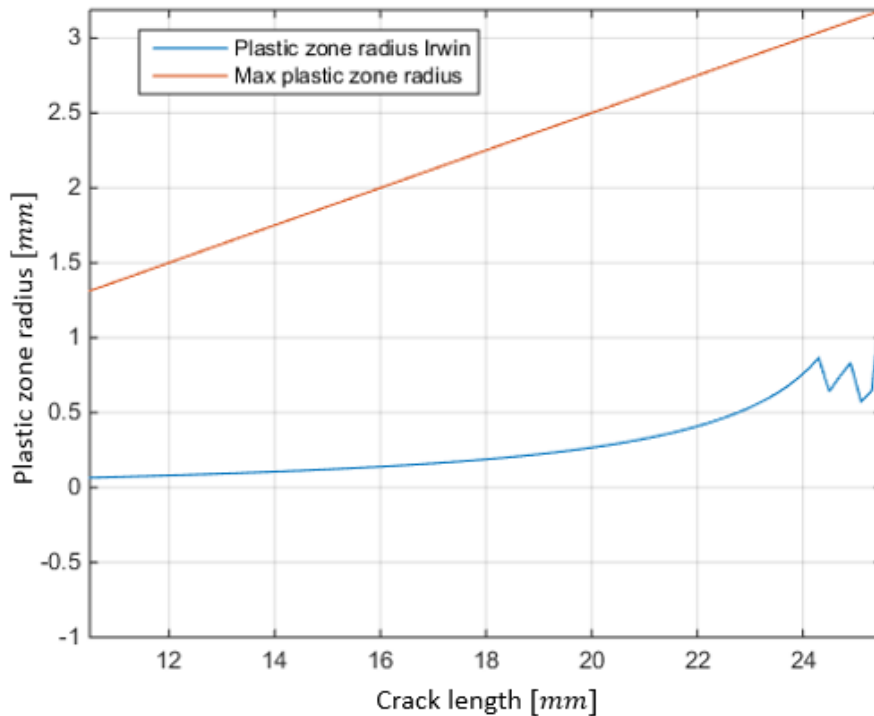


Figure 77: Radius of plastic zone from criteria of Irwin, and corresponding max value from monotonic loading

It is seen that the plastic zone radius from Irwin do not exceeds the max radius from monotonic loading.

## 10.4 Discussion of results

Results of the lifetime estimation due to numbers of cycles is more inaccurate due to estimation of the material constants  $C$  and  $n$ . The uncertainty of data selection from the experiment plays an role, where 6 values of the original data was selected for curve fit. A other significant issue is the analytical solution of the stress intensity factor compared with the results from ANSYS that show a different of approximately 10%. Which leads to an high error in number of cycles due to the fact that the  $\Delta K$  is powered by a factor of  $n = 4,1295$ .

# 11 Conclusion

The main focus of this Master Thesis was to create a numerical tool conducted in ANSYS to simulate the trajectories of a crack and estimate the lifetime due to cyclic loading of a structure.

## Trajectories

A study of the mesh configuration is conducted and the most optimal mesh for near crack-tip mesh and global mesh is obtained. The near crack-tip mesh is made from singular elements and with 4 layers of quadric elements. The global mesh consist of quadric elements with a corresponding size to the high of the crack, where followed relation is recommended, Mesh-size =  $0,8 \cdot h$ , see Figure 51.

The contours of the interaction integral is analysed, in order to obtain the most accurate results followed numbers of contours is chosen: 3, 4 and 5.

In section 10.1 the APDL code is compared to an experimental analysis, and it is seen that the trajectories is almost identical, the criteria of maximum tangential stress from Erdogan and Sih is used for further analyses. The APDL code is a powerful tool in order to obtain the crack trajectories from a numerical perspective.

The Mix-mode criteria showed almost identical behaviour, and from this the criteria from Tanaka is used for further analyses.

## Lifetime estimation

Different cack growth models is implemented in the APDL code in order to determine the number of cycles before fracture occur. The model of Paris is compared to an experimental analyses with mediocre results for different reason.

The main reason is the results from the stress intensity factors due to the determination of material constants, where a different of approximated 10% of the analytical solution and numerical solution is obtained. The difference between the experimental and numerical results become around 42.000 cycles with an error of 42%, if the different of 10% from the stress intensity factors is taking into account, an error of 10.000 cycles or 17% is obtained.

## 12 Bibliography

- [1] T. L. Anderson, *Fracture Mechanics, Fundamentals and Applications*, 2005.
- [2] R. I. Stephens, A. Fatemi, R. R. Stephens og H. O. Fuchs, *Metal Fatigue in Engineering*, 2001.
- [3] C. T. Sun and Z. H. Jin, *Fracture Mechanics*, 2012.
- [4] K. Ramesh, »Indian Institutes of Technology & Indian Institute of Science,« September 2014. [Online]. Available:  
<http://textofvideo.nptel.iitm.ac.in/video.php?courseId=112106065>.
- [5] »DTD Handbook,« June 2015. [Online]. Available:  
[http://www.afgrow.net/applications/DTDHandbook/sections/page2\\_2\\_0.aspx](http://www.afgrow.net/applications/DTDHandbook/sections/page2_2_0.aspx).
- [6] Y. Murakami, *Stress Intensity Factors Handbook*, 1988.
- [7] D. A. Russell, »Acoustics and Vibration Animations,« June 2015. [Online]. Available:  
<http://www.acs.psu.edu/drussell/Demos/waves/wavemotion.html>.
- [8] E. Sharon, S. P. Gross og J. Frineberg, »Local Crack Branching as a Mechanism for Instability in Dynamic Fracture,« *Physical Review Letters*, 1995.
- [9] F. Erdogan og G. C. Sih, »On the Crack Extension in Plates Under Plane Loading and Transverses,« *American Society of Mechanical Engineers*, 1963.
- [10] H. A. Richard, M. Fulland og M. Sander, »Theoretical Crack Path Prediction,« *Blackwell Publishing*, 2004.
- [11] K. Tanaka, »Fatigue Crack Propagation from a Crack Inclined to the Cyclic Tensile Axis,« *Engineering Fracture Mechanics*, 1974.
- [12] L. Liu, »Modelling of Mixed-Mode Fatigue Crack Propagation,« 2008.
- [13] P. Hübner, H. Scholsser, G. Pusch og H. Biermann, »Load History Effects in Ductile Cast Iron for Wind Turbine Components,« *ScienceDirect*, 2007.
- [14] M. J. Paris, N.-H. Kim og T. Davis, »Reanalyses of the Extended Finite Element Method for Crack Initiation and Propagation,« *AIAA*, 2010.

- [15] »University of Idaho,« 2015. [Online]. Available:  
[https://www.engr.uidaho.edu/thompson/courses/ME330/lecture/least\\_squares.html](https://www.engr.uidaho.edu/thompson/courses/ME330/lecture/least_squares.html).
- [16] M. C. Walters, C. H. Paulio og R. H. Dodds, »Interaction Integral Procedures for 3-D Curved Cracks Including Surface Traction,« *ELSEVIER*, 2005.
- [17] H. Yu, L. Wu, L. Guo, H. Wu og S. Du, »An Interaction Integral Method for 3D curved cracks in Nonhomogeneous Materials with Complex Interfaces,« *ELSEVIER*, 2009.
- [18] »ANSYS Help Viewer,« 2015.
- [19] R. D. Cook, D. S. Malkus, M. E. Plesha og R. J. Witt, Concepts and Applications of Finite Element Analysis, 2002.
- [20] M. C. M. Fernando , E. T. Moyer og H. Liebowitz, »A Near Optimal Crack Tip Mesh,« *Pergamon*, 1995.
- [21] E. Madenci og I. Guven, The Finite Element Method and Applications in Engineering Using ANSYS, 2006.
- [22] S. Wu, A. R. Ingraffea og M. Grigoriu, »Probabilistic Fracture Mechanics a Validation of Predictive Capability,« *Defense Technical Information Center*, 1990.
- [23] Z. Lu, J. Xu, L. Wang, J. Zhang og Y. Liu, »Curvilinear Fatigue Crack Growth Simulation and Validation under Constant Amplitude and Over Loading,« *American Society of Civil Engineers*, 2014.

## 13 Appendix 1

Installations of the UIDL and APDL files in ANSYS is described in this section, an example is conducted in order to show how the program is working.

1. From the attached CD, find the folder named “Crack modelling”, copy this folder to e.g. the desktop.
2. Find the ANSYS folders on the computer where UIDL and APDL files is placed, see Figure 78 (Typical placement of this files).

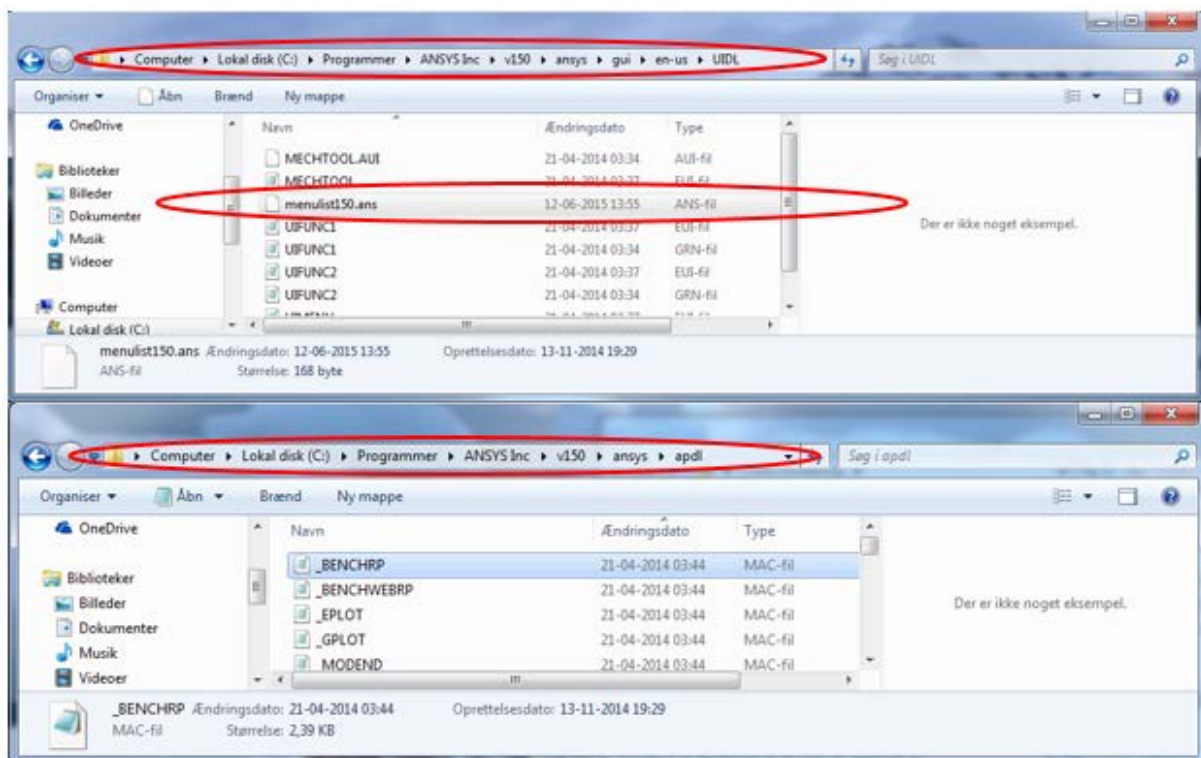


Figure 78 Folder for UIDL and APDL files

3. Copy the file from UIDL folder called “menulist150.ans” (150 = version 15.0), to the folder “Crack modelling”, see Figure 79.

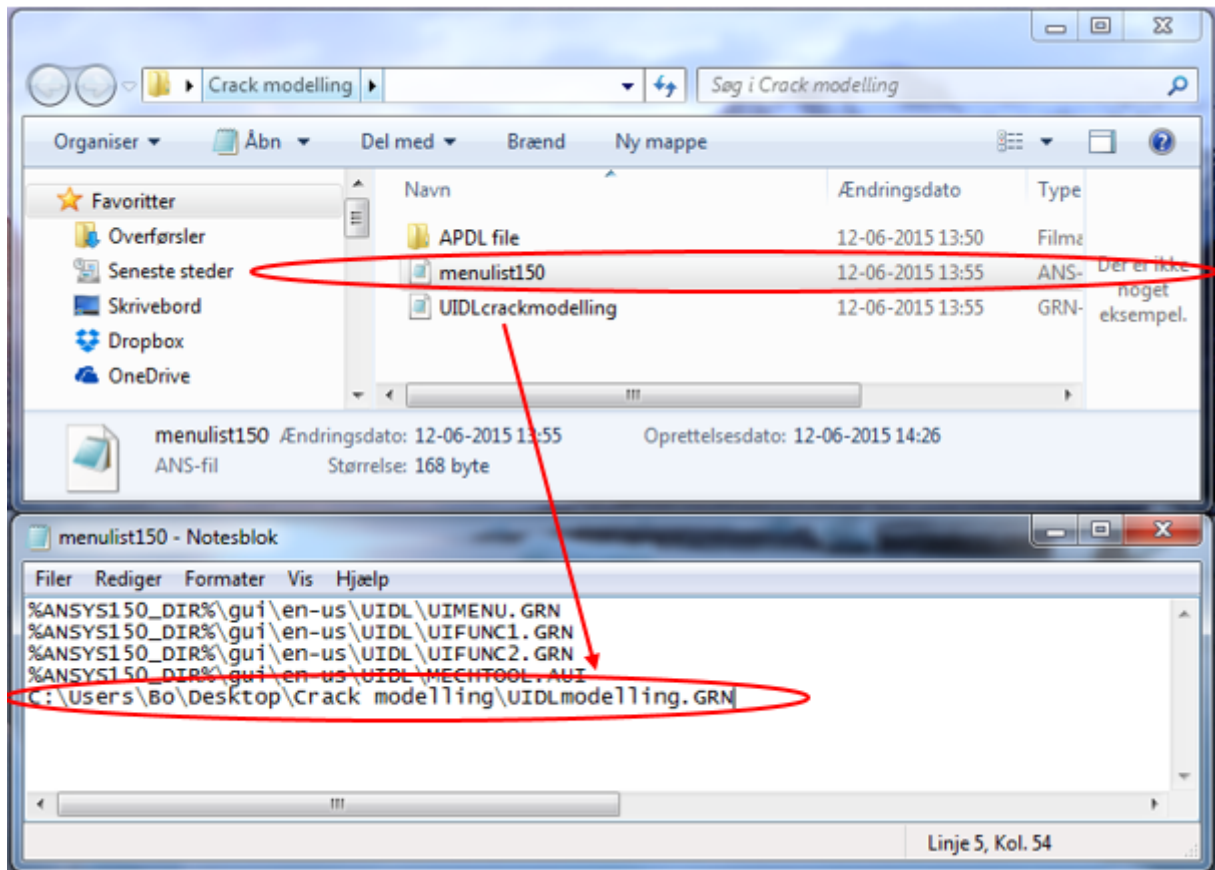


Figure 79 "Crack modellering" folder with "menulist150" open in notepad

4. Open the file "menulist150.ans", where the first four lines is directories for the ANSYS control files, create a new line with the directory of the folder "Crack modellering" with "\" and the filename "UIDLcrackmodellering.GRN", see Figure 79.
5. Cut the file "menulist150.ans" back to the folder of UIDL folder.
6. Open the folder "APDL file" and copy all the five files to the folder "APDL", see Figure 78.

The installations of the UIDL and APDL files is conducted, and ANSYS is ready to run with the new interface menu and APDL codes.

### Example of the program

1. Open the program “Mechanical APDL 15.0”, and type “plate” in the Command Prompt line, see fig Figure 80.

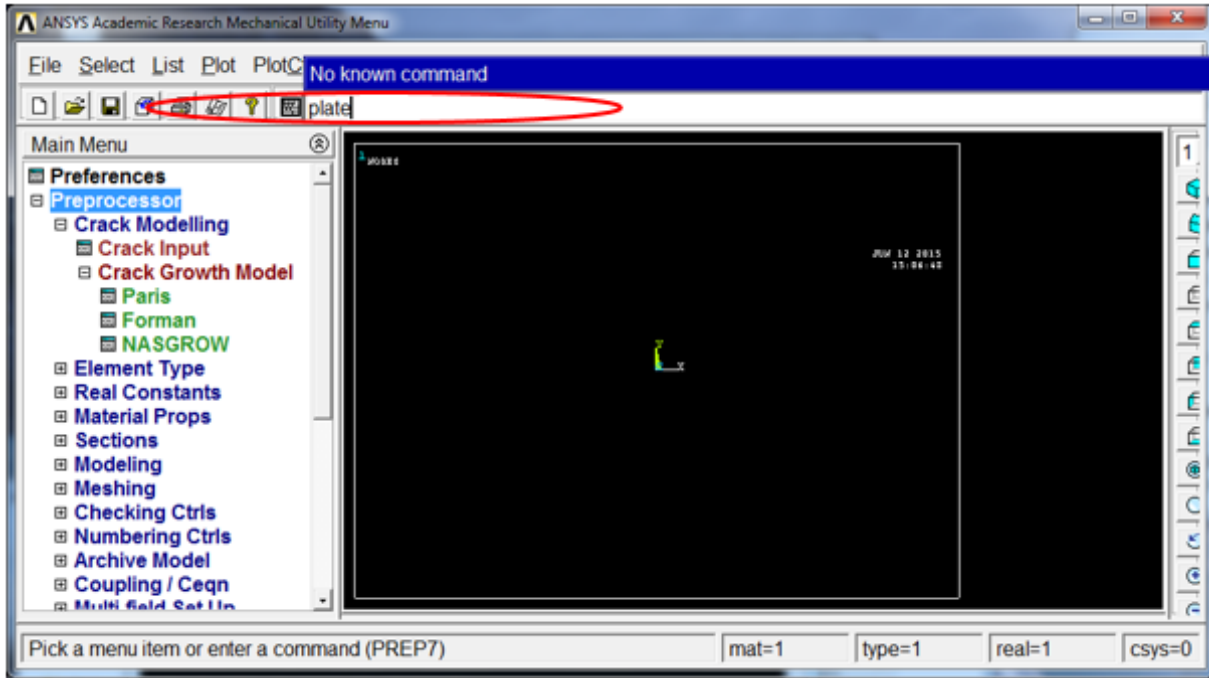


Figure 80 Modify GUI menu, with marked Command Prompt line

2. The command “plate” is a command for a plate with dimension of  $50 \times 75$  [mm], and boundary condition showed in Figure 81.

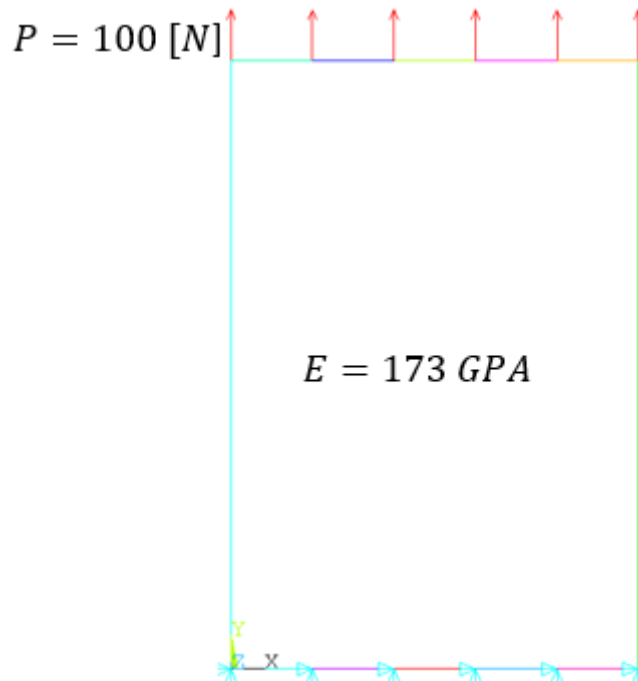


Figure 81 Boundary condition for plate

- Click on the “Crack Input” button and fill out the boxes with followed values, see Figure 82, and press “OK”.

Input for crack	
Coordinate of crack-edge and crack-tip	
Right edge side [X] and [Y]	0 49
Left edge side [X] and [Y]	0 50
Crack tip [X] and [Y]	10 49.5
Crack direction from crack-tip coordinate system	
Angle of crack-tip [DEG]	0
Global mesh size (Recommend 0.8*h)	
	1

Figure 82 Crack input with corresponding values

- Click on the “Paris” button, see Figure 80, and fill out the boxes with followed values, and a directory for the output file, click “OK” to start analysis, see Figure 83.

Crack Growth from Paris	
Material parameters for Paris	
Intercept coefficient [C] [E.G. = 1.5*10**(-10)]	3.1*10**(-10)
Slope of sigmoidal curve [n]	3
Number of steps [i]	40
Crack growth increment [da]	1
Write output parameters to file [i],[tip_x],[tip_y],[tip_theta],[d_theta],[K1_eff],[K2_eff] [Keq_max],[N_par],[D_K],[a_acc]	
Write file to	Desktop\Ansyscrack\output\test_plate.d
Press OK For Start Analysis	

Figure 83 Paris function block, with corresponding values

5. The crack trajectory of the plate is showed in Figure 84.

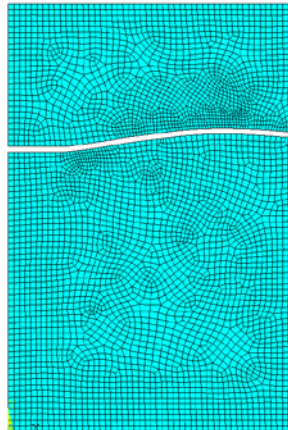


Figure 84 Results of analysis

6. The output file is showed in Figure 85, with corresponding terms of the value.

Number of steps	X-coor. Of crack-tip	Y-coor. Of crack-tip	$\theta_{cur}$	$\Delta\theta$	$K_{I\ eff}$	$K_{II\ eff}$	$K_{eq\ max}$	$N$	$\Delta K$	Accumulated crack length
1.00	10.00	49.50	6.39	6.39	203.40	-11.43	6.51	11698290.26	6.51	1.00
2.00	10.99	49.61	6.89	0.50	221.96	-0.97	7.10	9002456.69	7.10	2.00
3.00	11.99	49.73	7.50	0.60	240.18	-1.27	7.69	7104933.29	7.69	3.00
4.00	12.98	49.86	8.07	0.57	259.53	-1.30	8.30	5631845.25	8.30	4.00
5.00	13.97	50.00	8.47	0.40	279.80	-0.98	8.95	4494263.57	8.95	5.00
6.00	14.96	50.15	8.82	0.34	301.26	-0.91	9.64	3600653.03	9.64	6.00
7.00	15.95	50.30	9.13	0.31	324.08	-0.88	10.37	2892343.32	10.37	7.00
8.00	16.93	50.46	9.38	0.25	348.38	-0.77	11.15	2328185.91	11.15	8.00
9.00	17.92	50.62	9.57	0.19	374.32	-0.63	11.98	1876929.87	11.98	9.00
10.00	18.91	50.79	9.72	0.15	402.13	-0.51	12.87	1513898.00	12.87	10.00
11.00	19.89	50.96	8.58	-1.14	433.91	4.33	13.89	1204888.33	13.89	11.00
12.00	20.88	51.11	8.10	-0.48	466.18	1.95	14.92	971678.92	14.92	12.00
13.00	21.87	51.25	7.83	-0.27	500.97	1.16	16.03	783005.96	16.03	13.00
14.00	22.86	51.39	7.55	-0.28	538.84	1.30	17.24	629246.32	17.24	14.00
15.00	23.85	51.52	7.21	-0.34	580.17	1.74	18.57	504111.88	18.57	15.00
16.00	24.84	51.64	6.80	-0.41	625.48	2.24	20.02	402941.65	20.02	16.00
17.00	25.84	51.76	6.30	-0.50	675.42	2.93	21.61	319498.64	21.61	17.00
18.00	26.83	51.87	7.45	1.15	735.18	-7.38	23.53	247748.85	23.53	18.00
19.00	27.82	52.00	7.75	0.29	798.29	-2.05	25.55	193510.39	25.55	19.00
20.00	28.81	52.14	7.38	-0.37	868.26	2.80	27.78	150394.55	27.78	20.00
21.00	29.81	52.26	6.00	-1.38	946.47	11.39	30.29	116110.46	30.29	21.00
22.00	30.80	52.37	5.20	-0.80	1036.05	7.25	33.15	88520.27	33.15	22.00
23.00	31.80	52.46	4.31	-0.89	1138.67	8.81	36.44	66679.60	36.44	23.00
24.00	32.79	52.53	3.45	-0.86	1257.53	9.46	40.24	49502.72	40.24	24.00
25.00	33.79	52.59	2.57	-0.88	1396.28	10.71	44.68	36163.62	44.68	25.00
26.00	34.79	52.64	1.72	-0.85	1559.86	11.62	49.92	25937.68	49.92	26.00
27.00	35.79	52.67	0.87	-0.84	1754.68	12.93	56.15	18222.01	56.15	27.00
28.00	36.79	52.68	0.08	-0.79	1989.50	13.75	63.66	12501.27	63.66	28.00
29.00	37.79	52.69	-0.66	-0.74	2275.98	14.71	72.83	8349.89	72.83	29.00
30.00	38.79	52.67	-1.32	-0.66	2630.87	15.16	84.19	5406.18	84.19	30.00
31.00	39.79	52.65	-1.91	-0.59	3078.67	15.93	98.52	3373.65	98.52	31.00
32.00	40.79	52.62	-2.45	-0.53	3654.85	17.03	116.96	2016.42	116.96	32.00
33.00	41.79	52.57	-2.92	-0.47	4416.85	18.08	141.34	1142.48	141.34	33.00
34.00	42.79	52.52	-3.36	-0.44	5458.16	20.96	174.66	605.41	174.66	34.00
35.00	43.78	52.47	-3.76	-0.41	6943.33	24.66	222.19	294.09	222.19	35.00
36.00	44.78	52.40	-4.20	-0.43	9183.88	34.77	293.88	127.09	293.88	36.00
37.00	45.78	52.33	-4.67	-0.48	12847.36	53.51	411.12	46.42	411.12	37.00
38.00	46.78	52.25	-5.27	-0.60	19593.92	102.79	627.01	13.09	627.01	38.00
39.00	47.77	52.15	-6.12	-0.85	34765.09	256.83	1112.48	2.34	1112.48	39.00
40.00	48.77	52.05	-7.71	-1.59	86077.04	1193.12	2754.47	0.15	2754.47	40.00

Figure 85 Output file with corresponding terms of the value